INFORMATION TO USERS

The most advanced technology has been used to photograph and reproduce this manuscript from the microfilm master. UMI films the text directly from the original or copy submitted. Thus, some thesis and dissertation copies are in typewriter face, while others may be from any type of computer printer.

The quality of this reproduction is dependent upon the quality of the copy submitted. Broken or indistinct print, colored or poor quality illustrations and photographs, print bleedthrough, substandard margins, and improper alignment can adversely affect reproduction.

In the unlikely event that the author did not send UMI a complete manuscript and there are missing pages, these will be noted. Also, if unauthorized copyright material had to be removed, a note will indicate the deletion.

Oversize materials (e.g., maps, drawings, charts) are reproduced by sectioning the original, beginning at the upper left-hand corner and continuing from left to right in equal sections with small overlaps. Each original is also photographed in one exposure and is included in reduced form at the back of the book. These are also available as one exposure on a standard 35mm slide or as a 17" x 23" black and white photographic print for an additional charge.

Photographs included in the original manuscript have been reproduced xerographically in this copy. Higher quality 6" x 9" black and white photographic prints are available for any photographs or illustrations appearing in this copy for an additional charge. Contact UMI directly to order.

U·M·I

University Microfilms International
A Bell & Howell Information Company
300 North Zeeb Road, Ann Arbor, MI 48106-1346 USA
313/761-4700 800/521-0600

Reproduced with permission of the copyright owner. Further reproduction prohibited without permission.

Reproduced with permission of the copyright owner. Further reproduction prohibited without permission.

Order Number 9019875

Experimental and numerical study of low pressure mineral-melt equilibria in alkaline lavas

Camur, Mehmet Zeki, Ph.D.

University of Cincinnati, 1989

U·M·I
300 N. Zeeb Rd.
Ann Arbor, MI 48106

Reproduced with permission of the copyright owner. Further reproduction prohibited without permission.

Reproduced with permission of the copyright owner. Further reproduction prohibited without permission.

EXPERIMENTAL AND NUMERICAL STUDY OF LOW PRESSURE MINERAL-MELT EQUILIBRIA IN ALKALINE LAVAS

A dissertation submitted to the

Division of Graduate Studies and Research
of the University of Cincinnati

in partial fulfillment of the
requirements for the degree of

DOCTOR OF PHILOSOPHY

in the Department of Geology
of the College of Arts and Sciences

1989

by

Mehmet Zeki Camur

M.S., UNIVERSITY OF CINCINNATI, 1986

B.E., BLACKSEA UNIVERSITY, Turkey 1982

Reproduced with permission of the copyright owner. Further reproduction prohibited without permission.

UNIVERSITY OF CINCINNATI

November 17 19 89

I hereby recommend that the thesis prepared under my supervision by Mehmet Zeki Camur

entitled Experimental and Numerical Study of Low Pressure Mineral-Melt Equilibria in Alkaline Lavas

be accepted as fulfilling this part of the requirements for the degree of Doctor of Philosophy

Approved by:

Reproduced with permission of the copyright owner. Further reproduction prohibited without permission.

ABSTRACT

In recent years petrologists and geochemists initiated research projects aimed toward understanding low and high pressure crystallization of alkaline magmas. Isotopic and trace element data as well as theoretical calculations show that these magmas originate at source regions that are deeper than those of the tholeiitic magmas. Therefore, documentation of the geochemical characteristics of alkaline melts and coexisting minerals at high and low pressures, and construction of geochemical models for such melts are essential for constraining the chemistry and mineralogy of their source regions and for understanding the details of their low pressure fractionation. This dissertation is a contribution toward geochemistry and petrology of potassic alkaline rocks.

In order to analyze the phase equilibria in multiply saturated potassic alkaline systems, melting and crystal growth experiments were performed at one atmosphere total pressure and under the f_{O2} conditions similar to that defined by the QFM buffer. Range of temperature covered in this study is 1060-1250^{o}C. In addition, temperature and composition dependency of low pressure mineral-melt equilibria involving olivine, pyroxenes, plagioclase,

Reproduced with permission of the copyright owner. Further reproduction prohibited without permission.

nepheline, and leucite have been modeled using empirical equations.

In part I of this dissertation, chemical data from 60 experiments have been used to construct ternary pseudoliquidus phase diagrams to demonstrate the low pressure crystallization trends in potassic alkaline magmas as well as to evaluate olivine-, plagioclase-, alkali feldspar-, and leucite-melt relations. Experimental data obtained in this study show that at low pressures and f_{O2}~QFM, crystallization sequence in potassic alkaline magmas is olivine, pyroxene, leucite, plagioclase and by crystal fractionation, such magmas evolve toward alkali feldspar stability field. An important observation based on these experiments is that nepheline is not a stable phase in the presence of olivine, pyroxene, plagioclase and leucite. Corollary of this observation is that nepheline and plagioclase bearing (sodium-rich) alkaline lavas can not evolve from leucite and plagioclase bearing (potassium-rich) parental alkaline magmas. This observation also leads to the conclusion that coexistence of nepheline and leucite in an alkali basaltic melt is only possible in the absence of plagioclase.

Plagioclase coexisting with leucite in potassium-

Reproduced with permission of the copyright owner. Further reproduction prohibited without permission.

rich alkaline melts is calcium-rich. With decreasing temperature, leucite reacts with the melt (reaction relation) and produces potassium-rich alkali feldspar. Only after complete dissolution of leucite in the melt that plagioclase becomes sodium-rich.

Part II of this dissertation provides empirical mineral-melt equations that have been incorporated into a numerical model to predict equilibrium crystallization trends in basaltic melts. Using bulk chemical compositions of the starting materials in the experiments, equations successfully predict, at a given f_{O2} and temperature, compositions of multiply saturated melts as well as coexisting minerals. These generalized equations can be used to test equilibrium in basaltic lavas as well as to differentiate cumulate minerals from those forming from the melt. Finally, several mineral-melt geothermometers developed in this study can be used to retrieve temperature information from natural rocks.

Reproduced with permission of the copyright owner. Further reproduction prohibited without permission.

ACKNOWLEDGEMENTS

I gratefully acknowledge the assistance given by Professor Attila I. Kilinc: with his direction this dissertation was prepared. I thank my dissertation committee members Professor Arvid M. Johnson and Professor Craig Dietsch for their assistance and reviewing the text.

Special gratitude also goes to Professor Richard O. Sack for stimulating discussions and comments on the research and text, Professor Madeline Briskin for making me feel free to use her computer, and Professor Andrew J. Stolz for generously providing samples from Indonesia.

I would also like to thank Mark Philips, Amy Schmuckie, and Carl Heiger for their technical assistance.

This research was financially supported by the Department of Geology and the University Research Council of the University of Cincinnati. I would also acknowledge the Department of Atmospheric and Geological Sciences of Purdue University for providing free access to their electron microprobe.

Reproduced with permission of the copyright owner. Further reproduction prohibited without permission.

TABLE OF CONTENTS

Reproduced with permission of the copyright owner. Further reproduction prohibited without permission.

Reproduced with permission of the copyright owner. Further reproduction prohibited without permission.

LIST OF FIGURES

Reproduced with permission of the copyright owner. Further reproduction prohibited without permission.

Reproduced with permission of the copyright owner. Further reproduction prohibited without permission.

LIST OF TABLES

Page

Reproduced with permission of the copyright owner. Further reproduction prohibited without permission.

Reproduced with permission of the copyright owner. Further reproduction prohibited without permission.

PART I

EXPERIMENTAL STUDY OF LOW PRESSURE MELT-MINERAL EQUILIBRIA IN ALKALINE LAVAS FROM INDONESIA AND CHINA

Reproduced with permission of the copyright owner. Further reproduction prohibited without permission.

1.1 INTRODUCTION

Basaltic rocks are divided into three groups: 1) tholeiite basalts; 2) olivine tholeiite basalts; and 3) alkali basalts. Yoder and Tilley (1962) have proposed a simple classification system for basaltic rocks using the CIPW normative minerals forsterite, diopside, nepheline, and silica. Their generalized basalt tetrahedron (olivine-clinopyroxene-nepheline-silica) contains three compositionally distinct volumes separated by planes defined by the minerals olivine, clinopyroxene, and plagioclase and clinopyroxene, plagioclase, and orthopyroxene (Figure I.1).

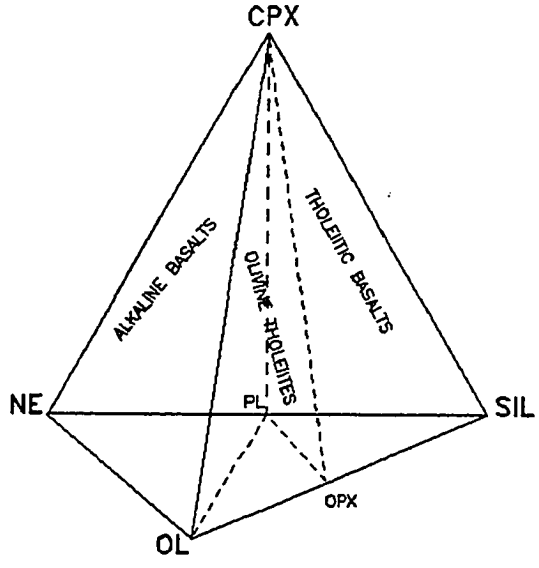

Figure I.1. Generalized basalt tetrahedron (after Yoder and Tilley 1962). OL=olivine; CPX=clinopyroxene; PL=plagioclase; NE=nepheline; OPX=orthopyroxene; SIL=silica.

Reproduced with permission of the copyright owner. Further reproduction prohibited without permission.

In Figure I.1, tholeiitic basalts plot within the silica-clinopyroxene-plagioclase-orthopyroxene volume; olivine tholeiites plot within the olivine-clinopyroxene-plagioclase-orthopyroxene volume, and basic alkaline lavas (basanites, olivine nephelinites etc.) plot within the clinopyroxene-plagioclase-olivine-nepheline volume.

My purpose in this experimental study is to analyze the compositional characteristics of both multiply saturated melts and their coexisting minerals in potassium-rich alkaline lavas as a function of temperature at one atmosphere pressure under controlled oxygen fugacity conditions.

Experimentally determined low pressure melt-mineral equilibria has been used extensively to study the evolution of basaltic magmas. In order to determine basaltic phase equilibria, experimental petrologists have used two types of starting materials in their experiments: (1) natural basalts and (2) two, three, and four-component, simplified synthetic basaltic systems. With the synthetic systems, phase relationships can easily be represented graphically and chemical trends can be shown for equilibrium or fractional crystallization. Using such diagrams, low pressure liquidus phase relationships of basaltic rocks have been established

Reproduced with permission of the copyright owner. Further reproduction prohibited without permission.

experimentally by Yoder and Tilley (1962), Schairer and Yoder (1960a), Schairer (1950), and other workers. However, these early experimental studies concentrated on the determination of phase relations. Complete sets of compositional data on coexisting phases were not collected for analytical study of the phase equilibria. Analytical data are vital for any quantitative analysis of mineral-melt equilibria under various pressure and temperature conditions.

Recently, experimental petrologists not only have been using rocks as starting materials in their experiments, but also have been routinely using the electron microprobe to collect chemical data on coexisting phases. In addition, solid buffers have been used extensively to control oxygen fugacity (f_{O2}) in experiments with mafic and ultramafic rocks. In early 1960 s, it was established that the oxygen fugacity strongly affects the sequence of crystallization and the compositions of minerals (Osborn, 1959).

As more experimental data using both natural systems and simple synthetic mineral systems have accumulated, discrepancies between these two approaches have become apparent. For example, Sack et al. (1987) used olivine tholeiites from different locations to

Reproduced with permission of the copyright owner. Further reproduction prohibited without permission.

experimentally study melt-mineral equilibria at one atmosphere pressure under controlled oxygen fugacity conditions. Sack et al. (1987) compared their experimental data with that of Presnall et al. (1978), who used the more simple synthetic system CaO-MgO-Al_2O_3-SiO_2 (CMAS) for their experiments. Sack et al. (1987) showed that the evolution trend of melts saturated with olivine, pyroxene, plagioclase, and +/- spinel in simple and natural systems is different (see Figure 3 in Sack et al. 1987).

Until recently, experimental petrologists studying basalts have concentrated their research mostly on tholeiites and olivine tholeiites. Alkaline rocks are volumetrically small among terrestrial basalts, and only a few experimental studies have been performed using natural alkaline rock compositions (Sack et al. 1987 and Gee and Sack, 1988). Nevertheless, a great deal of interest and controversy surround both the nature and the origin of their parental magmas. This is partly due to diverse and distinctive chemical compositions of alkaline lavas in comparison with tholeiites and partly due to information that their source regions are in deeper parts of the mantle compared to tholeiites. The characteristics of multiply saturated (evolved), potassium-rich (leucite-

Reproduced with permission of the copyright owner. Further reproduction prohibited without permission.

bearing) alkaline basaltic melts,-compositions of which reflect the processes of equilibrium crystallization and crystal fractionation at low pressures,-are not completely known and need to be experimentally studied.

My objectives in part I of this dissertation are as follows:

1) Experimental determination of the sequence of crystallization and the composition of minerals and coexisting melts in leucite-bearing (potassium-rich) alkaline lavas at low pressure as a function of temperature and composition.

2) Determination of any possible correlations between mineral and coexisting melt compositions using experimental data.

3) Construction of the multiply saturated liquidus diagrams for olivine, pyroxene, plagioclase, and leucite minerals for qualitative analysis of the phase relations in leucite-bearing alkaline lavas.

4) Evaluation of the reaction relations between feldspars-, leucite-, nepheline-, and melt in alkaline magmas.

Reproduced with permission of the copyright owner. Further reproduction prohibited without permission.

1.2 EXPERIMENTAL AND ANALYTICAL METHODS

1.2.1 Experimental Apparatus

Melting and crytal growth experiments have been performed using a one atmosphere, gas mixing, quench furnace in the Department of Geology of the University of Cincinnati. A detailed description of this furnace is given by Edgar (1973). During experimental runs, furnace input temperature was controlled by a Mode C unit manufactured by Deltech Inc. Temperature inside the furnace was monitored with a Pt-Pt-10%Rh thermocouple. Continuous temperature measurements during experimental runs indicated that the run temperatures have been maintained within +/- 2^{o}C of the set temperature.

In the experimental study of alkaline silicate compositions, it is important to control f_{O2}. Since f_{O2} strongly affects the sequence of crystallization and the compositions of minerals. The f_{O2} within the furnace was controlled by a gas mixture of 95.25% CO_2 and 4.75% CO which provides f_{O2} conditions similar to that defined by the quartz-fayalite-magnetite buffer (Denies et al. 1974). Reported f_{O2} values in Table I.A2 for each experimental run were calculated from known gas mixing ratio and the temperature using equations given by Denies et al. (1974). A desired gas mixture was adjusted using a flow meter manufactured by Matheson Inc.

Reproduced with permission of the copyright owner. Further reproduction prohibited without permission.

1.2.2 Starting Materials

Volcanic rocks were used as starting materials in the melting and crystal growth experiments and chemical analyses of them are listed in Table I.A1. These chemical analyses are projected onto the composition plane S-CA-M using the molecular percent equivalent of the procedure given in chapter 3 of B.V.S.P. (1981) (Figure I.2).

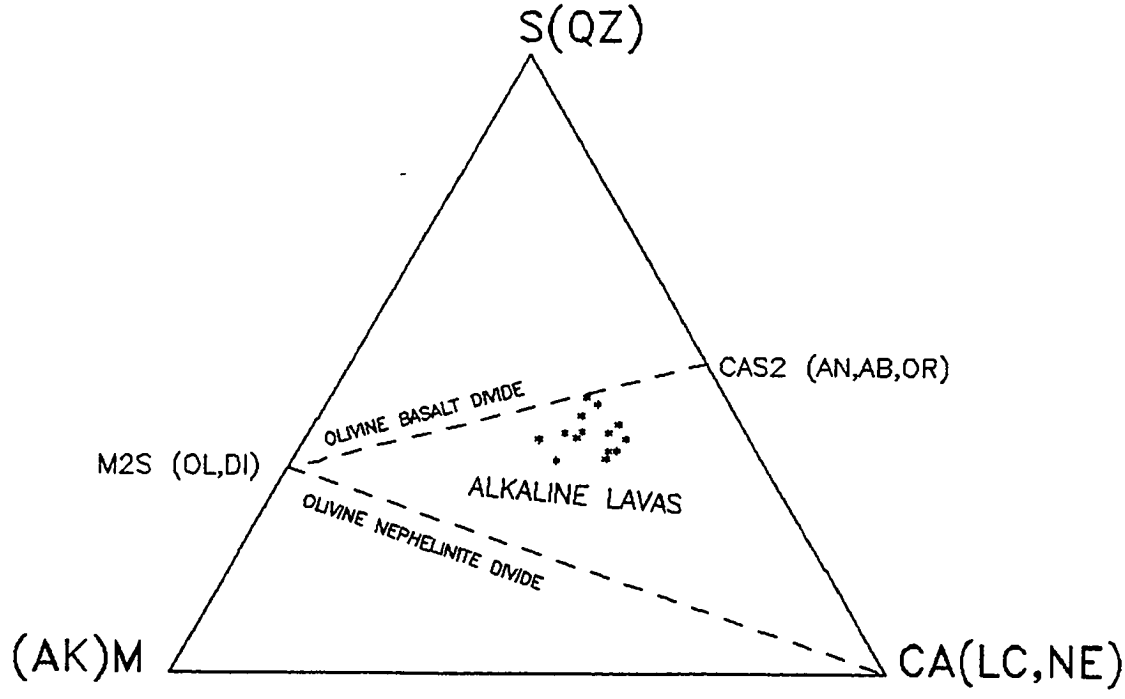

Figure I.2. The compositions of experimental starting materials projected into the system $CaO-MgO-Al_2O_3-SiO_2$ and onto composition plane S-CA-M. Molar oxides are combined as follows:
$CA=CaO+Al_2O_3+Fe_2O_3+3Na_2O+K_2O-1/3P_2O_5$, $M=FeO+MnO+MgO$, $S=SiO_2-2Na_2O-4K_2O$ (after B.V.S.P.,1981).
QZ=quartz, LC=leucite, NE=nepheline, OL=olivine, DI=diopside, AN=anorthite, AB=albite, OR=orthoclase, AK=akermanite.

Reproduced with permission of the copyright owner. Further reproduction prohibited without permission.

Sunda Arc Lavas, Indonesia:

Leucite basanites (samples 67127, 67130, 67137, 67145) are from the Batu Tara Volcano (Stolz et al. 1988). Olivine leucitites (samples 48114, 48115) are from the Sangenges Volcano. Olivine leucitite (sample 48134) and olivine tephrite (sample 48137) are from the Soromundi Volcano (Varne and Foden, 1986). These samples have been generously provided by Prof. A.J. Stolz (University of Tasmania, Australia).

Wudalianchi Lavas, China:

Late differentiates of leucite basanite magma (samples L-Low, L-Mid, L-Up, L-D, L-2) are from the Laoheishan Volcano and (sample H-5) from the Hoshaoshan Volcano. These samples were collected by Prof. A.I. Kilinc (University of Cincinnati, U.S.A.).

1.2.3 Experimental Procedures

Samples were ground to 5-10 micron size in a shatter box, mixed with polyvinyl alcohol as a binding agent, and then were compressed into pellets (about 0.5 grams). The pellets were broken into small fragments. A 0.40 millimeter diameter hole was drilled into small fragment of the pellets. They were hung onto 0.127 millimeter diameter iron electroplated platinum loops. The

Reproduced with permission of the copyright owner. Further reproduction prohibited without permission.

platinum loops and the sample fragments hanging from them were then loaded into the furnace.

One of the problems with this type of experiment is that iron from the samples diffuses into the platinum loops, despite the limited contact area between the samples and the platinum wires. In order to minimize this iron loss, the platinum wires were initially electroplated with iron (8-10 wt%; Grove, 1981) using a supersaturated ferrous sulfate (50 wt%)-ferrous ammonium sulfate (50 wt%) solution at a temperature of 65^{o}C and a current of 2 volts D.C.. To achieve the diffusion of electroplated iron into the wires, the electroplated platinum wires were then heated at 1200 ^{o}C for a period of 72 hours in the presence of 96% nitrogen-4% hydrogen gas stream.

Between 8-12 loops carrying samples were attached to a circular platinum wire (one millimeter in diameter) for each experimental run and suspended in the hot spot of the vertical quench furnace.

Duration of the experiments varied according to run temperatures, ranging from 48 hours for the highest temperature (1248 ^{o}C) to 995 hours for the lowest temperature (1062 ^{o}C). Experiments were terminated by

Reproduced with permission of the copyright owner. Further reproduction prohibited without permission.

dropping the samples into cold water which was injected into the bottom of the furnace immediately before quenching.

The difficulty of demonstrating equilibrium in experiments with multicomponent systems has been extensively discussed by Wyllie et al. in B.V.S.P. (1981 pg. 519). In my experiments, I have used the following positive criteria to judge whether or not a state of equilibrium has been achieved between minerals and melt: (a) presence of euhedral morphologies of crystals, (b) presence of uniform size of a given mineral, (c) presence of homogeneous composition of a given mineral at each experimental run, (d) presence of homogeneous glass composition in a given experimental run.

1.2.4 Analytical Procedures

Experimental run products were crushed in acetone and small chips were then mounted in epoxy, polished, and chemically analyzed using a 4-channel Cameca SX-50 electron microprobe at Purdue University. An accelerating voltage of 15 kV, beam current of 0.15-$0.3X10^{-7}$ amp., 30 second integration (counting) time , and one micron beam diameter were used in most analyses. In order to prevent alkali diffusion during glass analysis, the beam diameter was enlarged to 20 microns

Reproduced with permission of the copyright owner. Further reproduction prohibited without permission.

wherever possible. Samples were analyzed in sequence for Na, Cr, Ti, K, Mg, Mn, Fe, Si, Al, Ca, and P against the mineral standards; Amelia Albite (Na), 52NL11 (Cr), Di_2Ti (Ti), Orthoclase (K), Shallow Water Enstatite (Mg, Si), Hort (Mn), Fayalite (Fe), Anorthite (Ca, Al), and Apatite (P). Chemical analysis of the experimental run products together with the run conditions are given in Appendix I.A.

In order to quantify any alkali loss in glass analyses as a function of beam diameter and counting time, samples were analyzed using variable beam diameters and counting times. These analyses are listed in Appendix I.B. Using the glass with the lowest alkali content and a one micron beam diameter, weight percents of Na_2O and K_2O were measured at counting times of 5, 10, 20, and 30 seconds. These analyses show no detectable change in the concentrations of Na and K as a function of counting time. The effect of beam size on alkali loss during analysis was checked using beam diameters of 1, 5, 15, and 30 microns with a 30 second counting time. Except in glasses formed at high temperatures (~ 1250 ^{o}C) from experiments with the Wudalianchi lavas, in which there was a detectable Na loss (about 70%) with a one micron beam diameter, all other analyses show no

Reproduced with permission of the copyright owner. Further reproduction prohibited without permission.

correlation between beam diameter and measured concentrations of Na and K. Therefore, all analyses are reported without any correction.

Analyses of the glasses and the minerals in Table I.A3 represent the average of 2-4 individual good analysis of each product. Average deviations (+/-) for the reported concentrations of oxides analyzed in glasses from all of my experiments are as follow:

SiO_2=0.47	FeO_t=0.25	Na_2O=0.21
TiO_2=0.21	MnO=0.05	K_2O=0.10
Al_2O_3=0.23	MgO=0.21	P_2O_5=0.09
Cr_2O_3=0.03	CaO=0.13	

Where FeO_t is total iron concentration. Average deviations of oxides analyzed in minerals from all of my experiments are less than these values.

Reproduced with permission of the copyright owner. Further reproduction prohibited without permission.

1.3 MINERAL CHEMISTRY

1.3.1 Olivine

Olivine is the first mineral to crystallize in all experimental runs that include olivine as a run product. Olivine compositions range from 0.86 to 0.63 mole fraction forsterite (Mg_2SiO_4). Mole fraction forsterite shows a gradual decrease from high temperature olivine to low temperature olivine for a given bulk composition. Minor amounts of Ca and Mn in olivine correlate with increasing Fe concentration. Ca concentrations in olivine are relatively higher than those of Mn in all cases.

In general, Fe-Mg exchange between olivine and melt (glass) has a distribution coefficient ($K_D^{ol-melt}$) of about 0.3 +/- 0.03 (e.g. Roeder and Emslie, 1970, Walker et al., 1979). In some experiments, however, $K_D^{ol-melt}$ deviates from 0.3 +/- 0.03 and these experiments are listed below:

Sample I.D.	Run #	$K_D^{ol-melt}$
L-Mid	9	0.24
L-Up	8	0.26
L-Up	9	0.24
L-D	9	0.25
L-2	9	0.25
H-5	8	0.26
H-5	9	0.22

Reproduced with permission of the copyright owner. Further reproduction prohibited without permission.

Ferric iron concentrations in the melts used for $K_D^{ol-melt}$ calculations were determined from total iron values using Sack et al. 1980 ferric-ferrous equilibria equation. These seven experimental runs differ from those with $K_D^{ol-melt}=0.3$ +/-0.03 as follow: Experiments with $K_D^{ol-melt} < 0.3$ +/-0.03 include spinel and alkali feldspar as an additional crystallizing phases. It may be deduced that spinel and alkali feldspar crystallization may be responsible for relatively low $K_D^{ol-melt}$ values of these runs. $K_D^{ol-melt}$ values less then 0.3 were also reported by Sack et al. (1987) and Gee and Sack (1988) from similar melting experiments with alkaline lavas.

In order to quantify the equilibrium relationship between basaltic melt composition and the composition of coexisting olivine, experimental results reported in this study were coupled with the olivine-melt equilibrium data from Walker et al. (1979), Grove et al. (1982), Sack et al. (1987), and Gee and Sack (1988). Ferric iron concentrations in the melts were calculated from total iron values using Sack et al. 1980 ferric-ferrous equilibria equation. Using experimental data from 133 olivine-melt equilibria, the following empirical correlation between the compositions of olivine and coexisting melt as a function of temperature was

Reproduced with permission of the copyright owner. Further reproduction prohibited without permission.

established :

$$(I.1) \quad \text{Ln } X_{Fa} = (A/T) * (1-X_{MgO}) * \exp[X_{FeO}^{(1/3)}] + B$$

where,

X_{Fa} =Mole fraction of fayalite (Fe_2SiO_4) in olivine.
X_{FeO}=Mole fraction of FeO in melt.
X_{MgO}=Mole fraction of MgO in melt.
T =Equilibrium temperature in degrees Celcius.

A and B are the regression coefficients and have values of 3307.766 and -5.4879, respectively. The regression line has values of R^2=0.97 and correlation=0.987; the values R^2 and correlation relate to the precision of A and B. The regression line and the data used for the derivation of equation (I.1) are shown in Figure I.3.

I have performed two types of calculations using my data and data from the literature in order to quantify the prediction quality of equation (I.1): (1) for a given melt composition and equilibrium temperature, the mole fraction of fayalite in olivines was calculated and (2) for a given melt and olivine composition, equilibrium temperature was calculated. Average absolute values of calculated minus experimental results are about +/- 0.01 and +/- 11 ^{o}C in the first and second type of calculations, respectively.

Reproduced with permission of the copyright owner. Further reproduction prohibited without permission.

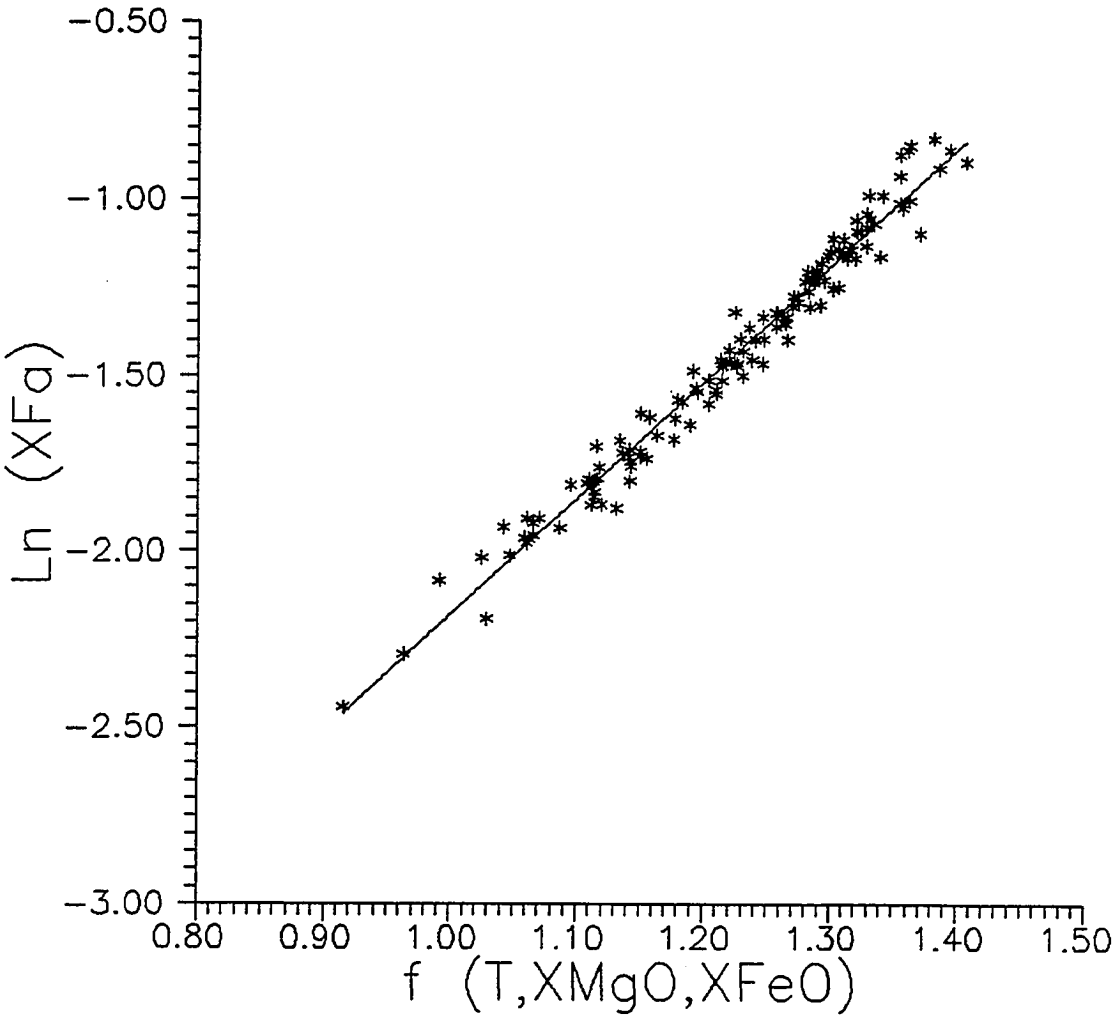

Figure I.3. Composition and temperature dependency of olivine-melt equilibria in basaltic composition space. $f=(1-X_{MgO})\exp[X_{FeO}^{(1/3)}]1000/T$.

The corresponding regression equation has a=3.3077, b=-5.4879, R^2=0.97, and correlation=0.987.

Reproduced with permission of the copyright owner. Further reproduction prohibited without permission.

The experimental data base used for the regression of equation (I.1) covers a wide range of basaltic compositions defined by the basaltic compositional space in Figure I.1. Therefore, equation (I.1) should be applicable to a variety of petrologic calculations (e.g. equilibrium temperature, olivine saturation, mineral cumulated versus original melt discrimination etc.) in basaltic composition space.

1.3.2 High-Calcium Pyroxene

High-Ca pyroxene is the second mineral to crystallize in all experimental runs that include olivine and pyroxene as run products. The compositional range of pyroxene in terms of the mole proportions of $Ca_2Si_2O_6$ (wollastonite), $Mg_2Si_2O_6$ (enstatite), and $Fe_2Si_2O_6$ (ferrosilite) components are Wo_{45-48}-En_{33-45}-Fs_{8-22} and Wo_{42-45}-En_{38-45}-Fs_{12-18} in the experiments with samples from Indonesia (leucite basanites, olivine leucitites and olivine tephrite) and from China (late differentiates of leucite basanites), respectively. Although Mg and Fe concentrations of pyroxenes in experiments from both localities are comparable, Ca and Al concentrations are higher in experiments with starting material from Indonesia and Na and Ti concentrations are higher in experiments with starting materials from China. Overall,

Reproduced with permission of the copyright owner. Further reproduction prohibited without permission.

pyroxene compositions cluster near the $CaMgSi_2O_6$ (diopside) corner of the quadrilateral composition space shown in Figure I.4.

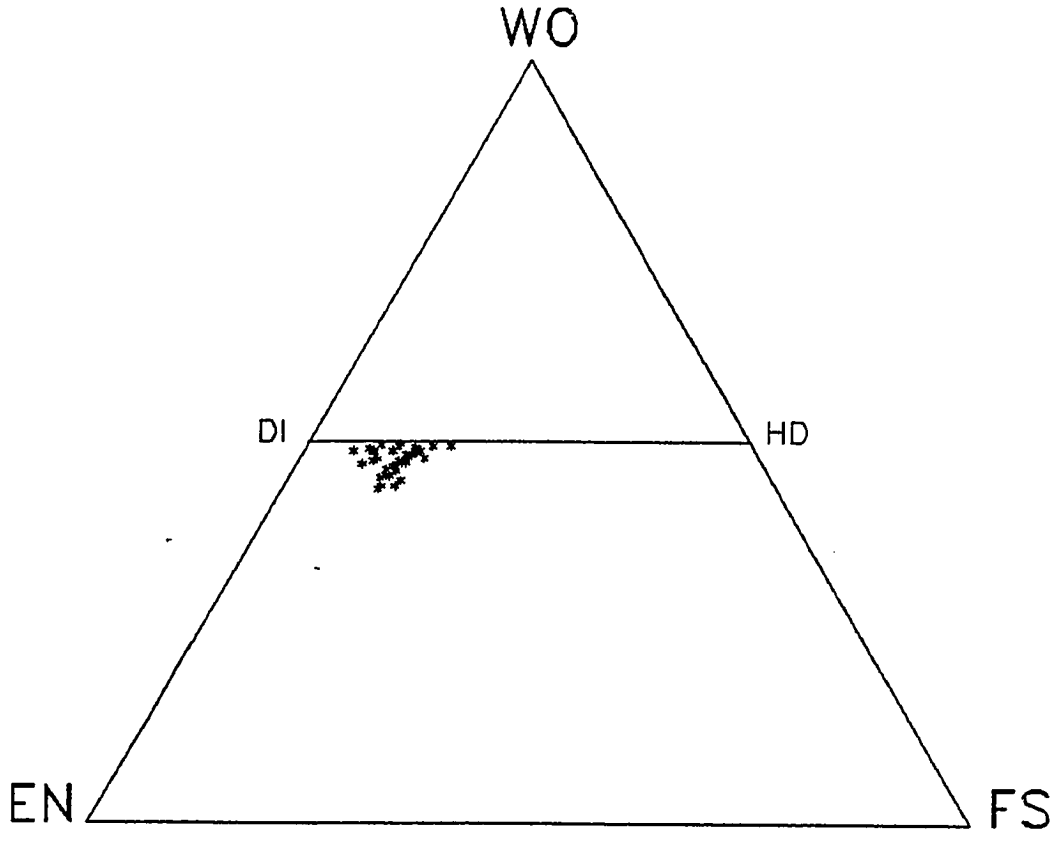

Figure I.4. Compositions of pyroxenes in experimental runs.
DI=diopside; HD=hedenbergite; EN=enstatite;
FS=ferrosilite; WO=wollastonite.

Reproduced with permission of the copyright owner. Further reproduction prohibited without permission.

1.3.3 Feldspars

Feldspar in the experimental runs with samples from Indonesia :

Plagioclase is the last phase to crystallize in my experiments, after olivine, high-Ca pyroxene, and leucite. Calcium concentration in plagioclase is very high, comparable to plagioclases from leucite bearing alkaline lavas (Gupta and Yagi, 1980). $CaAl_2Si_2O_8$ (anorthite), $NaAlSi_3O_8$ (albite), and $KAlSi_3O_8$ (orthoclase) components in plagioclase range from An_{89}-Ab_{26}-$Or_{5.8}$ to An_{68}-$Ab_{8.7}$-Or_2.

Feldspar in the experimental runs with samples from China:

In the experimental results of samples from China (except sample L-Up), alkali feldspars crystallize after olivine, high-Ca pyroxene, and spinel. Compositions range from An_0-Ab_8-Or_{60} to $An_{4.7}$-Ab_{35}-Or_{92}. In the sample L-D, alkali feldspar co-precipitates with plagioclase feldspar at 1062 ^oC and their compositions are $An_{0.5}$-$Ab_{11.4}$-$Or_{88.1}$ and An_{34}-Ab_{51}-Or_{15}, respectively.

There is a polynominal correlation between anorthite mole fractions in plagioclase and the CaO concentration in the melt phase saturated with olivine, high-Ca

Reproduced with permission of the copyright owner. Further reproduction prohibited without permission.

pyroxene, plagioclase, +/-leucite, and +/- alkali feldpar for bulk compositions used in this study. This relationship is depicted on Figure I.5. If one considers that the other Ca-bearing phase coexisting with the melt, high-Ca pyroxene, has nearly constant Ca concentration, the relationship between Ca concentration of plagioclase and the coexisting melt is not suprising. Nevertheless, this correlation is important to show the incompatibility of albite-rich plagioclase and leucite. Melt with the lowest CaO concentration (circle) on Figure I.5 is saturated with olivine, high-Ca pyroxene, plagioclase, and alkali feldspar but not leucite. While, the other melts (six-rayed stars) are saturated with olivine high-Ca pyroxene, plagioclase, and leucite but not alkali feldspar. Based on this information, it could be deduced that along the dashed line in Figure I.5, leucite would react with the melt to produce alkali feldspar. Only after complete dissolution of leucite in the melt that plagioclase becomes albite-rich. This deduction is consistent with the observation that in naturally occuring lavas, coexistence of albite-rich plagioclase and leucite are incompatible. Leucite-melt reaction relations will be discussed further in section 1.4.

Reproduced with permission of the copyright owner. Further reproduction prohibited without permission.

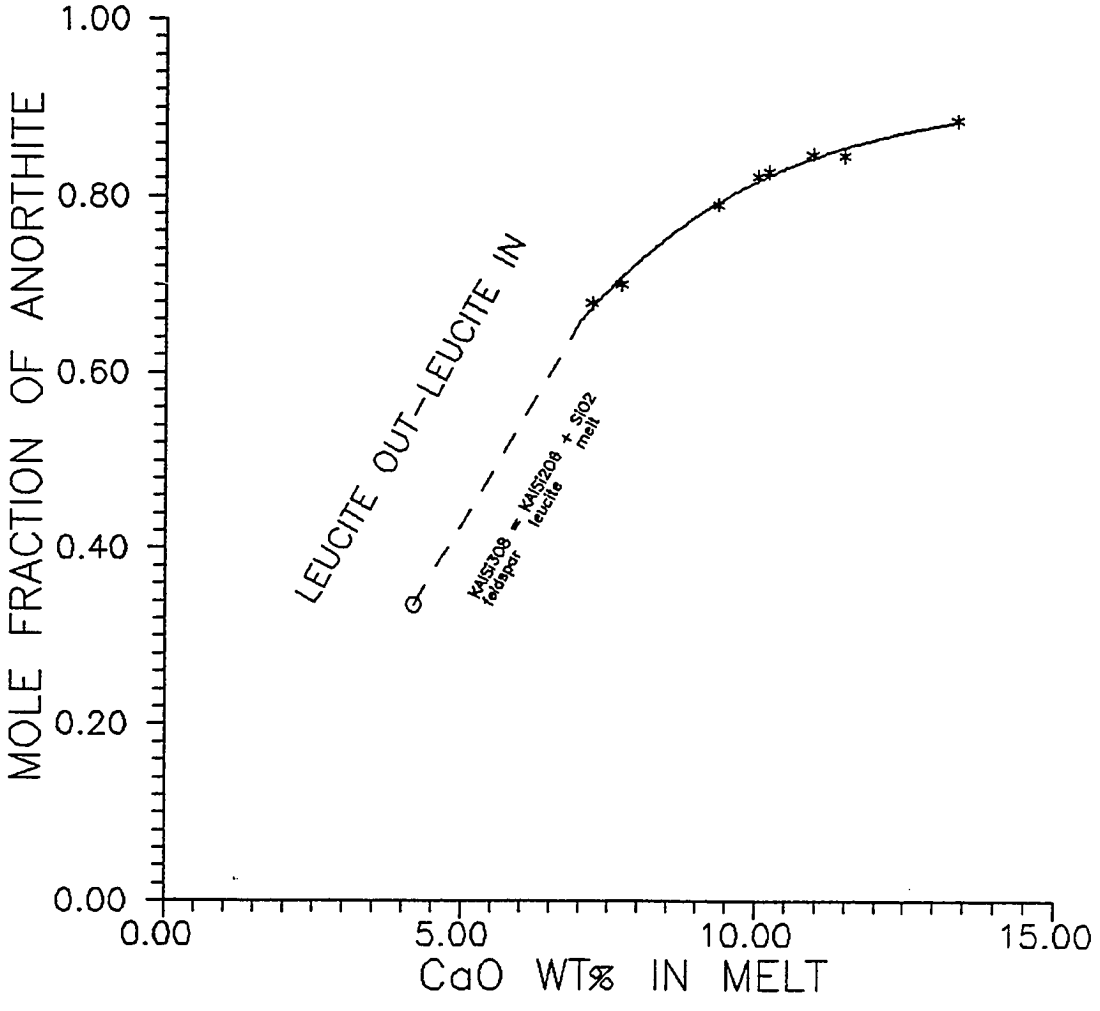

Figure I.5. Compositional relationship between mole fraction anorthite and wt% CaO in coexisting experimental melt. Melt compositions shown with (1) six-rayed star symbols are saturated with olivine, high -Ca pyroxene, plagioclase, and leucite:(2)circle symbol is saturated with olivine, high-Ca pyroxene, plagioclase, and alkali feldspar.

Reproduced with permission of the copyright owner. Further reproduction prohibited without permission.

1.3.4 Leucite

Leucite is present only in the experimental runs of samples from Indonesia, with the exception of sample 67137. In these runs leucite is the third crystallizing phase after olivine and high-Ca pyroxene. Mole fraction of $KAlSi_2O_6$ component varies only from 0.96 to 0.92. FeO concentration in leucites range from 0.74 wt% to 0.29 wt% and it is sometimes higher than that of Na_2O.

Reproduced with permission of the copyright owner. Further reproduction prohibited without permission.

1.4 LOW-PRESSURE COTECTICS

The evolution of leucite-bearing alkaline lavas under low pressure conditions may be qualitatively analyzed using the cotectics of multiply saturated melts coexisting with olivine, high-Ca pyroxene, feldspars, leucite, and with or without spinel. Due to the number of variables, multidimensional compositional spaces are required to represent such cotectics. In order to overcome this difficulty, multiply saturated melt compositions were transformed into normative compositions of the minerals coexisting with melt using the procedure given by Thompson (1982). Then, these normative minerals have been used to establish pseudoternary cotectic projections in two dimensional space.

1.4.1 Olivine - Pyroxene - Feldspars - Leucite - Cotectics

Based on the additive components Mg_2SiO_4 (forsterite), $CaMgSi_2O_6$ (diopside), $CaAl_2Si_2O_8$ (anorthite), $KAlSi_3O_8$ (sanidine), and $KAlSi_2O_6$ (leucite), and the exchange components $TiAl_2(MgSi_2)_{-1}$ (for high-Ca pyroxene), $Fe^{+3}(Al)_{-1}$ (for high-Ca pyroxene), $Fe^{+2}(Mg)_{-1}$ (for high-Ca pyroxene and olivine), $Mn(Mg)_{-1}$ (for high-Ca pyroxene and olivine), $Na(K)_{-1}$ (for feldspars and leucite), the pseudoternary diagram for olivine (OL),

Reproduced with permission of the copyright owner. Further reproduction prohibited without permission.

high-Ca pyroxene (DI), and alkali feldspar (AF) can be projected from plagioclase (PL) and leucite (LC) (Figure I.6). Spinel may coexist with the projected melt compositions; the presence or absence of spinel has a little affect on the position of the projected melt compositions. This set of components has been chosen because: (1) it represents all the minerals that coexist with the melt phase, and (2) it minimizes the scatter on the diagram and thus better defines the cotectics. Multiply saturated melt compositions that are expressed in terms of mole proportions of oxide components can be transformed to normative mineral compositions used in Figure I.6 by the following equations:

$$OL=0.5*(Al_2O_3+Fe_2O_3+FeO+MnO+MgO-CaO-Na_2O-K_2O)$$

$$DI=TiO_2-Al_2O_3-Fe_2O_3+CaO+Na_2O+K_2O$$

$$AF=SiO_2+2*TiO_2-0.5*(Al_2O_3+Fe_2O_3+FeO+MnO+MgO)-1.5*CaO-3.5*(Na_2O+K_2O)$$

On the basis of my experiments and the data of Sack et al. (1987), I have constructed the cotectics shown in Figure I.6. Multiply saturated melt compositions which are used to draw the cotectics are identified in the caption of Figure I.6. The OL+DI+PL+LC+/-SP cotectic is a best-fit line of the plotted data.

Reproduced with permission of the copyright owner. Further reproduction prohibited without permission.

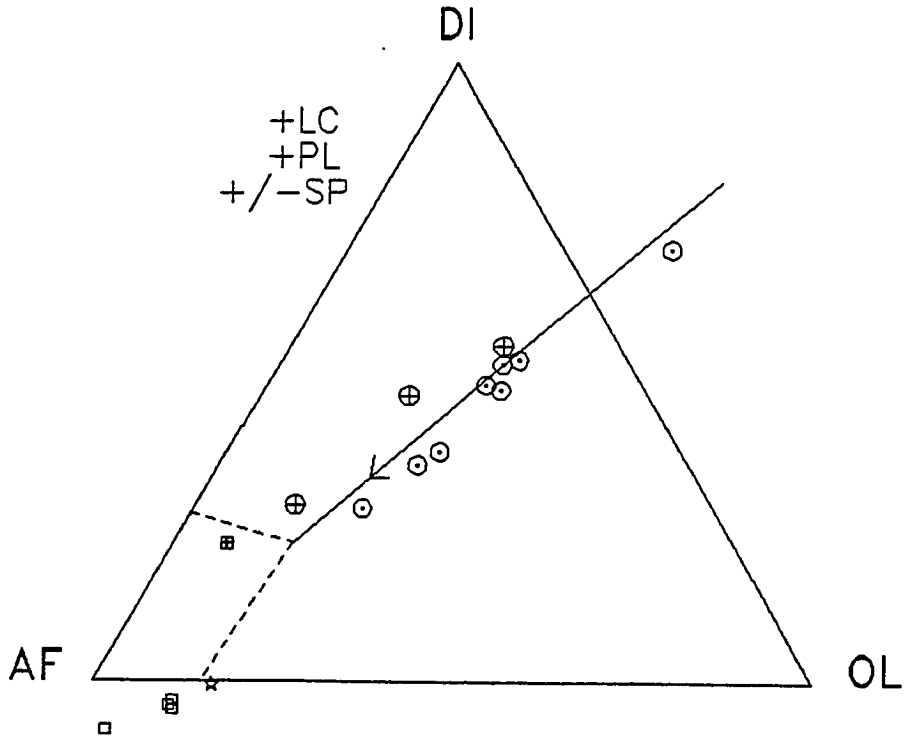

Figure I.6. One atmosphere (f_{O2} ~QFM) plagioclase + leucite +/- spinel saturated cotectics projected onto the composition plane defined by olivine, high-Ca pyroxene, and alkali feldspar normative components. The experimental melts plotted are
(1) saturated with olivine, high-Ca pyroxene, plagioclase, and leucite [circles with dots are the samples 48114, 48115, 67145 from run #6, the samples 48114, 48134, 67127, 67130, 67145 from run #7 (in this study)]:
(2) saturated with olivine, high-Ca pyroxene, plagioclase, leucite, and spinel [circles with cross are the sample BS-501 from run #13, the sample BS-501 from run #20, the sample 94-08A from run #24 (Sack et al. 1987)]:
(3) saturated with olivine, high-Ca pyroxene, alkali feldspar, and spinel [squares are the samples L-Low, L-Mid, L-2, H-5 from run #9 (in this study); square with cross is sample SAY-7E from run #21 (Sack et al. 1987)]:
(4) saturated with olivine, high-Ca pyroxene, plagioclase, alkali feldspar, and spinel [star is sample L-D from run #9 (in this study)].

Calculation procedures of the normative minerals and algorithms are given in the text.

Reproduced with permission of the copyright owner. Further reproduction prohibited without permission.

The melt compositions that plot on the cotectic saturated with OL+DI+PL+LC+/-SP evolve toward the alkali feldspar field. During this evolution, concentrations of SiO_2, Al_2O_3, Na_2O, and K_2O in the melt progressively increase and those of CaO and FeO decrease (Table I.A3). In Figure I.6 the boundaries of the alkali feldspar stability field have been approximated with dashed lines using melt compositions that coexist with olivine, high-Ca pyroxene, plagioclase, and alkali feldspar, but not leucite.

The data between simple synthetic systems and natural systems are disparate. In Figure I.6, once the melt composition reaches the alkali feldspar stability field, leucite may react with the melt and produce alkali feldspar through reaction:

(R I.1) $$\underset{\text{leucite}}{KAlSi_2O_6} + \underset{\text{melt}}{SiO_2} = \underset{\text{feld.}}{KAlSi_3O_8}$$

Because the activity of leucite is almost constant ($X^{leucite}$= 0.92-0.96), saturation of alkali feldspar in the melt will be governed by the activity of SiO_2 in the melt at constant pressure and temperature, according to R I.1. High SiO_2 activities in the melt phase drive R I.1 towards alkali feldspar. Thus, the observed SiO_2

Reproduced with permission of the copyright owner. Further reproduction prohibited without permission.

enrichment in the melt phase toward the alkali feldspar stability field (Table I.A3) is in agreement with R I.1. The temperature at which this reaction proceeds from left to right is 1150 +/-20 ^{o}C in the binary system $KAlSi_2O_6$-SiO_2 at one atmosphere pressure (Schairer and Bowen, 1938). In my study, at the temperature of 1149 +/-2^{o}C, none of the melt compositions are saturated with alkali feldspar. The equilibrium temperature for R I.1 has also been measured in two ternary systems at one atmosphere pressure: 1040 +/-10^{o}C in the system $CaMgSi_2O_6$-$NaAlSi_3O_8$-$KAlSi_2O_6$ (Sood et al. 1970) and 1100 +/- 10^{o}C in the system $CaMgSi_2O_6$-$KAlSi_2O_6$-SiO_2 (Schairer and Bowen 1938).

1.4.2 Olivine - Pyroxene - Feldspars - Leucite - Nepheline Cotectics

Using the additive components Mg_2SiO_4 (forsterite), $CaMgSi_2O_6$ (diopside), $CaAl_2Si_2O_8$ (anorthite), $NaAlSiO_4$ (nepheline), $KAlSi_2O_6$ (leucite), and exchange components $TiAl_2(MgSi_2)_{-1}$ (for high-Ca pyroxene), $Fe^{+3}(Al)_{-1}$ (for high-Ca pyroxene), $Fe^{+2}(Mg)_{-1}$ (for high-Ca pyroxene and olivine), $Mn(Mg)_{-1}$ (for high-Ca pyroxene and olivine), $NaSi(CaAl)_{-1}$ (for plagioclase), experimental compositions of multiply saturated melts were recast and plotted on the pseudoternary diagram olivine (OL), high-Ca pyroxene

Reproduced with permission of the copyright owner. Further reproduction prohibited without permission.

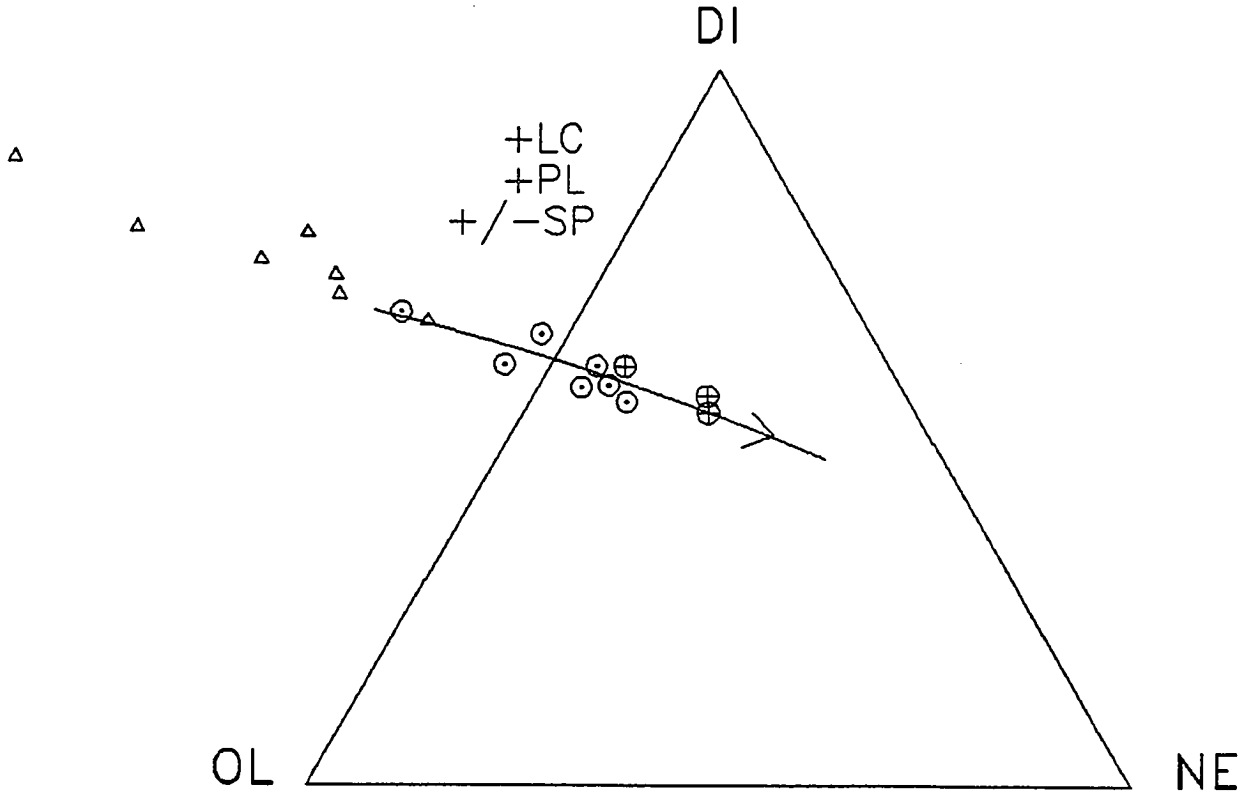

Figure I.7. One atmosphere (f_{O2} ~QFM) plagioclase + leucite +/- spinel saturated cotectic projected onto the composition plane defined by olivine, high-Ca pyroxene, and nepheline normative components. The experimental melts plotted are the same as given in the caption of Fig. I.6. Triangles represent tholeiitic melt compositions saturated with olivine, pyroxene, and plagioclase (Walker et al., 1979)

Calculation procedure of the normative minerals and algorithms are given in the text.

Reproduced with permission of the copyright owner. Further reproduction prohibited without permission.

(DI), and nepheline (NE) projected from the plagioclase (PL) and leucite (LC) apex (Figure I.7). Spinel may coexist with the projected melt compositions; the presence or absence of spinel has a little affect on the position of the projected melt compositions. This set of components has been chosen because it allows comparison between Na-rich and K-rich alkaline melts and it reduces the scatter on the diagram thus better defines the cotectic. Multiply saturated melt compositions that are expressed in terms of mole proportions of oxide components can be transformed to normative mineral compositions used in Figure I.7 by the following equations:

$$OL=0.5*(Al_2O_3+Fe_2O_3+FeO+MnO+MgO-CaO-Na_2O-K_2O)$$

$$DI=TiO_2-Al_2O_3-Fe_2O_3+CaO+Na_2O+K_2O$$

$$NE=-0.5*SiO_2-TiO_2+0.25*(Al_2O_3+Fe_2O_3+FeO+MnO+MgO)+0.75*CaO+2.75*Na_2O+1.75*K_2O$$

On the basis of my experiments and the data of Sack et al. (1987), the cotectic shown in Figure 7 was constructed. Multiply saturated melt compositions that are used to the draw the cotectic are identified in the caption of Figure I.6. The OL+DI+PL+LC+/-SP cotectic is a best fit line of the plotted data. Multiply saturated tholeiitic melt compositions (triangles) are also plotted

Reproduced with permission of the copyright owner. Further reproduction prohibited without permission.

on Figure I.7 to show the consistency between my experimental data and the data of Walker et al. (1979).

In Figure I.7, the melt compositions plot on OL+DI+PL+LC+/-SP cotectic move away from the OL-DI edge of the triangle upon further cooling. In K-rich alkaline magmas, melt compositions saturated with OL+DI+PL+LC+/-SP mineral assemblage evolve toward the stability field of alkali feldspar rather than towards that of nepheline. Although there are not enough experimental data to prove this statement with Figure I.7, the validity of this interpretation may be shown using a thermodynamic argument. For the composition space shown on Figure I.7, there are two possible reactions that buffer a_{SiO2} in the melt phase. These are: (1) leucite-melt reaction (R I.1) and (2) nepheline-melt reaction:

(R I.2) $0.5\ \underset{\text{nepheline}}{NaAlSiO_4} + \underset{\text{melt}}{SiO_2} = 0.5\ \underset{\text{feld.}}{NaAlSi_3O_8}$

Log a_{SiO2} versus temperature calculations for alkaline lavas indicate that these two silica buffer reactions follow parallel trends and the mineral stability fields of leucite and nepheline do not overlap at any temperature for a given bulk composition (Figure I.8). This means that if either of these silica buffer

Reproduced with permission of the copyright owner. Further reproduction prohibited without permission.

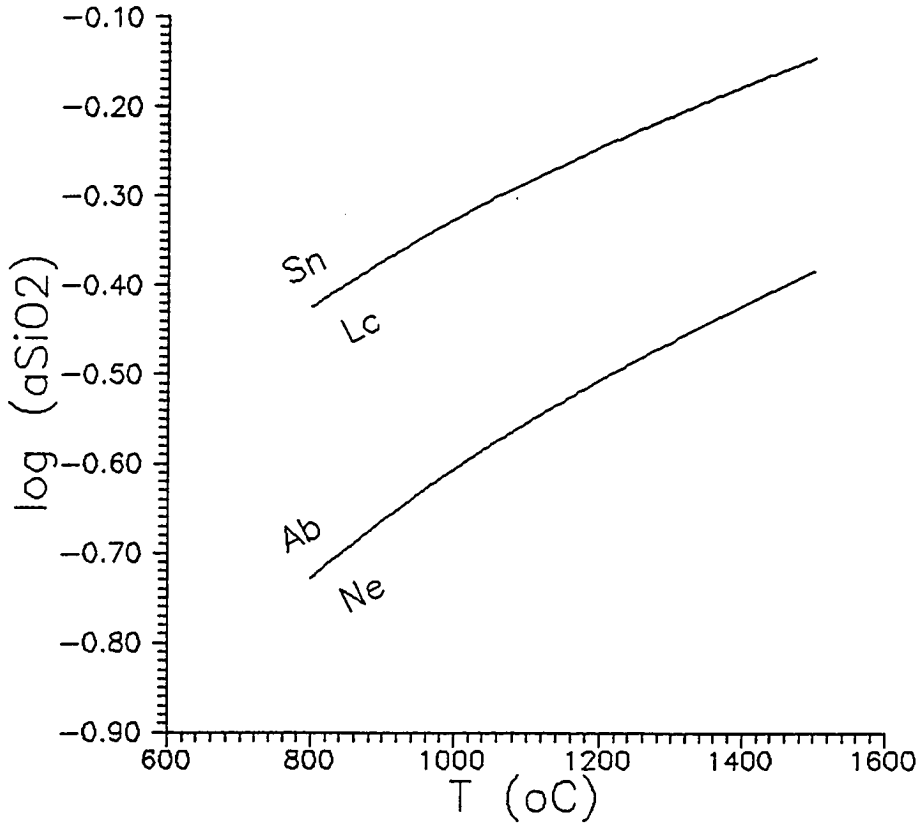

Figure I.8 Log a_{SiO2} versus temperature plotted for sanidine-leucite and nepheline-albite silica buffer reactions evaluated at one bar pressure (after Ghiorso and Carmichael, 1987).

reactions is in progress, the other would not take place under equilibrium crystallization conditions. Since the melt compositions plotted on Figure I.7 are saturated with leucite -not nepheline- and plagioclase coexisting with leucite is rich in the anorthite component -not albite-, R I.1 is the likely reaction to take place upon decreasing temperature and increasing a_{SiO2} for these melt compositions. Therefore, an alkali feldspar stability field must exist in Figure I.7.

Reproduced with permission of the copyright owner. Further reproduction prohibited without permission.

The termination of OL+DI+PL+LC+/-SP cotectic may be better understood with Figure I.9. This pseudoternary diagram is projected from the olivine and leucite corners to the DI-NE-AF plane and includes all the minerals shown in Figure I.7. This projection, was first used by Sack et al. (1987) is abandened in this study because the OL+DI+PL+LC+/-SP cotectic (dashed line) is extremely sensitive to Na_2O and CaO concentrations in the melt phase. The reason for this is that in the algorithm used by Sack et al. (1987), normative nepheline and diopside components of the melt phase are defined as $2*Na_2O$ and CaO (mole proportions), respectively. Nevertheless, the diagram is useful to show that the OL+DI+PL+LC+/-SP cotectic in this composition space terminates at alkali feldspar stability field -not at nepheline.

An important observation based on these experiments is that nepheline is not a stable phase in the presence of olivine, high-Ca pyroxene, plagioclase, and leucite. Corollary of this observation is that nepheline and plagioclase bearing (Na-rich) alkaline lavas can not evolve from leucite and plagioclase bearing (K-rich) parental alkaline magmas. This observation also leads to the conclusion that coexistence of nepheline and leucite in an alkaline basaltic melt is only possible in the absence of plagioclase.

Reproduced with permission of the copyright owner. Further reproduction prohibited without permission.

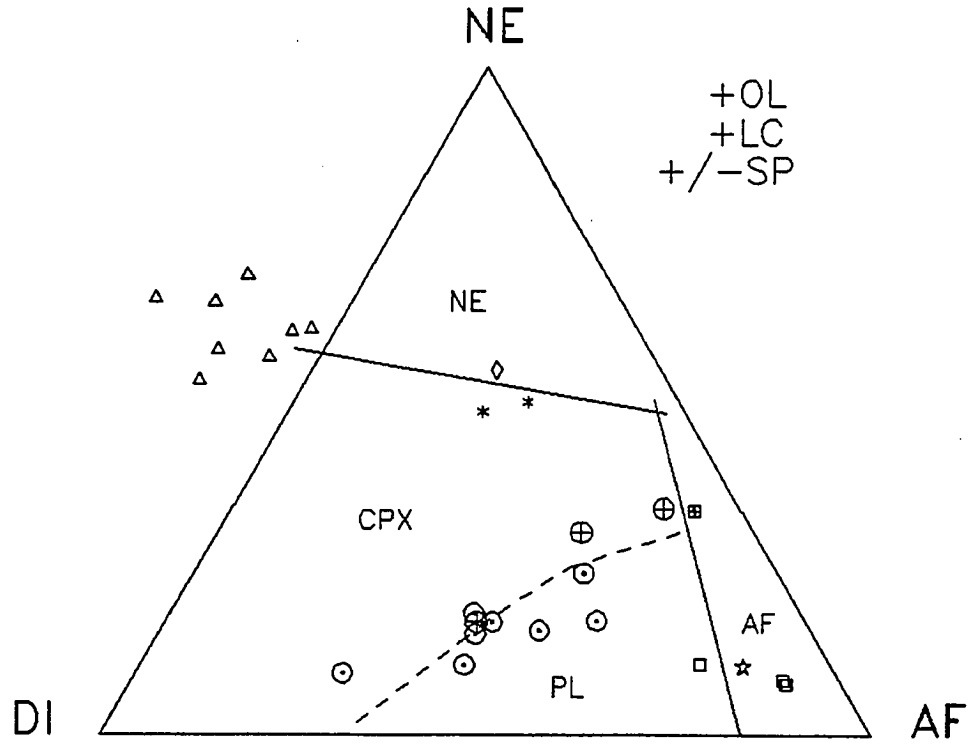

Figure I.9 Pseudoternary, pseudoliquidus diagram for experimental melts
(1) saturated with minerals given in the caption of Figure I.6:
(2) saturated with olivine, high-Ca pyroxene, leucite, nepheline [triangles are the samples B-12, B-10, C-15 from run #6, sample A-4 from run #7; samples A-3, A-4, A-5, B-7, B-11 from run #13 (Gee and Sack, 1988)]:
(3) saturated with olivine, leucite, nepheline [diamond is the sample B-12 from run #14 (Gee and Sack, 1988)]:
(4) saturated with high-Ca pyroxene, leucite, nepheline [six-rayed stars are the sample 20421 from run #20 and from run #21 (Sack et al. 1987)].

Calculation procedures of normative minerals on the diagram are given in the caption of Fig. 9 in Sack et al. 1987.

Reproduced with permission of the copyright owner. Further reproduction prohibited without permission.

1.5 APPLICATIONS TO NATURAL LAVA COMPOSITIONS

The validity and applications of the pseudoternary diagrams established in this study may be shown using natural lava compositions. For this purpose, I have plotted a total of 26 leucite-bearing lava compositions from different volcanoes on Figures I.10 and I.11. Sample identification of these lavas in the original study and in this study are listed in Table I.1.

Lava compositions A, B, C, D, and E are the Vico lavas from the Roman volcanic region, Italy, studied by Cundari and Mattias (1974), and classified as phonolitic leucite tephrite (A), tephritic leucite phonolite (B, C, and D), and leucite trachyte (E). These rocks consist of olivine + clinopyroxene + plagioclase + leucite + alkali feldspar +/- nepheline. Cundari and Mattias (1974) reported that these rocks represent low pressure differentiation products of one parental magma in the region. This interpretation is consistent with the clustering of the lava compositions on or near to the low pressure OL+DI+PL+LC+/-SP and OL+PL+LC+AF+/-SP cotectics established in this study (Figure I.10).

Lava compositions from F through J also are from the Roman volcanic region, Italy. These lavas were studied

Reproduced with permission of the copyright owner. Further reproduction prohibited without permission.

Table I.1. Identification of the lava samples used in Figures I.10 and I.11.

SAMPLE I.D.	ADAPTED SAMPLE I.D.	LAVA NAME
PLT-176	A	Phonolitic leucite tephrite
LTP-21	B	Tephritic leucite phonolite
TLP-154	C	"
TLP-185B	D	"
LTR-189	E	Leucite trachyte
90-05	F	Leucite phonolite
9	G	"
88-17	H	Leucite trachyte
89-21	I	"
8	J	" (av. of 5)
6	K	"
3	L	Phonolitic leucite tephrite (av.of 14)
CND-4	M	Leucitite
BYT-2	N	"
TUL-14	O	"
1	P	Leucite trachybasalt
2	Q	"
3	R	"
1	S	Leucite tephrite
6	T	"
3	U	Leucitophyre
C2911	V	Phonolitic glass
C2799	W	Trachytic glass
T174	X	Phonolite
2	Y	Leucite phonolite
5	Z	Trachyte

Reproduced with permission of the copyright owner. Further reproduction prohibited without permission.

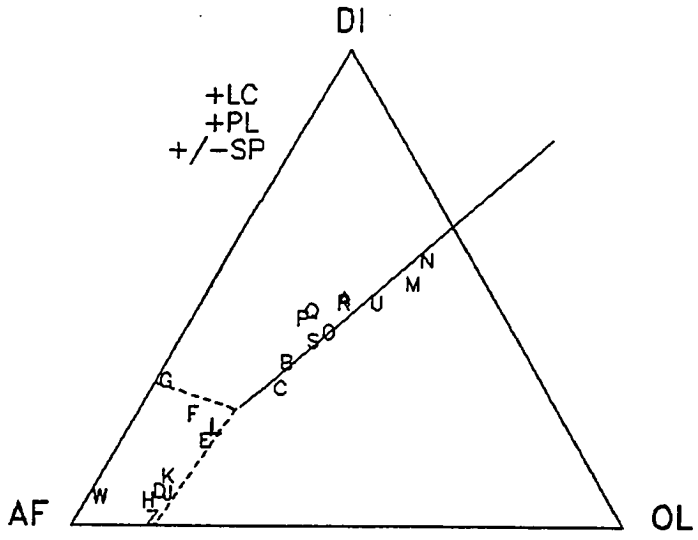

Figure I.10. Experimental cotectics shown on Figure I.6 compared with leucite-bearing lavas. Discriptions of the lavas are given in the text.

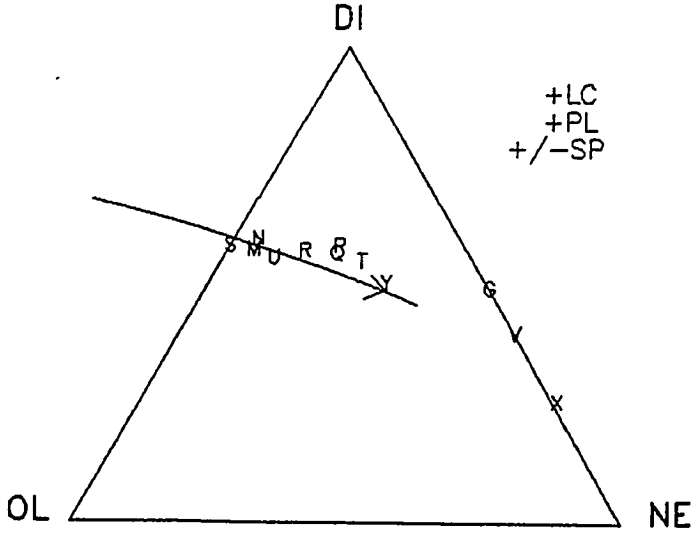

Figure I.11. Experimental cotectic shown on Figure I.7 compared with leucite-bearing lavas. Discriptions of the lavas are given in the text.

Reproduced with permission of the copyright owner. Further reproduction prohibited without permission.

by Baldridge et al. (1981). Compositions G and J are taken from Fudali (1963). Samples F and G are leucite phonolites and samples H, I, and J are leucite trachytes. These samples were reported to contain a phenocryst aasemblage of clinopyroxene + plagioclase + leucite and a groundmass assemblage of clinopyroxene + plagioclase + leucite + alkali feldspar +/- nepheline. Note that leucite phonolites F and G plot near to the DI+LC+PL+AF+/-SP cotectic whereas leucite trachytes (H, I, and J) plot near to the OL+PL+LC+AF+/-SP cotectic. This implies that leucite phonolites and leucite trachytes represents the crystallization trends of two separate parental magma compositions. The lavas from the Vulsinian (K) and Rocca (L) volcanoes, Italy, have a similar mineralogy to the lavas H, I, J and also plot near OL+PL+LC+AF+/-SP cotectic. The lava compositions K and L are taken from Gupta and Yagi (1980).

Trachyte from Gough Island (Z) taken from Le Maitre (1962) contains olivine + clinopyroxene + plagioclase + alkali feldspar (but not leucite) and is located on the AF-OL edge of the Figure I.10. The composition of Z represents a late differentiation product of parental alkali olivine basalt magma (Le Maitre, 1962). Samples V and W are phonolitic and trachytic glass compositions,

Reproduced with permission of the copyright owner. Further reproduction prohibited without permission.

respectively, from Bufumbira, Uganda (Ferguson and Cundari, 1975). Ferguson and Cundari (1975) reported that the phonolitic glass (V) is the very last product of a leucitite magma trend represented by the sequence: leucite tephrite --> tephritic leucitite --> leucitite --> phonolitic leucitite. Ferguson and Cundari (1975) interpreted the trachytic glass (W) as the last differentiation product of a phonolitic tephrite magma and they suggested the differentiation sequence for it to be leucite tephrite --> phonolitic leucite tephrite --> tephritic leucite phonolite --> latite --> trachyte. Indeed the phonolitic glass composition (V) of Ferguson and Cundari (1975) plots on the nepheline side of Figure I.11 and the tracytic glass composition (W) plots near the alkali feldspar corner of the Figure I.10. A phonolitic lava composition (X) is from an olivine nephelinite series in Eastern Uganda (King, 1965) and it plots in the nepheline stability field in Figure I.11.

Leucite trachybasalt lava compositions (P, Q, and R) are from Tristan da Cunha Island (Baker et al. 1964). These lavas are composed of olivine + high-Ca pyroxene + plagioclase + leucite and they plot close to and on the OL+DI+PL+LC+/-SP cotectic, both in Figures I.10 and I.11. Leucite tephrites (S and T) and leucitophyre (U) lava

Reproduced with permission of the copyright owner. Further reproduction prohibited without permission.

compositions are from Java Island, Indonesia (Gupta and Yagi, 1980) and they plot near to and on the cotectic OL+DI+PL+LC+/-SP (Figures I.10 and I.11).

Leucitite compositions (M,N, and O) are from New South Wales, Australia, and these lavas have been studied by Cundari (1973). These lavas consist of olivine + clinopyroxene + leucite + feldspars and minor amounts of biotite, amphibole, and nepheline. Crystallization pressures for the lavas are considered to be lower than 2 kb and they do plot near the cotectic OL+DI+PL+LC+/-SP (Figures I.10 and I.11).

In summary, all the lava compositions plotted on Figures I.10 and I.11 confirm the validity of the cotectics for leucite bearing alkaline lavas. Figures I.10 and I.11 could be used to determine the low-pressure differentiation of evolved alkaline magmas. It should be noted, however, that more melting experiments at low temperatures (< 1060 ^{o}C) are needed to further define the terminations of alkali feldspar-, plagioclase-, and nepheline-bearing alkali melts in natural systems.

Reproduced with permission of the copyright owner. Further reproduction prohibited without permission.

PART II

NUMERICAL MODELING OF LOW PRESSURE ANHYDROUS MELT-MINERAL EQUILIBRIA IN BASALTIC COMPOSITION SPACE

Reproduced with permission of the copyright owner. Further reproduction prohibited without permission.

2.1 INTRODUCTION

In order to understand thermochemical processes that take place in the Earth's interior, geochemists study volcanic rocks. Coexisting glass (melt) and mineral compositions in lavas provide information about pressure (P), temperature (T), and compositional (X) characteristics of the Earth's interior where their magmas originate or are subsequently processed.

The fundamental approach used for the determination of these variables (P, T, and X), is to perform equilibrium melting and crystal growth experiments using samples of lavas. In these experiments, the samples are subjected to different P and T conditions and, for each P and T, compositions of melt and coexisting mineral(s) are determined.

A serious limitation of the data gathered in this experimental approach is that experiments cover only a narrow compositional space. Specific experimental results are extrapolated to the other comparable compositions with phase diagrams (i.e Figure I.6 in part I of this study) which provide qualitative analysis of melt-mineral equilibria in an extrapolated compositional range.

Reproduced with permission of the copyright owner. Further reproduction prohibited without permission.

The idea of predicting melt-mineral equilibria observed in volcanic rocks has recently been an intriguing research topic for many geochemists. However, the application of equilibrium thermodynamics to melt-mineral phase relations has been very much model dependent due to insufficient data on the structural properties of natural silicate melts. As Bottinga et al. (1981) summarized, existing simple silicate structure models i.e the so-called random network model, the molten salt model (Tempkin model), and the polymer model, are presently not applicable to the multicomponent silicate melt systems.

A number of stoichiometric models that assign a set of most likely structural units to a melt phase, also have been proposed. These models include: (1) ideal-mixing models of Burnham (1975, 1979a, 1979b), Bottinga and Richet (1978), Nielsen and Dungan (1983) and (2) regular solution models of Ghiorso et al. (1980, 1983, 1985) and Berman and Brown (1984).

Among these models, Bottinga and Richet 's (1978) and Berman and Brown 's (1984) models have only been applied to binary and ternary systems, respectively. Burnham's (1975) model on the other hand is applicable only to felsic melts. Currently, the models of Nielsen

Reproduced with permission of the copyright owner. Further reproduction prohibited without permission.

and Dungan (1983) and Ghiorso et al. (1983, 1985), within their limitations are the most comprehensive ones that can be used to simulate melt-mineral equilibria in magmatic systems.

Nielsen and Dungan (1983) have modified the "two lattice" models of Bottinga and Weill (1972) and Drake (1976b) for the melt phase. Nielsen and Dungan have calibrated equilibrium distribution constants for melt-mineral reactions as a function of temperature. In their treatment of mineral-melt equilibrium, they assumed ideal mixing for intra-melt lattices and no inter-mixing between the melt lattices. Therefore, any non-ideal behaviour in the system is forced to be included in a temperature dependent linear function. The model of Nielsen and Dungan (1983) covers olivine-, pyroxene-, plagioclase-, rhombohedral oxides-, and spinel-melt equilibria at low pressures in anhydrous mafic systems. Detailed statistical analysis to check the internal consistency of the model is not given; however, they report that their model reproduces the input data base to within +/- 20 ^{o}C and +/- 3.1 wt% for oxides in the minerals (Nielsen and Dungan, 1983). This model is limited to alkali-poor basaltic compositions in its application because modeled solid phases do not include

Reproduced with permission of the copyright owner. Further reproduction prohibited without permission.

nepheline or leucite. Furthermore, the compositional range of the experimental data base which was used to determine the distribution coefficients by least square regression is limited to alkali-poor basaltic compositions.

Ghiorso et al. (1980, 1983) have developed a "regular solution" model assuming that melt phase is composed of a set of mineral-like components with structures based on eight oxygens. They have calibrated binary symmetric interaction parameters ($W_{i,j}$) from melt-mineral reactions as a function of melt components in the form defined by the regular solution model of Margules. Any non-ideality in the melt phase is forced to be included in the $W_{i,j}$ parameters. Their model covers olivine-, pyroxene-, plagioclase-, leucite-, melilite-, spinel-, and rhombohedral oxides-melt equilibria at both low and high pressures in hydrous and anhydrous systems. The model reproduces the temperatures of the input anhydrous data base to within +/- 22-77^{o}C standard deviation with correlation coefficients ranging from 0.01 to 0.56. Their large experimental data base extends to alkali-rich basaltic compositions. Although this model covers more variables (e.g. pressure, H_2O etc.) than the other models and is built on very large anhyrous

Reproduced with permission of the copyright owner. Further reproduction prohibited without permission.

experimental data base, the following limitations of the model needed to be considered:

1) A large error is associated with temperature prediction. Consequently, the error associated with temperature prediction would propigate into calculations of melt-mineral equilibria (Ghiorso et al. 1983, Table 5).

2) The accesible mineral phases, olivine, plagioclase, and pyroxenes in the model do not extend into the composition space of alkalic rocks. This limitation is acknowledged by Ghiorso (1988) in SILMIN computer program of the model.

3) The high pressure and hydrous experimental data bases are rather limited.

In summary, no present model has succesfully predicted melt-mineral equilibria in alkali silicate composition space. The main reason for this is the fact that the proposed models are inevitably empirical in nature i.e., based on regression coefficients. These coefficients in turn are completely dependent upon the data base used in the regression analysis. Unsatisfactory results predicted by the model of Ghiorso et al. (1983), despite its large experimental data base,

Reproduced with permission of the copyright owner. Further reproduction prohibited without permission.

may indicate that the regular solution model is not applicable to the wide range of silicate melt compositions, at least in the binary symmetric form. In conclusion, no model has passed the ultimate test of "usefulness" in the prediction of melt-mineral equilibria observed in alkaline rocks.

Because thermodynamic solution models for liquids (melts) are presently not realistic enough to apply to naturally occuring melt-mineral equilibria, any attempt to model such equilibria is destined to be empirical. However, if the experimental data base used in empirical modeling is large enough and both the variables and the organization of variables in the empirical function sufficient enough to absorb non-ideality observed in melt-mineral reactions, then such models may be used: (1) to quantify the internal consistency of experimental data and (2) to predict phase equilibria in magmatic systems. With these goals in mind, my purpose is to establish a model for the quantitative analysis of low pressure anhydrous melt-mineral equilibria observed in tholeiitic and alkalic basalts.

Specifically my objectives are as follows:

(1) To show the internal consistency of basaltic experimental mineral-melt equilibrium data that were

Reproduced with permission of the copyright owner. Further reproduction prohibited without permission.

collected at different laboratories.

(2) To drive compositionally independent, internally consistent, empirical melt-mineral equilibrium equations from one atmosphere anhydrous experimental data on basaltic rocks ranging from alkali-rich to alkali-poor compositions.

(3) to incorporate these equations into a model to simulate equilibrium crystallization of basaltic rocks at low pressures under anhydrous conditions.

Reproduced with permission of the copyright owner. Further reproduction prohibited without permission.

2.2 METHODOLOGY

In order to express any chemical equilibria between melt and mineral phases in a given system, components representing all phases must be defined. As previously stated, due to lack of our understanding of short-range and long-range structural organizations of silicate melts, formulation of melt components is currently arbitrary. However, any postulated set of chemical components must cover the compositional range of interest and an internally consistent standard state thermodynamic data for these components must exist. The melt components that satisfy these conditions are given by Ghiorso et al. (1983,1985) and are used in this study (Table II.1). These stoichiometric units are identical or similar, in both structure and composition, to the mineral phases that coexist with basic melts. Indeed, the existence of such stoichiometric units is implied by X-ray radial-distribution analysis (Taylor and Brown, 1979). Mineral phases and their end-member components used for the modeling are listed in Table II.2. The choice of mineral phases is dictated by the phases that are present in the experimental data base with the exception of spinel.

Reproduced with permission of the copyright owner. Further reproduction prohibited without permission.

Table II.1. Conversion of moles of simple oxides into moles of adapted new melt components (n_i).

$n_1 = 0.25\ [nSiO_2 - 0.5(nFeO + nMnO + nMgO + nCaO) - nNa_2O - nK_2O]$

$n_2 = 0.25\ nTiO_2$

$n_3 = 0.375\ nAl_2O_3$

$n_4 = 0.375\ nCr_2O_3$

$n_5 = 0.375\ nFe_2O_3$

$n_6 = 0.25\ nFeO$

$n_7 = 0.25\ nMnO$

$n_8 = 0.25\ nMgO$

$n_9 = 0.25\ nCaO$

$n_{10} = 0.375\ nNa_2O$

$n_{11} = 0.375\ nK_2O$

$n_{12} = 0.625\ nP_2O_5$

Chemical formulae of new melt components:

1= Si_4O_8
2= Ti_4O_8
3= $Al_{16/3}O_8$
4= $Cr_{16/3}O_8$
5= $Fe_{16/3}O_8$
6= $Fe_4Si_2O_8$
7= $Mn_4Si_2O_8$
8= $Mg_4Si_2O_8$
9= $Ca_4Si_2O_8$
10= $Na_{16/3}Si_{8/3}O_8$
11= $K_{16/3}Si_{8/3}O_8$
12= $P_{16/5}O_8$

* After Ghiorso et al. (1983)

Reproduced with permission of the copyright owner. Further reproduction prohibited without permission.

Table II.2. Modeled minerals and end-member components.

MINERAL		END-MEMBER COMPONENTS		CHEMICAL FORMULA
OLIVINE	(OL)	Forsterite	(Fo)	Mg_2SiO_4
		Fayalite	(Fa)	Fe_2SiO_4
CLINOPYROXENE	(CPX)	Clino-enstatite	(Cen)	$Mg_2Si_2O_6$
		Clino-ferrosilite	(Cfs)	$Fe_2Si_2O_6$
		Diopside	(Di)	$CaMgSi_2O_6$
ORTHOPYROXENE	(OPX)	Ortho-enstatite	(Oen)	$MgSiO_3$
		Ortho-ferrosilite	(Ofs)	$FeSiO_3$
PLAGIOCLASE	(PL)	Anorthite	(An)	$CaAl_2Si_2O_8$
		Albite	(Ab)	$NaAlSi_3O_8$
		Sanidine	(Sn)	$KAlSi_3O_8$
NEPHELINE	(NE)	Nepheline	(Ne)	$NaAlSiO_4$
		Kalsilite	(Ks)	$KAlSiO_4$
LEUCITE	(LC)	Dehydrated Analcime	(Da)	$NaAlSiO_6$
		Leucite	(Le)	$KAlSiO_6$

Reproduced with permission of the copyright owner. Further reproduction prohibited without permission.

2.2.1 Thermodynamics of a Chemical Reaction

The equilibrium condition for coexisting mineral and melt phases in a solution can be expressed by writing chemical reactions between components of the mineral phase and components of the melt phase.

If the products and the reactants of a reaction are in chemical equilibrium, then the equilibrium condition can be expressed as:

$$(1) \qquad \sum_{i=1}^{nr} c_i \ \mu^{p}_{i,P,T} = 0$$

where nr is the number of components in the reaction and c_i is the stoichiometric coefficient of component i in the reaction (c_i is positive for products and negative for reactants). $\mu^{p}_{i,P,T}$ is the chemical potential of component i in phase p ,at pressure (P) and temperature (T) of equilibrium.

By definition, the chemical potential of the ith component in phase p is :

$$(2) \qquad \mu^{p}_{i,P,T} = \mu^{o,p}_{i,Pr,Tr} + RT\ln a^{p}_{i} \quad \text{or}$$

Reproduced with permission of the copyright owner. Further reproduction prohibited without permission.

$$\mu^{p}_{i,P,T} = G^{o,p}_{i,Pr,Tr} + RT\ln a^{p}_{i} \quad (3)$$

$\mu^{o,p}_{i,Pr,Tr}$ equals $G^{o,p}_{i,Pr,Tr}$ and is the chemical potential (μ) or the molal Gibbs free energy of formation (G) of the pure component i in phase p from its elements at standard state pressure (Pr) and temperature (Tr). R is the universal gas constant. a_i is the activity of the ith component in phase p, defined as:

$$a^{p}_{i} = X^{p}_{i} * \gamma^{p}_{i} \quad (4)$$

where X^{p}_{i} and γ^{p}_{i} are the mole fraction and the activity coefficient respectively, of the ith component in phase p.

The standard state for phases adopted in this study is one in which the activities of the components of pure (stoichiometric) phases are unity at any pressure and temperature. Therefore Tr=T and Pr=P, where T and P stand for equilibrium temperature and pressure, respectively.

Applying this standard state, substituting eq. (3) into equation (1), and rearranging, the equilibrium

Reproduced with permission of the copyright owner. Further reproduction prohibited without permission.

condition for a given reaction can be expressed as:

$$(5) \qquad \Delta G^{o}_{r,P,T} = -RT\ln \prod_{i=1}^{nr} a_i^{c} \quad .$$

$\Delta G^{o}_{r,P,T}$ is the Gibbs free energy change for the reaction involving pure components of melt and mineral phases at P and T. $\prod_{i=1}^{nr} a_i$ is the product of the activities of the components in the reaction each raised to its stoichiometric reaction coefficient (c is negative for reactants and positive for products). $\Delta G^{o}_{r,P,T}$ for a reaction between the components of melt and mineral phases is expressed as:

$$(6) \qquad \Delta G^{o}_{r,P,T} = c_i[G^{o,mineral}_{i,f,P,T}] - \sum_{i=1}^{nm} c_i[G^{o,melt}_{i,f,P,T}]$$

where nm is the number of melt components needed to balance a given reaction and c_i=1 for mineral components. $G^{o}_{i,f,P,T}$ is the apparent standard molal Gibbs free energy of formation of ith component from its elements at a given pressure and temperature in superscripted phase. Detailed equations to evaluate $G^{o}_{i,f,P,T}$ are given in Appendix II.A. Using equations (4), (5), and (6), the chemical equilibrium between mineral and melt phase

Reproduced with permission of the copyright owner. Further reproduction prohibited without permission.

components can be expressed as:

$$(7) \quad \Delta G^{o}_{r,P,T} = \sum_{i=1}^{nm} c_i[RT\ln(X_i^{melt} * \gamma_i)] - [RT\ln a_i^{mineral}]$$

Evaluation of the right hand side of equation (7) requires formulation of the excess Gibbs free energies (G_{ex}) for both melt and mineral (solid) phases. There have been numbers of studies to formulate G_{ex} of mineral solutions found in magmatic systems (for summary see Ganguly and Saxena, 1987). Nevertheless, either due to limitations in various models or due to lack of enough experimental data, or both these formulations do not yield satisfactory results. For example, the most current, comprehensive models for olivine, clinopyroxene, and orthopyroxene solid solutions are those developed by Davidson and Lindlsey (1985,1989). Recently Sack and Ghiorso (1989) showed that Davidson and Lindsley's models cannot correctly reproduce the non-ideality observed in and among these phases (but Sack and Ghiorso (1989) did not themselves formulate a model that did). Sack and Ghiorso argued that any formulation for clinopyroxene and orhopyroxene will not be complete unless Al^{+3} and Fe^{+3} are included in models of these phases. Furthermore, there is not any comprehensive G_{ex}

Reproduced with permission of the copyright owner. Further reproduction prohibited without permission.

formulation at all for nepheline and leucite.

In light of existing G_{ex} formulations for minerals, I have adapted activities based on ideal solution models. These formulations are given in Appendix II.B. The excess Gibbs energies of the reactions (non-ideality of the reactions) are then empirically modeled as a function of melt composition, temperature, and oxygen fugacity (f_{O2}).

In order to formulate excess energies of reactions (REX) empirically, linear correlations between REX and temperature have initially been established using coexisting mineral and melt phases equilibriated at a known temperature and pressure, and from given standard state thermodynamic properties of the components in the reaction. Because temperature in this correlation is both the dependent and the independent variable due to temperature dependence of standard state data, this correlation has been interpolated to the mole fraction of melt components and oxygen fugacity using the modified form of the ferric-ferrous equilibria equation of Sack et al.(1980). The following empirical formulation of REX is then applied to the melt-mineral equilibria:

Reproduced with permission of the copyright owner. Further reproduction prohibited without permission.

$$(8)\quad REX=C_1+T\{C_2+C_3[C_4 lnf_{O2}+ln(X_{FeO}/X_{Fe2O3})+(\sum_{i=1}^{n}\frac{CN_i*X_i}{CD_i*X_i}+CN13)]\}$$

where,

X_i= Mole fraction of ith melt component,

n=Number of melt components (=12),

T=Equilibrium temperature in degrees Kelvin, and

C_i, CN_i,CD_i are the reaction excess energy coefficients to be regressed. From equations (7) and (8),

$$(9)\quad \overset{o}{\Delta G}_{r,P,T} - \sum_{i=1}^{nm} c_i[RTlnX_i^{melt}] + [RTlna_i^{mineral}] =$$

$$C_1+T\{C_2+C_3[C_4 lnf_{O2}+ln(X_{FeO}/X_{Fe2O3})+(\sum_{i=1}^{n}\frac{CN_i*X_i}{CD_i*X_i}+CN13)]\}\ .$$

Note that, there are as many equation (9) as the number of mineral components in the model. Modeled melt-mineral reactions are given in Table II.C1. The quantities on the left hand side of equation (9) can be calculated from the compositions of coexisting mineral and melt phases equilibriated at a known temperature and pressure and from given standard state chemical potential properties

Reproduced with permission of the copyright owner. Further reproduction prohibited without permission.

of the components in the reaction. Standard state thermodynamic properties of the end member components of minerals and the melt components are listed in Table II.A1 and II.A2, respectively. The unknowns in equation (9) then reduce to REX coefficients. The values of these coefficients may be determined using large numbers of equilibrium melting and crystal growth experiments that cover the entire compositional range of interest. Because each melt-mineral experimental data will result in a statement in the form of equation (9), values of the REX coefficients become overdetermined, but by using a least square numerical procedure, the values of the REX coefficients may be approximated.

References for the experimental data base and the number of melt-mineral statements applied to equation (9) are listed in Table II.3 (the data base will be referred to repeatedly below). Rock names for the starting bulk compositions in the experiments also are given in Table II.3. The experimental data base is limited to experiments that were performed under controlled oxygen fugacity defined by the QFM oxygen buffer. All experimental results are accepted and used in the regression analysis. Regressed values of the REX coefficients are listed in Table II.C2.

Reproduced with permission of the copyright owner. Further reproduction prohibited without permission.

Table II.3. References for the experimental data base and the number of melt-mineral statements.

Reference	OL	CPX	OPX	PL	NE	LC
Gee and Sack 1988 (1)	-	-	-	-	9	18
Grove et. al. 1982 (2)	28	14	6	41	-	-
Sack et. al. 1987 (3)	66	37	-	45	2	19
Walker et. al. 1979 (4)	8	10	-	14	-	-
Total	102	61	6	100	11	37

Starting bulk compositions in the experiments are represented by the following rock names:

(1) Melilite Nephelinite

(2) Basaltic Andesite

(3) Basanite, Minette, Leucite Basanite, Leucitite, Basanite-Tephrite, Olivine Basalt, Tholeiite, Olivine-Andesite, Alkali Olivine Basalt, Trachybasalt, High-Alumina Basalt

(4) Tholeiite

Reproduced with permission of the copyright owner. Further reproduction prohibited without permission.

2.3 INTERNAL CONSISTENCY OF THE MODEL

Using regressed REX coefficients on the right hand side of equation (9), four sets of calculations outlined below have been carried out with the experimental data base in order to check the internal consistency of the model. These calculations are detailed below.

1) For given values of f_{O2} and melt and mineral compositions, the temperature of melt-mineral equilibrium was calculated using both component reactions separately and together in a given mineral. For example, for olivine-melt equilibria, forsterite-melt and fayalite-melt reactions were initially used independently to calculate the equilibrium temperature. Then, these two reactions were combined as one equation (under equilibrium conditions, both equations must be equal to zero) and solved for temperature and the result reported as olivine. All of my calculated results were then compared with experimental temperatures: the sum of the absolute values of residuals divided by the total number of cases is reported as average deviation in Table II.4. The overall average deviation of these calculations is about +/- $1^{o}K$ (column a in Table II.4).

Reproduced with permission of the copyright owner. Further reproduction prohibited without permission.

Table II.4: Results of internal consistency calculations using regressed REX coefficients given in Table II.C2.

	Average deviations (+/-)				
	a	b		c	c'
	$T(^oK)$	$X^{mineral}$	$[X^{mineral}$,	$T(^oK)]$	Correl.
Forsterite	1.02	0.03	0.02		0.95
Fayalite	2.21	0.02	0.02		0.95
OLIVINE	0.79			0.65	0.99
C-enstatite	2.66	0.03	0.03		0.40
C-ferrosilite	2.58	0.02	0.02		0.40
Diopside	0.73	0.04	0.03		
CLINOPYROXENE	1.23			0.42	0.99
Enstatite	0.19	0.01	0.009		0.96
Ferrosilite	0.40	0.008	0.009		0.96
ORTHOPYROXENE	0.08			0.05	1.00
Anorthite	0.20	0.03	0.03		0.85
Albite	0.94	0.03	0.03		0.85
Sanidine	2.55	0.005	0.004		
PLAGIOCLASE	0.86			0.10	1.00
Nepheline	0.33	0.03	0.03		0.50
Kalsilite	1.47	0.04	0.03		0.50
NEPHELINE	0.65			0.27	0.99
Leucite	0.33	0.05	0.01		0.48
Dehyd. Analc.	0.88	0.01	0.01		0.48
LEUCITE	0.39			0.30	1.00

Reproduced with permission of the copyright owner. Further reproduction prohibited without permission.

2) For given values of f_{O2}, experimental temperature, and melt composition, the mole fractions of mineral components were calculated by simultaneously solving end-member component reactions of a given mineral. These results were then compared with experimental mole fraction and the overall average deviation of these calculations is about +/- 0.025 (column b in Table II.4).

3) For given values of melt composition and f_{O2}, both the equilibrium temperature and the mole fractions of mineral components were calculated by simultaneously solving end-member component reactions of a given mineral. In these calculations one of the mole fractions of a set of mineral components is written in terms of the other(s) (the sum of mole fractions of components in a phase is equal to one). These results were then also compared with experimental temperatures and mole fractions: the overall average deviation for temperature is about +/- 0.3 and for mole fraction of mineral components is about +/- 0.02 (column c in Table II.4). Predicted versus experimental data correlations for these calculations are listed in column c' in Table II.4. Predicted versus experimental temperatures and mole fractions of mineral components are plotted in Figure II.1 and Figure II.2, respectively. In both

Reproduced with permission of the copyright owner. Further reproduction prohibited without permission.

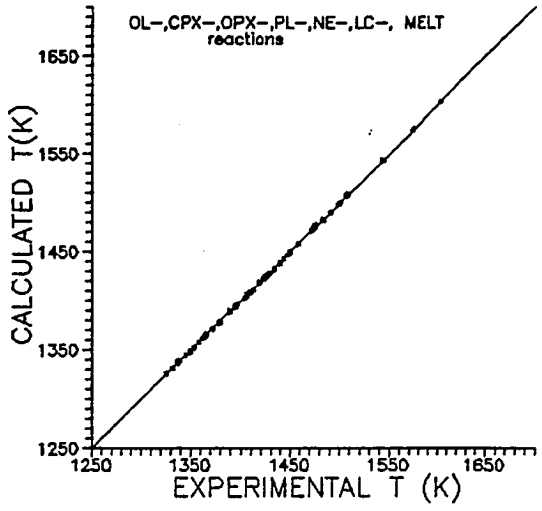

Figure II.1. Plot of calculated versus experimental temperature results. Correlation=0.99.

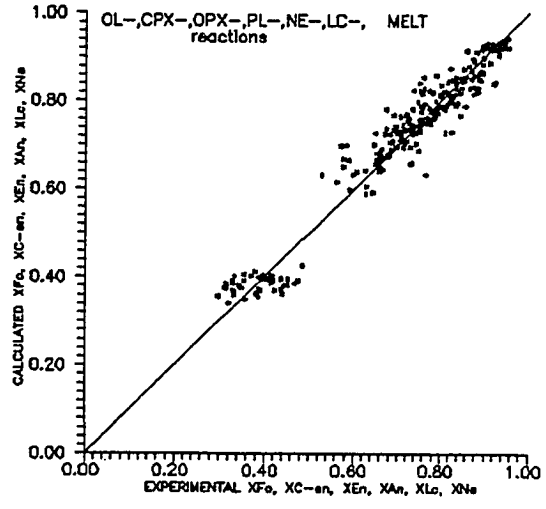

Figure II.2. Plot of calculated versus experimental mole fraction results. Correlation=0.98.
Temperatures and mole fractions are calculated for given values of melt composition and f_{O2} (procedure #3 in text).
OL=olivine, CPX=clinopyroxene, OPX=orthopyroxene, PL=plagioclase, NE=nepheline, LC=leucite. XFo=mole fraction of forsterite, XC-en=mole fraction of clinoenstatite, XEn= mole fraction of enstatite, XAn= mole fraction of anorthite, XNe=mole fraction of nepheline, XLc=mole fraction of leucite.

Reproduced with permission of the copyright owner. Further reproduction prohibited without permission.

figures, data from equilibria involving different reactions have been combined into one comprehensive plot. In both figures, 100% correlation is shown by the solid line. The calculated overall correlation for the data in Fig. II.1 and Fig. II.2 is 0.99 and 0.98, respectively. Most of the scatter in Fig. II.2 is caused by anorthite and clino-enstatite points. Figure II.3 shows predicted versus calculated mole fractions of the mineral components without anorthite and clino-enstatite points.

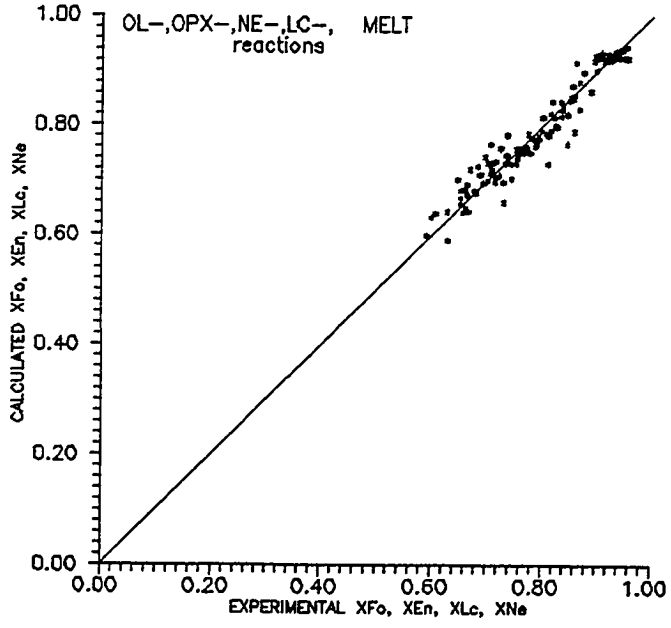

Figure II.3. Plot of calculated versus experimental mole fraction of forsterite, enstatite, leucite, and nepheline.

Reproduced with permission of the copyright owner. Further reproduction prohibited without permission.

4) For given values of bulk composition, temperature, and f_{O2}, the compositions of coexisting melt and mineral phases, and their proportions, have been calculated for a system open to oxygen (equilibrium crystallization calculations). These multiple saturation calculations were carried out for the bulk compositions listed below (Sack et al., 1987), not for the entire experimental data base.

Rock name	Sample I.D.	Temperature
Alkali Olivine Basalt	(CSQ-3)	1121 and 1092.5°C
Leucite Basanite	(94-08)	1116 and 1133°C
Olivine Basalt	(SSC-2)	1116 and 1092.5°C
Olivine Basalt	(SSC-1)	1121°C
Basanite Tephrite	(K-15)	1092.5°C
Basanite Tephrite	(K-14)	1116°C
Basanite	(BS-501)	1116 and 1092.5°C
Trachybasalt	(TB-253)	1133°C
Leucite Basanite	(9418)	1133°C
High-Alumina Basalt	(HC-63)	1137°C

The results of these calculations and the applied numerical programming procedure are given in Appendix II.D. Average deviations of the calculated melt

Reproduced with permission of the copyright owner. Further reproduction prohibited without permission.

compositions in terms of wt% of oxides are (+/-): SiO_2=1.4; Al_2O_3=1.2; Fe_2O_3=0.3; FeO=1.5; MgO=1.1; CaO=1.2; Na_2O=0.5; and K_2O=1.0. The multiply saturated melt compositions calculated in these computations were recast into diopside, forsterite, and nepheline normative components of Sack et al. (1987) and plotted on a ternary diagram (Figure II.4). It should be noted that with the exception of a few points, all my calculated compositions plot on or near Sack et al.'s (1987) experimentally determined FO+DI+PL+/-SP cotectic (dashed line). A logarithmic best fit line (solid line in Figure II.4), drawn using the calculated data points only, is in close agreement with Sack et al.'s (1987) best fit line determined using experimental data (dashed line).

In summary, all four sets of calculations to check the internal consistency of my model have given good results. Based on these calculations, therefore, I can conclude that the model I have developed is internally consistent.

Reproduced with permission of the copyright owner. Further reproduction prohibited without permission.

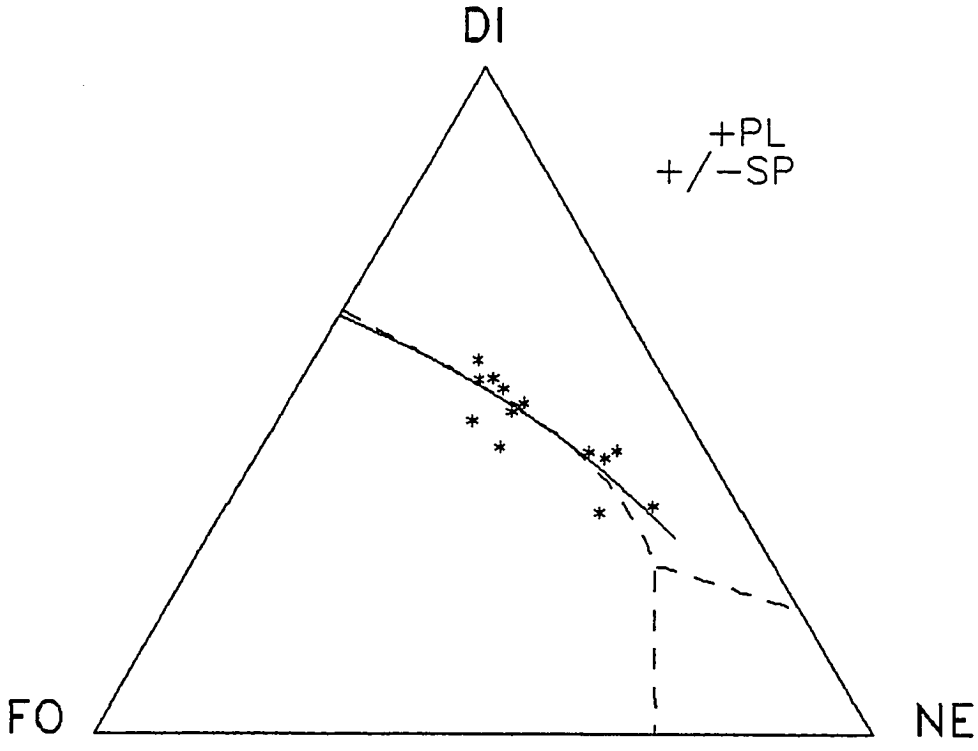

Figure II.4. Plot of calculated (solid line) versus experimental (dashed line from Sack et al. 1987) one atmosphere olivine, high-Ca pyroxene, plagioclase cotectic for alkalic basalts. Normative mineral calculation procedure is given in the caption of Figure 5 of Sack et al. 1987. Stars represent calculated melt compositions saturated with olivine, pyroxene, plagioclase, and +/- leucite.

Reproduced with permission of the copyright owner. Further reproduction prohibited without permission.

2.4 APPLICATION OF REX COEFFICIENTS TO NEW DATA

The validity of my general model -equations- was checked using data that was not incorporated into the regression of the model REX coefficients. For this purpose, I have used my own experimental data base listed in Appendix I.A. My data base inludes 49 olivine-melt, 36 clinopyroxene-melt, 12 plagioclase-melt, and 14 leucite-melt equilibrium statements. Ferric and ferrous iron concentrations in the data base were calculated from total iron using the equation of Sack et al. (1980).

Calculations 1, 2, and 3 that were explained in the previous section were also carried out for my experimental data:

1) For given values of f_{O2} and melt and mineral compositions, the temperature of melt-mineral equilibrium was calculated using both the component reactions separately and together in a given mineral. The overall average deviation of these calculations is about +/- 1.7 ^{o}K (column a in Table II.5).

2) For given values of f_{O2}, experimental temperature, and melt composition, the mole fractions of mineral components were calculated by simultaneously solving end-member component reactions of a given mineral and then

Reproduced with permission of the copyright owner. Further reproduction prohibited without permission.

Table II.5. Results of application calculations using regressed REX coefficients given in Table II.C2.

	Average deviations (+/-)				
	a	b	c		c'
	$T(^oK)$	$X^{mineral}$	$[X^{mineral}, T(^oK)]$		Correl.
Forsterite	1.93	0.07	0.03		0.90
Fayalite	2.12	0.02	0.03		0.90
OLIVINE	0.84			1.24	0.99
C-enstatite	2.60	0.06	0.03		0.27
C-ferrosilite	3.20	0.09	0.04		0.27
Diopside	1.20	0.11	0.03		
CLINOPYROXENE	2.16			0.55	0.99
Anorthite	0.60	0.09	0.08		0.99
Albite	2.85	0.07	0.09		0.99
Sanidine	2.70	0.01	0.09		
PLAGIOCLASE	0.68			0.28	1.00
Leucite	0.67	0.10	0.01		0.89
Dehyd. Analc.	1.22	0.009	0.01		0.89
LEUCITE	0.42			0.60	0.99

Reproduced with permission of the copyright owner. Further reproduction prohibited without permission.

compared with experimental mole fractions. The overall average deviation of these calculations is about +/- 0.06 (column b in Table II.5).

3) For given values of melt composition and f_{O2}, both the equilibrium temperature and the mole fractions of mineral components were calculated by simultaneously solving end-member component reactions of a given mineral and then compared with the experimental temperature and the mole fractions. Predicted versus experimental data correlations for these calculations are listed in column c' in Table II.5. The overall average deviation for temperature is about +/- 0.7 and for mole fractions of mineral components is about +/- 0.04 (column c in Table II.5). Predicted versus experimental temperatures and mole fractions of mineral components also are plotted in Figure II.5 and Figure II.6, respectively. In these figures 100% correlation is shown by the solid line. The calculated overall correlations for the data in Figure II.5 and Figure II.6 are 1.00 and 0.98, respectively.

Reproduced with permission of the copyright owner. Further reproduction prohibited without permission.

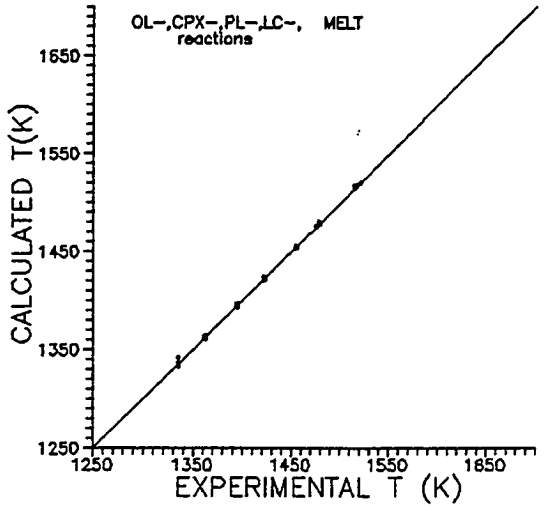

Figure II.5. Plot of calculated versus experimental temperature results using experimental data from this study. Correlation=1.00.

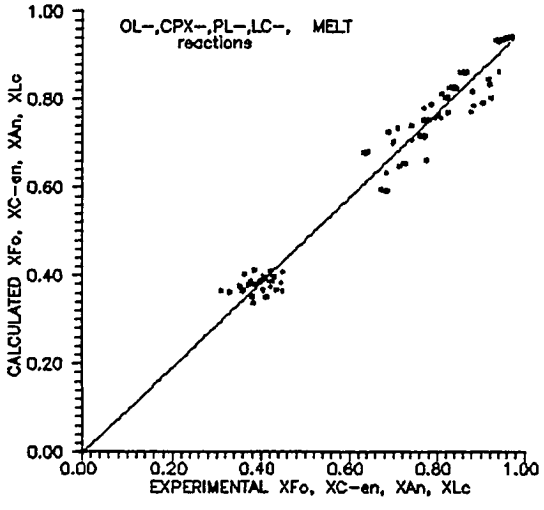

Figure II.6. Plot of calculated versus experimental mole fraction results using experimental data from this study. Correlation=0.98.

Temperatures and mole fractions are calculated for given values of melt composition and f_{O2} (procedure #3 in text). Abbreviations are the same as given in the caption of Figure II.2.

Reproduced with permission of the copyright owner. Further reproduction prohibited without permission.

2.5 DISCUSSION OF THE MODEL

The model is successful in the prediction of melt-mineral equilibria observed in basaltic rocks. Although the predictions of mole fractions of mineral components are not as good as temperature predictions, they are better than the predictions from currently available models.

There are many applications of the model. In the previous sections, I have only performed equilibrium crystallization calculations and have shown that the model can accurately predict mineral and melt compositions. Equilibrium crystallization calculations are, in fact, the fundamental computations to evaluate fractional crystallization, mixing, and assimilation processes that can take place in a magma chamber, and understanding these processes can ultimately be used to establish the physical and the thermochemical history of a magma chamber. One of the advantages of my model over others is that it includes f_{O2} as an additional variable which can be used to evaluate equilibrium relations between the melt and mineral phases under varying f_{O2} conditions. It is, however, possible to eliminate this variable in the reaction equations by substituting a desired temperature-dependent oxygen fugacity buffer

Reproduced with permission of the copyright owner. Further reproduction prohibited without permission.

equation.

Finally, one might argue that any realistic formulation of melt-mineral equilibria should include the non-ideality of mineral solutions. I would like to report that, in my earlier attempts to develop a model, I have used Davidson and Lindsley's (1989) non-ideal clinopyroxene, orthopyroxene, and olivine model; and Newton and Haselton's (1981) non-ideal plagioclase model, and have regressed the REX coefficients. An internal consistency check with these formulations actually gave better results (e.g. the average deviation on mole fractions of olivine components is about +/- 0.001). However, after carefully examining Sack and Ghiorso 's (1989) results, I have decided that it is better to built a model on constraints that are well established. With this decision, of course, I had hoped that the REX coefficients would include the non-ideality present in a reaction. Internal and external data applications of the model show that any non-ideality of melt-mineral reaction has indeed reasonably included by these coefficients.

As a final note, it should be remembered that all the computations were carried out for the melt and mineral phases in a composition space that is covered by the experimental data base used in the regression of the

Reproduced with permission of the copyright owner. Further reproduction prohibited without permission.

REX coefficients. Because this data set ranges in bulk compositions from andesitic basalt to leucite basanite, the model should be applicable in this range of composition space (covering the compositions set forth in the introduction). In addition, the model is compositionally independent within this wide ranging composition space.

Reproduced with permission of the copyright owner. Further reproduction prohibited without permission.

2.6 MELT-MINERAL GEOTHERMOMETERS

Although the equations that were developed in the previous sections could make excellent melt-mineral geothermometers, the application of these equations as geothermometers requires that ferric and ferrous iron concentrations in the melt phase be known. However, ferric and ferrous iron concentrations cannot be directly determined by electron microprobe analysis which is extensively used to determine the compositions of coexisting melt and mineral phases in a lava. Therefore, in order to calculate the equilibrium temperature of coexisting melt and mineral phases, different set of reaction excess energy coefficients were calibrated as a function of temperature and f_{O2}. These coefficients are abbreviated here as GREX coefficients. The formulation for GREX is derived from the previously determined correlation between temperature and excess energies of reactions and from the correlation between temperature and oxygen fugacity:

(10) $$GREX=CG_1+T[CG_2+CG_3 \ln f_{O2}]$$

where

CG_1, CG_2, and CG_3 are the GREX coefficients for the different melt-mineral geothermometers. Using the same

Reproduced with permission of the copyright owner. Further reproduction prohibited without permission.

Table II.6. Regressed melt-mineral geothermometer (GREX) coefficients.

	CG_1	CG_2	CG_3
R1	-518350	207.05799	-7.21243
R2	-352370	129.45328	-5.58287
R3	-739482	312.98160	-9.39285
R4	-569468	241.99766	-7.44094
R5	-767390	322.64211	-9.82254
R6	-369921	121.10167	-6.39422
R7	-284734	87.47372	-5.28286
R8	-1013700	396.19365	-14.16174
R9	-938700	353.41560	-13.83726
R10	-943919	342.92182	-14.27480
R11	-500241	204.72758	-6.49531
R12	-509408	199.06909	-6.79166
R13	-728830	297.86964	-9.48779
R14	-714678	286.13694	-9.58381

Reproduced with permission of the copyright owner. Further reproduction prohibited without permission.

experimental data base (Table II.3) and melt-mineral reactions (Table II.C1) discussed previously, the GREX coefficients are calibrated and listed in Table II.6.

For given values of f_{O2} and melt and mineral compositions (in experimental data base), the temperature of melt-mineral equilibrium was calculated both using the component reactions separately and together in a given mineral. Average absolute values of calculated minus experimental temperatures are reported as average deviations in Table II.7. The overall average deviation is about +/- 4.2°K. The correlation between the calculated and the experimental temperature for a given mineral is also listed in Table II.7. In these calculations, the total iron concentration in melts is assumed to be ferrous iron. Predicted versus experimental temperatures are shown in Figure II.7.

The calibrated GREX coefficients were used to reproduce the temperatures of my experimental data reported in Appendix I.A (data that was not included in the derivation of the GREX coefficients). Calculated versus experimental temperature correlations and the average deviations determined in these applications are listed in Table II.8. In these calculations, the total iron concentration in melts is assumed to be ferrous iron.

Reproduced with permission of the copyright owner. Further reproduction prohibited without permission.

Table II.7. Results of temperature calculations using regressed geothermometer coefficients (GREX) given given in Table II.6.

	Average deviations (+/-) T (^{o}K)	correlation
Forsterite	4.9	
Fayalite	5.8	
OLIVINE	5.0	0.99
Clino-enstatite	6.1	
Clino-ferrosilite	6.6	
Diopside	5.2	
CINOPYROXENE	5.5	0.97
Ortho-enstatite	2.5	
Ortho-ferrosilite	2.8	
ORTHOPYROXENE	2.6	0.99
Anorthite	5.3	
Albite	5.6	
Sanidine	5.7	
PLAGIOCLASE	5.4	0.98
Nepheline	1.4	
Kalsilite	2.3	
NEPHELINE	1.6	0.99
Leucite	3.5	
Dehyd. Analcime	3.7	
LEUCITE	3.6	0.99
OVERALL		0.99

Reproduced with permission of the copyright owner. Further reproduction prohibited without permission.

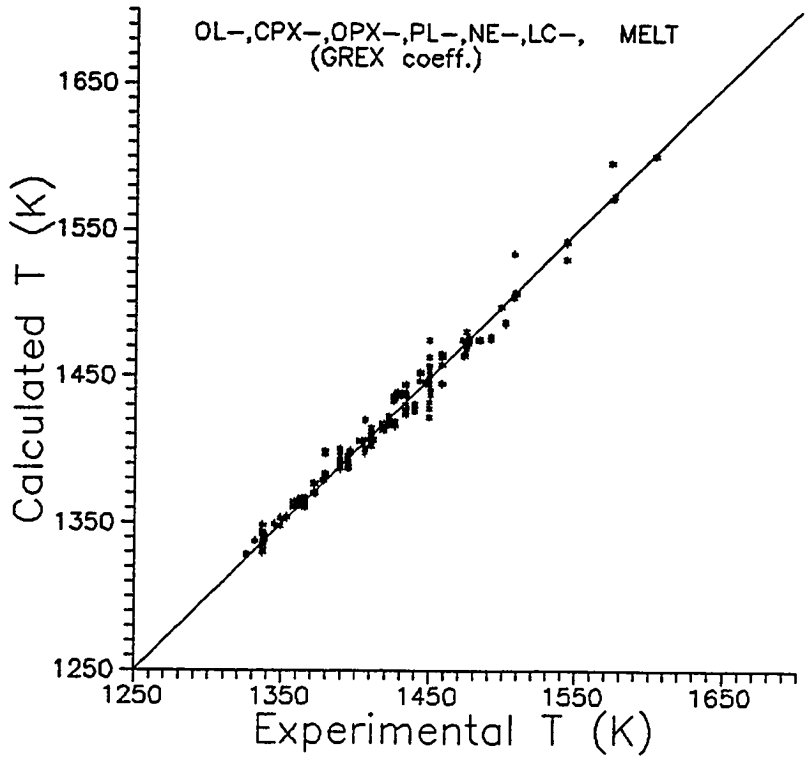

Figure II.7. Plot of calculated versus experimental temperature results using regressed geothermometer coefficients given in Table II.6. Abbreviations are the same as those given in the caption of Figure II.2.

Finally, in order to constrain the f_{O2} sensitivity of the calculated temperatures, several calculations on different mineral and melt compositions have been carried out using each geothermometer equation seperately. These calculations indicated that +/- 0.3 miscalculation of $\ln f_{O2}$ would shift the calculated equilibrium temperature about +/- 6°C.

Reproduced with permission of the copyright owner. Further reproduction prohibited without permission.

Table II.8. Results of application temperature calculations using regressed geothermometer coefficients (GREX) given in Table II.6.

	Average deviations	
	(+/-) T (^{o}K)	correlation
Forsterite	3.20	
Fayalite	1.60	
OLIVINE	1.49	0.99
Clino-enstatite	6.69	
Clino-ferrosilite	9.26	
Diopside	3.82	
CINOPYROXENE	6.05	0.99
Anorthite	1.66	
Albite	4.98	
Sanidine	1.38	
PLAGIOCLASE	2.09	0.99
Leucite	1.48	
Dehyd. Analcime	2.89	
LEUCITE	2.18	0.99
OVERALL		0.99

Reproduced with permission of the copyright owner. Further reproduction prohibited without permission.

For an initial application the derived melt-mineral geothermometers can be used to determine the equilibrium temperature of coexisting melt and mineral phases assuming that total iron of the melt is ferrous iron at a given f_{O2}. This calculation can also be performed by substituting any temperature dependent oxygen buffer equation in place of f_{O2}. The calculated temperature, in turn can be used to estimate ferric and ferrous iron concentrations in a melt using the equations of Sack et al. (1980) or Kilinc et al. (1983). On the other hand, if the equilibrium temperature is fixed, one can calculate f_{O2} using coexisting melt and mineral phases and can evaluate change of f_{O2} (if any) in a magma as a function of melt and mineral compositions.

Geoscientists trying to understand the fluid dynamics behaviour of magma chambers are currently applying previously established empirical relations to determine the change in density and viscosity of a magma as a function of temperature (for example, Sparks et al., 1984). However, the error in estimating temperature with these empirical relations ranges up to +/- 50^{o}C (e.g. Roeder and Emslie, 1970). The geothermometers developed here can be used for far more accurate results.

Other applications of the derived melt-mineral

Reproduced with permission of the copyright owner. Further reproduction prohibited without permission.

geothermometers are numerous. Finally, I would like to point out that in any application, one has to be aware that the calculated temperature is a function of f_{O2} (equation 10) and therefore, several calculations at different f_{O2} should be done to evaluate the sensitivity of calculated temperatures as a function of f_{O2} for a given melt and mineral compositions. It should also be remembered that these geothermometers have been derived using an experimental data base that covers f_{O2} values defined by the QFM oxygen buffer only.

Reproduced with permission of the copyright owner. Further reproduction prohibited without permission.

REFERENCES

Baker, P.E., Gass, I.G., Harris, P.G., and Le Maitre R. W., 1964, The volcanological report of the Royal Society expedition to Tristan da Cunha; Philos. Trans. R. Soc. London Ser. A., v.256, p.439-578.

Baldridge, W., Carmichael, I.S.E., and Albee, A.L., 1981, Crystallization paths of leucite-bearing lavas: examples from Italy; Cont. Min. Pet., v.76, p.321-335.

Berman, R.G. and Brown, T.H., 1984, A thermodynamic model for multicomponent melts, with application to the system $CaO-Al_2O_3-SiO_2$; Geochim. Cosmochim. Acta, v. 48, p.661-678.

Beswick, A.E. and Carmichael, I.S.E., 1978, Constraints on Mantle source compositions imposed by phosphorus and rare-earth elements;Cont. Min. Pet., v.67, p.317 -330.

Bottinga, Y., Weill, D.F., and Richet, P., 1981, Thermodynamic modelling of silicate melts; in Thermo -dynamics of Minerals and Melts, Newton, R.C., Navrotsky, A., and Wood, B.J. (eds.), p.207-245. Springer press.

Bottinga, Y. and Richet, P., 1978, Thermodynamics of liquid silicates, a preliminary report;Earth Planet. Sci. Lett., v.40, p.382-400.

Bottinga, Y. and Weill, D.F., 1972, The viscosity of magmatic silicate liquids: a model calculation; Am. J. Sci., v.272, p.438-475.

Brown, F.H. and Carmichael, I.S.E., 1969, Quaternary volcanoes of the Lake Rudolf region:1. The basanite -tephrite series of the Korath Range;Lithos, v.2, p. 239-260.

Burnham, C.W., 1979a, The importance of volatile constituents; in The Evolution of the Igneous Rocks, 50 th Anniversary Perspectives, p.439-478. Princeton University press.

Burnham, C.W., 1975, Water and magmas: a mixing model; Geochim. Cosmochim. Acta, v.39, p.1077-1084.

Reproduced with permission of the copyright owner. Further reproduction prohibited without permission.

B.V.S.P., 1981, Experimental petrology of basalts and their source rocks; in Basaltic Volcanism on the Terrestrial Planets, p. 494-630. Pergamon press.

Cundari, A., 1973, Petrology of the leucite-bearing lavas in New South Wales; J. Geol. Soc. Australia, v.20, p.465-492.

Cundari, A. and Mattias, P.P., 1974, Evolution of the Vico Lavas, Roman Volcanic Region, Italy; Bull. Volcan., v.38, p.98-114.

Davidson, P.M. and Lindsley, D.H., 1989, Thermodynamic analysis of pyroxene-olivine-quartz equilibria in the system CaO-MgO-FeO-SiO_2; Am. Miner., v.74, p.18-30.

Davidson, P.M. and Lindsley, D.H., 1985, Thermodynamic analysis of quadrilateral pyroxenes part II: Model calibration from experiments and applications to geothermometry;Cont. Min. Pet., v.91, p.390-404.

Denies, P., Nafziger, R.H., Ulmer, G.C., and Woermann, E., 1974, Temperature-Oxygen Fugacity Tables for Selected Gas Mixtures in the System C-H-O at One Atmosphere Total Pressure; Bull. Earth Min. Sci. Exper. Sta., no.88, 129 p. Penn State Univ. press.

Drake, M.J., 1976b, Plagioclase-melt equilibria; Geochim. Cosmochim. Acta, v.40, p.457-466.

Edgar, A.D., 1973, Experimental Petrology, 217 p. Oxford Press.

Ferguson, A.K. and Cundari, A., 1975, Petrological aspects and evolution of the leucite-bearing lavas from Bufumbira, South West Uganda; Cont. Min. Pet.,v. 50, p.25-46.

Fudali, R.F., 1963, Experimental studies bearing on the origin of pseudoleucite and associated problems of alkalic rock systems;Geol. Soc. Amer. Bull., v.74, p. 1101-1126.

Ganguly, J. and Saxena, S.K., 1987, Mixtures and Mineral Reactions, 291 p. Springer-Verlag press.

Ganguly, J., 1982, Mg-Fe order-disorder of ferro-magnesian silicates; in Ad. in phys. geochemistry, Saxena, S.K. (ed.), v.2, p.58-99. Springer press.

Reproduced with permission of the copyright owner. Further reproduction prohibited without permission.

Gee, L.L. and Sack, R.O., 1988, Experimental petrology of of melilite nephelinites;J. Petrol., v.29, p. 1233-1255.

Ghiorso, M.S. and Carmichael, I.S.E., 1987, Modeling magmatic systems: Petrologic applications; in Thermodynamic Modeling of Geologic Materials, Carmichael, I.S.E. and Eugster H.P. (eds.): Rev. Miner., v.17, p.467-499.

Ghiorso, M.S., 1985, Chemical mass transfer in magmatic processes:I. Thermodynamic relations and numerical algorithms;Cont. Min. Pet., v.90, p.107-120.

Ghiorso, M.S., Carmichael, I.S.E., Rivers, M.L., and Sack, R.O., 1983, Gibbs free energy of mixing of natural silicate liquids: an expanded regular solution approximation for the calculation of magmatic intensive variables;Cont. Min. Pet., v.84, p.107-145.

Ghiorso, M.S. and Carmichael, I.S.E., 1980, Regular solution model for met-aluminuous silicate liquids: Applications to geothermometry, immiscibility and the source regions of basic magmas;Cont. Min. Pet., v.71, p.323-342.

Grove, T.L., Gerlach, D.C., and Sand, T.W., 1982, Origin of calc-alkaline series lavas of Medicine Lake Volcano by fractionation, assimilation and mixing; Cont. Min. Pet., v.80, p.160-182.

Grove, T.L., 1981, Use of FePt alloys to eliminate the iron loss problem in 1 atm. gas mixing experiments: Theoretical and practical considerations; Cont. Min. Pet., v.78, p.298-304.

Gupta, A.K., Venkatesawaran, G.P., Lidiak, E.G., and Edgar, A.D., 1973, The system diopside-nepheline-akermanite-leucite and its bearing on the genesis of alkali-rich mafic ultramafic rocks; J. Geol., v.81, p. 209-218.

Gupta, A.K. and Yagi, K., 1980, Petrology and Genesis of leucite bearing rocks, 253 p. Springer-Verlag press.

Helgeson, H.C., Delany, J.M., Nesbitt, H.W., and Bird, D.K., 1978, Summary and critique of the thermodynamic properties of rock-forming minerals; Am. J. Sci., v. 278-A, p.1-221.

Reproduced with permission of the copyright owner. Further reproduction prohibited without permission.

Kilinc, A., Carmichael, I.S.E., Rivers, M.L., and Sack, R.O., 1983, The ferric-ferrous ratio of natural silicate liquids equilibriated in air;Cont. Min. Pet.,v. 83, p.136-140.

King, B.C., 1965, Petrogenesis of the alkaline igneous rock suites of the volcanic and intrusive centres of Eastern Uganda;J. Petrol., v.6, p.67-100.

Kushiro, I., 1975, On the nature of silicate melt and its significance in magma genesis: regularities in the shift of liquidus boundaries involving olivine, pyroxene, and silica minerals; Am. J. Sci., v.275, p.411-431.

Le Maitre, R.W., 1962, Petrology of volcanic rocks Gough Island, South Atlantic;Geol. Soc. Amer. Bull., v.73, p.1309-1340.

Mc Callister, R.H., Finger, L.W., and Ohashi, Y., 1976 Intercrystalline Fe^{2+}-Mg equilibria in three natural Ca-rich clinopyroxenes;Am. Miner., v.61, p.671-676.

Newton, R.C. and Haselton, H.I., 1981, Thermodynamics of the garnet-plagioclase-Al_2SiO_5-quartz geobarometer; in Ad. in phys. geochemistry, v.1, p.131-148. Springer press.

Nielsen, R.L. and Dungan, M.A., 1983, Low-pressure mineral-melt equilibria in natural anhydrous mafic systems;Cont. Min. Pet., v.84, p.310-326.

Osborn, E.F., 1959, Role of oxygen pressure in the crystallization and differentiation of basaltic magma; Am. J. Sci., v.259, p.609-647.

Presnall, D.C., Dixon, S.A., Dixon, J.R., O'Donell, T.H., Brenner, N.L., and Schrock, R.L., 1978, Liquidus phase relations on the join diopside-forsterite-anorthite from 1 atm to 20 kbar: their bearing on the generation and crystallization of basaltic magma; Cont. Min. Pet., v.66, p.203-220.

Press, W.H., Flannery, B.P., Teukolsky, S.A., and Vetterling, W.T., 1986, Numerical Recipes, 818 p. Cambridge University press.

Roeder, P.L. and Emslie, R.F., 1970, Olivine-liquid equilibrium; Cont. Min. Pet., v.29, p.275-289.

Reproduced with permission of the copyright owner. Further reproduction prohibited without permission.

Sack, R.O. and Ghiorso, M.S., 1989, Importance of considerations of mixing properties in establishing an internally consistent thermodynamic database: thermochemistry of minerals in the system Mg_2SiO_4-Fe_2SiO_4-SiO_2;Cont. Min. Pet., v.102, p.41-68.

Sack, R.O., Walker, D., and Carmichael, I.S.E., 1987, Experimental petrology of alkalic lavas: constraints on cotectics of multiple saturation in natural basic liquids;Cont. Min. Pet., v.96, p.1-23.

Sack, R.O., Carmichael, I.S.E., and Ghiorso, M.S., 1980, Ferric-ferrous equilibria in natural silicate liquids at 1 bar;Cont. Min. Pet., v.75, p.369-376.

Schairer, J.F. and Bowen, N.L., 1938, The system diopside -leucite-silica; Am. J. Sci., v.35-A, p.289-309.

Sood, M.K., 1981, Modern Igneous Petrology. John Wiley & Sons press.

Sood, M.K., Platt, R.G., and Edgar, A.D., 1970, Phase equilibrium relations in portions of the system diopside-nepheline-kalsilite-silica and their importance in the genesis of alkaline rocks; Can. Miner., v.10, p.380-394.

Sorensen, H. (ed.), 1974, The Alkaline Rocks, 622 p. John Wiley & Sons press.

Sparks, R.S.J. and Huppert, H.E., 1984, Density changes during the fractional crstallization of basaltic magmas: fluid dynamic implications; Cont. Min. Pet., v.85, p. 300-309.

Stolz, A.J., Varne, R., Wheller, G.E., Foden, J.D., and Abbott, M.J., 1988, The geochemistry and petrogenesis of K-rich alkaline volcanics from the Batu Tara volcano, eastern Sunda arc; Cont. Min. Pet., v.98, p.374-389.

Takahashi, E. and Kushiro, I., 1983, Melting of dry peridotite at high pressure and basalt magma genesis; Amer. Min., v.68, p.859-879.

Taylor, M. and Brown, G.E., 1979, Structure of silicate mineral glasses;Geochim. Cosmochim. Acta, v.43, p.61 -75.

Reproduced with permission of the copyright owner. Further reproduction prohibited without permission.

Thompson, J.B. Jr, 1982, Composition space: an algebraic and geometric approach;in Reviews in Mineralogy, Ferry, J.M. (ed.), v.10, p.1-31.

Varne, R. and Foden, J.D., 1986, Geochemical and isotopic systematics of eastern Sunda arc volcanics: implications for mantle sources and mantle mixing processes; in The origin of Arcs, Wezel, F.C. (ed.), p. 159-189. Elsevier Press.

Walker, D., Shibata, T. and De Long, S.E., 1979, Abyssal tholeiites from the ocenographer fracture zone;Cont. Min. Pet., v.70, p.111-125.

Wood, B.J. and Nicholls, J., 1978, The thermodynamic properties of reciprocal solid solutions; Cont. Min., Pet., v.66, p.389-400.

Yoder, H.S. and Tilley, C.E., 1962, Origin of basalt magmas: an experimental study of natural and synthetic rock systems; J. Petrol., v.3, p.342-532.

Reproduced with permission of the copyright owner. Further reproduction prohibited without permission.

APPENDIX I.A

Chemical analysis of experimental starting materials and experimental run products

Reproduced with permission of the copyright owner. Further reproduction prohibited without permission.

Chemical analysis of the starting materials has been performed using a Rigaku-3070 X-ray fluorescence spectrometer at the University of Cincinnati. A tube voltage of 50 kV and a tube current of 50 mA were used in all analyses.

Table I.A1. Chemical analysis of experimental starting materials.

	SAMPLE I.D.						
	48114	48115	48134	48137	67127	67130	67137
SiO_2	45.51	45.51	46.65	45.43	50.34	49.23	50.46
TiO_2	0.89	0.93	0.94	0.97	0.72	0.84	0.84
Al_2O_3	11.72	12.02	14.34	15.64	16.90	14.84	17.21
FeO_t	9.68	10.61	9.67	10.10	7.39	8.00	7.82
MnO	0.17	0.19	0.19	0.22	0.17	0.17	0.17
MgO	12.92	11.16	8.98	6.38	6.47	8.18	5.92
CaO	13.61	13.40	11.92	11.43	8.98	10.56	9.62
Na_2O	1.68	1.93	2.59	2.80	2.90	4.89	4.55
K_2O	3.40	5.07	3.79	5.23	5.82	3.58	4.16
P_2O_5	0.61	0.83	0.46	0.89	0.82	1.00	0.89
TOTAL	100.19	101.65	99.53	99.09	100.51	101.29	101.64

	SAMPLE I.D.						
	67145	L-LOW	L-MID	L-UP	L-D	L-2	H-5
SiO_2	45.40	53.47	55.39	54.04	50.89	53.11	51.53
TiO_2	1.07	2.22	2.30	2.29	2.24	2.29	2.15
Al_2O_3	17.60	14.72	13.24	12.01	11.21	12.53	12.57
FeO_t	9.10	7.15	7.74	7.78	9.17	8.32	8.78
MnO	0.19	0.13	0.12	0.12	0.15	0.13	0.15
MgO	5.71	5.21	5.81	6.10	9.39	7.38	8.34
CaO	10.75	5.10	4.96	5.06	7.22	5.68	7.24
Na_2O	2.88	4.40	3.86	3.39	3.73	3.78	4.22
K_2O	4.88	6.05	5.95	5.71	4.87	5.35	4.58
P_2O_5	1.32	0.99	0.92	0.86	1.07	0.83	0.97
TOTAL	98.90	99.44	100.29	97.36	99.94	99.40	100.53

FeO_t =Total iron concentration.

Reproduced with permission of the copyright owner. Further reproduction prohibited without permission.

Table I.A2: Experimental run conditions

SAMPLE I.D.	RUN #	DURATION (hours)	Log f_{O2}	TEMPERATURE (Celcius)	RUN PRODUCTS
48114	3	48	-7.756	1248	GL+OL
	5	384	-8.643	1181	GL+OL+CPX
	6	485	-9.097	1149	GL+OL+CPX+LC+PL
	7	600	-9.504	1121.5	GL+OL+CPX+LC+PL
48115	4	168	-8.316	1205	GL+OL+CPX+LC
	5	384	-8.643	1181	GL+OL+CPX+LC
	6	485	-9.097	1149	GL+OL+CPX+LC+PL
48134	3	48	-7.756	1248	GL
	5	384	-8.643	1181	GL+OL+CPX
	7	600	-9.504	1121.5	GL+OL+CPX+LC+PL
48137	3	48	-7.756	1248	GL
	1	24	-8.343	1203	GL+CPX
	6	485	-9.097	1149	GL+CPX+LC
	7	600	-9.504	1121.5	GL+CPX+LC+PL
67127	3	48	-7.756	1248	GL
	5	384	-8.643	1181	GL+OL+CPX+LC
	6	485	-9.097	1149	GL+OL+CPX+LC
	7	600	-9.504	1121.5	GL+OL+CPX+LC+PL
67130	3	48	-7.756	1248	GL
	6	485	-9.097	1149	GL+OL+CPX
	7	600	-9.504	1121.5	GL+OL+CPX+LC+PL
67137	2	48	-7.819	1243	GL
	4	168	-8.316	1205	GL+OL
	6	485	-9.097	1149	GL+OL+CPX+PL
	7	600	-9.504	1121.5	GL+OL+CPX+PL
67145	3	48	-7.756	1248	GL
	4	168	-8.316	1205	GL
	5	384	-8.643	1181	GL
	6	485	-9.097	1149	GL+OL+CPX+LC+PL
	7	600	-9.504	1121.5	GL+OL+CPX+LC+PL

Abbreviations: GL=glass; OL=olivine; CPX=high-Ca pyroxene
PL=plagioclase feldspar; LC=leucite.

Reproduced with permission of the copyright owner. Further reproduction prohibited without permission.

Table I.A2: Experimental run conditions, cont.

SAMPLE I.D.	RUN #	DURATION (hours)	Log f_{O2}	TEMPERATURE (Celcius)	RUN PRODUCTS
L-LOW	4	168	-8.316	1205	GL+OL
	7	600	-9.504	1121.5	GL+OL+CPX
	9	995	-10.442	1062	GL+OL+CPX+SN+SP
L-MID	2	48	-7.819	1243	GL+OL
	4	168	-8.316	1205	GL+OL
	6	485	-9.097	1149	GL+OL
	7	600	-9.504	1121.5	GL+OL+CPX
	8	800	-10.006	1089	GL+OL+CPX
	9	995	-10.442	1062	GL+OL+CPX+SN+SP
L-UP	2	48	-7.819	1243	GL+OL
	4	168	-8.316	1205	GL+OL
	5	384	-8.643	1181	GL+OL
	7	600	-9.504	1121.5	GL+OL+CPX
	8	800	-10.006	1089	GL+OL+CPX
	9	995	-10.442	1062	GL+OL+CPX+SP
L-D	4	168	-8.316	1205	GL+OL
	6	485	-9.097	1149	GL+OL+CPX
	7	600	-9.504	1121.5	GL+OL+CPX
	8	800	-10.006	1089	GL+OL+CPX
	9	995	-10.442	1062	GL+OL+CPX+SN+PL+SP
L-2	2	48	-7.819	1243	GL+OL
	4	168	-8.316	1205	GL+OL
	5	384	-8.643	1181	GL+OL
	8	800	-10.006	1089	GL+OL+CPX+SP
	9	995	-10.442	1062	GL+OL+CPX+SN+SP
H-5	2	48	-7.819	1243	GL+OL
	4	168	-8.316	1205	GL+OL
	1	24	-8.343	1203	GL+OL
	8	800	-10.006	1089	GL+OL+CPX+SP
	9	995	-10.442	1062	GL+OL+CPX+SN+SP

Abbreviations: GL=glass; OL=olivine; CPX=high-Ca pyroxene
PL=plagioclase feldspar; LC=leucite
SP=spinel; SN=alkali feldspar.

Reproduced with permission of the copyright owner. Further reproduction prohibited without permission.

Table I.A3. Chemical analysis of experimental run products.

SAMPLE I.D. : 48114

	SiO_2	TiO_2	Al_2O_3	Cr_2O_3	FeO_t	MnO	MgO	CaO	Na_2O	K_2O	P_2O_5	TOTAL
R# 3												
GL	46.83	0.91	11.55	0.04	9.72	0.15	8.81	15.62	1.11	2.50	0.38	97.62
OL	39.44	0.00	0.14	0.05	12.45	0.24	45.21	0.78	0.00	0.00	0.04	98.35
R# 5												
GL	45.86	0.91	15.30	0.02	11.08	0.16	5.76	12.96	1.29	3.50	0.50	97.32
OL	38.47	0.01	0.00	0.02	19.40	0.25	40.17	0.73	0.00	0.00	0.02	99.05
CPX	51.16	0.35	2.72	0.19	5.15	0.06	15.15	23.80	0.13	0.02	0.02	98.73
R# 6												
GL	46.08	1.21	14.55	0.01	13.03	0.18	4.63	11.47	1.38	3.78	0.82	97.11
OL	37.47	0.06	0.02	0.00	25.32	0.33	34.65	0.75	0.02	0.01	0.04	98.66
CPX	52.90	0.07	1.54	0.16	3.62	0.06	16.12	24.14	0.13	0.02	0.02	98.78
LC	54.93	0.02	22.93	0.02	0.62	0.00	0.01	0.00	0.52	20.32	0.00	99.37
PL	46.88	0.01	32.59	0.01	0.73	0.02	0.25	16.97	1.36	0.53	0.02	99.37
R# 7												
GL	45.73	1.51	14.52	0.00	14.29	0.26	3.67	10.03	2.28	3.78	1.00	97.05
OL	36.33	0.06	0.06	0.00	31.11	0.51	30.17	0.82	0.01	0.02	0.04	99.13
CPX	47.59	0.85	6.43	0.13	9.53	0.17	10.89	22.89	0.40	0.08	0.06	99.02
LC	55.33	0.04	23.54	0.05	0.37	0.04	0.00	0.00	0.83	19.76	0.01	99.97
PL	46.96	0.17	32.97	0.01	0.91	0.00	0.29	16.12	1.63	0.44	0.04	99.54

FeO_t =Total iron concentration.

Reproduced with permission of the copyright owner. Further reproduction prohibited without permission.

Table I.A3. Chemical analysis of experimental run products, cont.

SAMPLE I.D. : 48115

	SiO_2	TiO_2	Al_2O_3	Cr_2O_3	FeO_t	MnO	MgO	CaO	Na_2O	K_2O	P_2O_5	TOTAL
R# 4												
GL	44.29	1.14	12.29	0.03	12.18	0.20	6.74	15.04	1.22	3.56	0.61	97.30
OL	38.42	0.01	0.05	0.03	17.15	0.29	41.46	1.02	0.00	0.00	0.10	98.53
CPX	51.42	0.44	2.84	0.20	4.65	0.06	15.18	23.91	0.10	0.00	0.01	98.81
LC	54.39	0.03	22.34	0.00	0.71	0.00	0.05	0.00	0.41	20.48	0.01	98.40
R# 5												
GL	43.84	1.11	13.13	0.02	13.52	0.18	5.96	14.33	1.21	3.45	0.88	97.61
OL	38.55	0.00	0.07	0.00	20.61	0.32	38.51	1.09	0.01	0.03	0.03	99.22
CPX	51.48	0.62	3.03	0.19	5.29	0.04	14.62	24.12	0.14	0.01	0.00	99.54
LC	54.87	0.04	22.60	0.01	0.74	0.00	0.02	0.00	0.43	20.57	0.03	99.29
R# 6												
GL	42.26	1.21	14.77	0.02	15.49	0.29	4.89	13.36	1.06	2.98	0.94	97.26
OL	37.28	0.03	0.04	0.01	26.80	0.39	33.27	0.90	0.01	0.01	0.05	98.77
CPX	50.08	0.52	3.90	0.03	6.62	0.00	13.80	24.08	0.10	0.04	0.04	99.21
LC	54.63	0.06	22.79	0.03	0.47	0.02	0.00	0.00	0.43	20.52	0.04	98.99
PL	45.73	0.10	33.66	0.00	0.76	0.09	0.15	17.64	0.96	0.44	0.02	99.52

FeO_t =Total iron concentration.

Reproduced with permission of the copyright owner. Further reproduction prohibited without permission.

Table I.A3. Chemical analysis of experimental run products, cont.

SAMPLE I.D. : 48134

	SiO_2	TiO_2	Al_2O_3	Cr_2O_3	FeO_t	MnO	MgO	CaO	Na_2O	K_2O	P_2O_5	TOTAL
R# 3												
GL	46.25	0.95	13.47	0.03	10.43	0.19	7.63	13.46	1.87	3.05	0.36	97.69
R# 5												
GL	46.58	1.02	15.95	0.00	10.47	0.19	5.35	12.09	1.77	3.66	0.48	97.55
OL	38.42	0.00	0.04	0.02	19.65	0.32	40.20	0.73	0.02	0.03	0.02	99.45
CPX	48.38	0.69	5.89	0.01	7.50	0.14	12.90	23.22	0.34	0.02	0.03	99.12
R# 7												
GL	47.93	1.35	15.29	0.01	13.39	0.28	3.34	9.36	2.27	4.19	0.82	98.24
OL	36.42	0.06	0.15	0.01	30.38	0.61	29.78	0.96	0.01	0.03	0.15	98.56
CPX	49.34	0.75	4.69	0.11	7.92	0.19	12.73	22.83	0.27	0.02	0.02	98.85
LC	55.38	0.00	23.43	0.03	0.48	0.00	0.00	0.08	0.86	19.51	0.02	99.79
PL	47.41	0.05	32.37	0.03	1.23	0.03	0.25	15.71	1.86	0.65	0.06	99.65

FeO_t =Total iron concentration.

Reproduced with permission of the copyright owner. Further reproduction prohibited without permission.

Table I.A3. Chemical analysis of experimental run products, cont.

SAMPLE I.D. : 48137

	SiO_2	TiO_2	Al_2O_3	Cr_2O_3	FeO_t	MnO	MgO	CaO	Na_2O	K_2O	P_2O_5	TOTAL
R# 3												
GL	45.17	0.96	14.38	0.01	10.77	0.21	5.38	13.01	1.87	3.93	0.57	96.26
R# 1												
GL	45.72	0.95	14.80	0.00	10.69	0.22	5.35	12.67	2.16	4.47	0.56	97.59
CPX	50.60	1.41	5.95	0.09	0.15	0.15	16.53	24.10	0.12	0.02	0.04	99.16
R# 6												
GL	44.84	1.04	15.30	0.04	13.26	0.29	4.75	12.17	1.90	3.62	0.71	97.89
CPX	50.54	0.53	4.38	0.00	6.39	0.16	13.65	23.50	0.15	0.01	0.04	99.35
LC	55.27	0.07	23.46	0.02	0.54	0.02	0.00	0.00	0.63	20.06	0.02	100.06
R# 7												
GL	43.33	1.26	14.19	0.02	16.22	0.32	3.82	11.14	2.13	3.14	1.08	96.65
CPX	46.49	1.04	7.26	0.01	8.42	0.21	11.55	23.06	0.25	0.01	0.00	98.32
LC	54.34	0.10	23.45	0.01	0.49	0.02	0.02	0.00	0.81	19.49	0.00	98.71
PL	45.83	0.01	34.10	0.00	0.87	0.00	0.11	16.73	1.33	0.33	0.02	99.33

FeO_t =Total iron concentration.

Reproduced with permission of the copyright owner. Further reproduction prohibited without permission.

Table I.A3. Chemical analysis of experimental run products, cont.

SAMPLE I.D. : 67127

	SiO_2	TiO_2	Al_2O_3	Cr_2O_3	FeO_t	MnO	MgO	CaO	Na_2O	K_2O	P_2O_5	TOTAL
R# 3												
GL	50.89	0.76	15.56	0.03	6.64	0.13	6.27	10.06	1.99	4.83	0.46	97.62
R# 5												
GL	51.31	0.84	17.02	0.03	6.85	0.10	4.55	9.38	2.03	5.34	0.41	97.86
OL	39.04	0.00	0.03	0.02	16.30	0.26	43.05	0.52	0.01	0.01	0.03	99.27
CPX	48.86	0.72	5.09	0.08	7.53	0.16	13.67	22.34	0.25	0.03	0.01	98.74
LC	55.93	0.00	22.26	0.03	0.29	0.02	0.00	0.00	0.61	20.00	0.00	99.14
R# 6												
GL	50.69	0.81	16.60	0.01	8.35	0.15	3.99	8.67	2.43	5.30	0.94	97.91
OL	38.21	0.00	0.03	0.02	21.01	0.31	39.23	0.44	0.01	0.00	0.04	99.30
CPX	50.56	0.32	3.09	0.23	5.40	0.10	15.45	23.30	0.23	0.01	0.00	98.69
LC	54.90	0.10	22.48	0.03	0.49	0.00	0.01	0.00	0.68	19.64	0.00	98.33
R# 7												
GL	50.85	1.03	16.46	0.01	9.32	0.14	3.37	7.71	2.67	5.24	1.43	98.22
OL	37.27	0.03	0.03	0.04	25.91	0.49	33.94	0.52	0.00	0.04	0.07	98.34
CPX	47.29	0.89	6.89	0.09	7.52	0.18	13.17	22.62	0.29	0.00	0.05	98.99
LC	57.13	0.03	22.68	0.00	0.45	0.00	0.00	0.00	0.89	19.02	0.07	100.27
PL	49.38	0.13	30.08	0.04	0.93	0.02	0.30	13.99	2.63	1.04	0.04	98.59

FeO_t =Total iron concentration.

Reproduced with permission of the copyright owner. Further reproduction prohibited without permission.

Table I.A3. Chemical analysis of experimental run run products, cont.

SAMPLE I.D. : 67130

	SiO_2	TiO_2	Al_2O_3	Cr_2O_3	FeO_t	MnO	MgO	CaO	Na_2O	K_2O	P_2O_5	TOTAL
R# 3												
GL	49.14	0.89	13.78	0.06	7.72	0.19	8.15	12.09	2.30	3.18	0.63	98.13
R# 6												
GL	49.56	0.88	17.02	0.01	8.18	0.20	4.00	8.82	3.01	4.83	0.77	97.28
OL	37.91	0.00	0.02	0.00	19.98	0.36	39.69	0.57	0.01	0.01	0.05	98.59
CPX	50.76	0.56	3.86	0.18	4.82	0.14	14.63	23.10	0.24	0.02	0.07	98.38
R# 7												
GL	50.72	0.89	17.71	0.02	8.34	0.15	3.24	7.21	3.81	5.27	1.04	98.40
OL	38.09	0.00	0.02	0.00	23.11	0.48	37.17	0.55	0.01	0.00	0.05	99.48
CPX	48.45	1.02	5.58	0.14	7.08	0.15	13.25	22.42	0.30	0.06	0.00	98.45
LC	55.23	0.11	23.23	0.02	0.38	0.00	0.00	0.00	0.80	19.40	0.06	99.23
PL	50.17	0.07	30.81	0.03	1.06	0.00	0.27	13.64	2.91	0.98	0.06	100.00

FeO_t =Total iron concentration.

Reproduced with permission of the copyright owner. Further reproduction prohibited without permission.

Table I.A3. Chemical analysis of experimental run products, cont.

SAMPLE I.D. : 67137

	SiO_2	TiO_2	Al_2O_3	Cr_2O_3	FeO_t	MnO	MgO	CaO	Na_2O	K_2O	P_2O_5	TOTAL
R# 2												
GL	48.58	0.82	16.05	0.03	8.02	0.21	6.13	10.74	2.69	3.50	0.65	97.42
R# 4												
GL	49.17	0.83	16.12	0.02	8.03	0.20	5.97	10.74	2.60	3.60	0.58	97.86
OL	38.65	0.08	1.06	0.10	14.80	0.36	43.48	0.84	0.00	0.00	0.06	99.43
R# 6												
GL	50.39	1.04	16.91	0.01	8.70	0.17	4.06	8.98	2.59	4.48	0.64	97.96
OL	38.35	0.07	0.04	0.01	20.77	0.35	38.63	0.59	0.02	0.03	0.15	99.01
CPX	50.65	0.55	4.17	0.33	5.45	0.13	14.77	22.71	0.22	0.02	0.01	99.01
PL	48.15	0.01	32.97	0.01	0.56	0.03	0.18	15.75	2.03	0.50	0.02	100.22
R# 7												
GL	50.79	1.24	16.86	0.02	9.53	0.21	3.26	7.98	2.55	4.84	1.08	98.37
OL	37.41	0.09	0.06	0.02	26.14	0.55	33.91	0.65	0.00	0.03	0.10	98.96
CPX	49.06	0.97	6.16	0.04	8.44	0.16	12.62	22.18	0.37	0.04	0.06	100.10
PL	47.77	0.08	32.45	0.00	0.74	0.01	0.14	15.53	2.12	0.43	0.03	99.30

FeO_t =Total iron concentration.

Reproduced with permission of the copyright owner. Further reproduction prohibited without permission.

Table I.A3. Chemical analysis of experimental run products, cont.

SAMPLE I.D. : 67145

	SiO_2	TiO_2	Al_2O_3	Cr_2O_3	FeO_t	MnO	MgO	CaO	Na_2O	K_2O	P_2O_5	TOTAL
R# 3												
GL	46.93	1.11	16.67	0.00	9.63	0.21	5.42	11.90	2.01	3.80	0.72	98.37
R# 4												
GL	46.54	1.09	16.40	0.01	9.46	0.20	5.37	11.83	2.03	3.80	0.78	97.50
R# 6												
GL	46.95	1.25	15.64	0.03	11.62	0.19	4.61	10.94	2.07	4.05	0.94	98.27
OL	37.85	0.04	0.03	0.02	23.06	0.42	36.89	0.69	0.02	0.00	0.04	99.06
CPX	50.55	0.69	3.64	0.05	6.25	0.14	14.25	23.13	0.18	0.02	0.00	98.90
LC	55.55	0.17	23.30	0.02	0.41	0.01	0.00	0.00	0.72	19.77	0.02	99.93
PL	46.76	0.00	33.92	0.01	0.74	0.05	0.15	16.88	1.39	0.42	0.03	100.33
R# 7												
GL	45.27	1.84	14.36	0.03	14.31	0.31	3.84	10.22	2.40	3.78	1.42	97.78
OL	36.77	0.00	0.04	0.04	30.59	0.58	30.66	0.71	0.02	0.01	0.01	99.43
CPX	49.14	0.89	4.74	0.05	7.68	0.20	12.72	22.48	0.24	0.02	0.03	98.19
LC	55.87	0.01	22.92	0.01	0.43	0.00	0.02	0.00	0.84	19.89	0.02	100.01
PL	46.78	0.03	33.79	0.04	0.73	0.01	0.09	16.46	1.63	0.40	0.03	99.99

FeO_t =Total iron concentration.

Reproduced with permission of the copyright owner. Further reproduction prohibited without permission.

Table I.A3. Chemical analysis of experimental run products, cont.

SAMPLE I.D. : L-LOW

	SiO_2	TiO_2	Al_2O_3	Cr_2O_3	FeO_t	MnO	MgO	CaO	Na_2O	K_2O	P_2O_5	TOTAL
R# 4												
GL	55.02	2.14	14.55	0.03	6.83	0.10	4.74	5.72	3.51	5.21	0.58	98.43
OL	38.88	0.10	0.01	0.09	15.19	0.22	43.51	0.35	0.00	0.00	0.06	98.43
R# 7												
GL	54.86	1.96	16.22	0.02	5.94	0.09	2.58	4.81	2.98	5.84	0.51	95.81
OL	38.16	0.00	0.04	0.05	21.06	0.26	39.67	0.38	0.00	0.01	0.09	99.71
CPX	50.91	1.13	2.13	0.16	6.48	0.15	15.28	21.79	0.40	0.06	0.03	98.51
R# 9												
GL	59.88	1.54	18.02	0.01	5.31	0.06	1.36	2.97	1.76	5.59	0.80	97.30
OL	36.71	0.12	0.07	0.00	28.01	0.40	34.12	0.35	0.02	0.04	0.09	99.94
CPX	48.93	1.88	4.08	0.18	7.81	0.16	14.82	21.24	0.49	0.05	0.12	99.76
SN	62.53	0.16	20.53	0.00	0.36	0.00	0.01	0.95	3.87	9.95	0.04	98.40

FeO_t =Total iron concentration.

Reproduced with permission of the copyright owner. Further reproduction prohibited without permission.

Table I.A3. Chemical analysis of experimental run products, cont.

SAMPLE I.D. : L-MID

	SiO_2	TiO_2	Al_2O_3	Cr_2O_3	FeO_t	MnO	MgO	CaO	Na_2O	K_2O	P_2O_5	TOTAL
R# 2												
GL	54.12	2.20	14.20	0.03	6.96	0.13	5.90	5.41	3.26	5.20	0.57	97.98
OL	39.26	0.00	0.02	0.05	13.26	0.20	45.49	0.34	0.00	0.00	0.18	98.80
R# 4												
GL	55.08	2.31	14.85	0.01	6.64	0.09	4.44	5.49	3.48	5.39	0.37	98.12
OL	38.92	0.05	0.39	0.14	15.37	0.26	43.33	0.36	0.00	0.00	0.07	98.86
R# 6												
GL	56.34	2.16	15.66	0.02	5.93	0.08	3.23	5.68	3.07	5.61	0.38	98.16
OL	38.31	0.02	0.03	0.04	18.08	0.26	41.23	0.40	0.00	0.03	0.40	98.78
R# 7												
GL	56.02	1.71	16.54	0.01	5.49	0.07	2.27	4.18	3.13	6.41	0.35	96.18
OL	37.73	0.11	0.01	0.04	21.86	0.33	38.82	0.39	0.00	0.01	0.30	99.61
CPX	50.11	1.27	2.31	0.03	6.55	0.11	14.83	22.29	0.46	0.07	0.04	98.07
R# 8												
GL	51.89	2.18	16.20	0.04	7.89	0.13	3.55	7.22	2.54	4.97	1.43	98.04
OL	38.47	0.11	0.03	0.00	20.55	0.32	39.76	0.54	0.01	0.02	0.04	99.85
CPX	50.76	1.18	2.33	0.08	6.77	0.11	15.07	22.03	0.41	0.04	0.04	98.82
R# 9												
GL	59.65	1.59	18.43	0.03	5.54	0.07	1.38	3.03	1.79	5.48	0.77	97.76
OL	36.79	0.00	0.01	0.02	27.86	0.44	33.31	0.40	0.00	0.05	0.32	99.19
CPX	49.31	1.54	3.49	0.20	6.95	0.08	14.71	21.61	0.45	0.10	0.21	98.65
SN	62.06	0.14	25.17	0.00	0.41	0.00	0.00	0.00	0.88	15.15	0.02	103.84

FeO_t =Total iron concentration.

Reproduced with permission of the copyright owner. Further reproduction prohibited without permission.

Table I.A3. Chemical analysis of experimental run products, cont.

SAMPLE I.D. : L-UP

	SiO_2	TiO_2	Al_2O_3	Cr_2O_3	FeO_t	MnO	MgO	CaO	Na_2O	K_2O	P_2O_5	TOTAL
R# 2												
GL	54.56	2.22	14.17	0.03	6.91	0.11	5.68	5.34	3.53	5.30	0.66	98.48
OL	39.06	0.00	0.02	0.02	13.91	0.20	44.66	0.21	0.00	0.00	0.09	98.17
R# 4												
GL	54.81	2.25	14.54	0.01	6.84	0.12	4.45	5.60	3.50	5.40	0.60	98.10
OL	39.02	0.03	0.02	0.07	15.83	0.24	42.84	0.31	0.00	0.00	0.11	98.45
R# 5												
GL	55.92	2.30	15.17	0.00	6.28	0.09	3.86	5.39	3.03	5.43	0.32	97.79
OL	39.24	0.01	0.03	0.04	16.52	0.20	43.05	0.33	0.01	0.01	0.08	99.49
R# 7												
GL	54.58	2.27	16.08	0.05	6.51	0.07	2.86	5.28	3.24	5.73	1.05	97.72
OL	38.00	0.11	0.02	0.08	21.52	0.29	38.37	0.37	0.00	0.00	0.13	98.89
CPX	50.50	2.10	4.32	0.17	7.53	0.14	13.66	20.34	0.57	0.38	0.12	99.83
R# 8												
GL	58.18	1.83	17.23	0.02	5.54	0.05	1.76	5.54	1.53	5.67	0.57	97.92
OL	37.63	0.01	0.00	0.04	24.93	0.42	36.05	0.37	0.00	0.01	0.04	99.51
CPX	50.42	1.18	2.74	0.18	7.01	0.19	16.20	21.89	0.36	0.05	0.07	100.29
R# 9												
GL	58.79	1.66	17.61	0.03	5.50	0.11	1.33	2.97	1.75	5.52	0.82	96.09
OL	36.42	0.06	0.00	0.00	27.63	0.41	33.05	0.37	0.00	0.01	0.25	98.21
CPX	51.03	1.74	3.51	0.01	7.28	0.14	13.85	22.36	0.57	0.06	0.17	100.72

FeO_t =Total iron concentration.

Reproduced with permission of the copyright owner. Further reproduction prohibited without permission.

Table I.A3. Chemical analysis of experimental run products, cont.

SAMPLE I.D. : L-D

	SiO_2	TiO_2	Al_2O_3	Cr_2O_3	FeO_t	MnO	MgO	CaO	Na_2O	K_2O	P_2O_5	TOTAL
R# 4												
GL	51.15	1.95	14.07	0.07	7.72	0.11	5.55	8.16	3.38	4.40	0.75	97.29
OL	39.58	0.00	0.01	0.06	14.75	0.22	44.09	0.44	0.01	0.00	0.08	99.23
R# 6												
GL	52.21	2.29	15.78	0.01	7.70	0.13	3.93	7.42	2.91	4.75	0.70	97.80
OL	38.65	0.00	0.03	0.04	18.75	0.32	40.59	0.48	0.00	0.02	0.07	98.93
CPX	52.32	0.78	1.70	0.63	4.66	0.10	15.51	22.46	0.34	0.03	0.02	98.53
R# 7												
GL	52.18	2.26	17.00	0.02	7.42	0.14	3.21	6.88	2.49	5.15	1.32	98.07
OL	38.38	0.10	0.01	0.00	21.09	0.29	39.38	0.45	0.03	0.02	0.09	99.85
CPX	50.32	1.49	3.37	0.97	6.93	0.14	14.30	22.30	0.42	0.04	0.06	100.30
R# 8												
GL	52.34	2.35	17.91	0.02	6.93	0.11	2.48	5.48	2.58	5.54	1.33	97.07
OL	37.27	0.06	0.01	0.03	24.46	0.39	36.52	0.42	0.02	0.02	0.06	99.27
CPX	49.99	1.92	2.52	0.08	7.20	0.12	14.41	22.00	0.48	0.04	0.08	98.84
R# 9												
GL	54.48	1.73	18.45	0.04	6.65	0.13	1.75	4.20	2.12	5.09	1.10	95.74
OL	36.80	0.07	0.01	0.03	27.48	0.45	33.85	0.46	0.03	0.01	0.06	99.24
CPX	49.70	1.54	4.03	0.14	6.99	0.20	14.79	21.81	0.51	0.09	0.06	99.86
PL	56.81	0.17	26.37	0.01	0.49	0.00	0.03	6.47	5.42	2.48	0.05	98.30
SN	60.08	0.24	25.37	0.02	0.62	0.01	0.11	0.10	1.33	15.65	0.08	103.60

FeO_t =Total iron concentration.

Reproduced with permission of the copyright owner. Further reproduction prohibited without permission.

Table I.A3. Chemical analysis of experimental run products, cont.

SAMPLE I.D. : L-2

	SiO_2	TiO_2	Al_2O_3	Cr_2O_3	FeO_t	MnO	MgO	CaO	Na_2O	K_2O	P_2O_5	TOTAL
R# 2												
GL	53.18	2.22	14.05	0.02	7.46	0.12	6.15	6.18	3.53	4.88	0.65	98.41
OL	39.40	0.00	0.03	0.09	13.13	0.20	45.18	0.35	0.00	0.00	0.17	98.54
R# 4												
GL	53.72	2.37	14.40	0.03	7.16	0.13	4.88	6.44	3.44	4.86	0.55	97.96
OL	39.16	0.04	0.04	0.07	15.51	0.24	43.54	0.36	0.00	0.00	0.05	99.00
R# 5												
GL	54.16	2.24	14.83	0.03	6.67	0.09	4.24	6.12	3.24	5.10	0.46	97.16
OL	38.98	0.06	0.01	0.04	16.64	0.19	42.36	0.37	0.02	0.00	0.11	98.76
R# 8												
GL	56.36	1.91	18.09	0.03	5.56	0.05	1.77	4.10	1.93	5.70	1.18	96.70
OL	37.30	0.00	0.01	0.02	24.68	0.37	36.57	0.40	0.00	0.05	0.05	99.46
CPX	51.07	1.22	2.09	0.12	6.92	0.14	15.57	21.48	0.34	0.04	0.04	99.04
R# 9												
GL	58.59	1.59	18.45	0.03	5.33	0.08	1.40	3.00	1.88	5.37	0.81	96.53
OL	36.68	0.00	0.00	0.02	28.63	0.39	32.87	0.36	0.00	0.04	0.08	99.07
CPX	48.26	1.72	3.76	0.16	7.32	0.12	13.41	22.15	0.37	0.11	0.88	98.26
SN	60.97	0.07	25.19	0.00	0.37	0.02	0.03	0.29	1.03	14.90	0.39	103.24

FeO_t =Total iron concentration.

Reproduced with permission of the copyright owner. Further reproduction prohibited without permission.

Table I.A3. Chemical analysis of experimental run products, cont.

SAMPLE I.D. : H-5

	SiO_2	TiO_2	Al_2O_3	Cr_2O_3	FeO_t	MnO	MgO	CaO	Na_2O	K_2O	P_2O_5	TOTAL
R# 2												
GL	50.97	2.07	13.70	0.06	7.94	0.15	6.74	7.79	3.49	4.11	0.79	97.81
OL	39.67	0.00	0.02	0.04	12.91	0.23	45.00	0.33	0.00	0.00	0.11	98.30
R# 4												
GL	51.25	2.14	14.54	0.04	7.68	0.12	5.56	8.22	3.42	4.19	0.74	97.90
OL	39.00	0.04	0.07	0.07	15.34	0.22	43.61	0.51	0.00	0.00	0.18	99.01
R# 1												
GL	50.58	1.90	14.02	0.01	8.05	0.10	5.65	8.09	3.80	4.38	1.02	97.56
OL	39.80	0.04	0.08	0.05	14.45	0.22	44.29	0.38	0.02	0.01	0.06	99.36
R# 8												
GL	52.69	2.15	17.88	0.02	7.16	0.13	2.22	5.06	2.05	5.35	1.03	96.01
OL	37.26	0.02	0.01	0.03	25.56	0.39	35.64	0.43	0.01	0.03	0.08	99.46
CPX	48.94	1.42	3.77	0.07	6.86	0.14	14.41	22.38	0.45	0.03	0.01	98.48
R# 9												
GL	58.92	0.12	25.66	0.00	0.49	0.04	0.11	7.14	2.50	5.48	0.10	100.55
OL	36.08	0.04	0.01	0.00	27.36	0.45	33.22	0.40	0.02	0.02	0.04	97.63
CPX	49.78	2.02	3.32	0.09	6.79	0.15	13.61	21.93	0.53	0.05	0.02	98.28
SN	60.55	0.26	24.37	0.00	0.53	0.07	0.12	0.16	1.45	14.22	0.06	101.78

FeO_t =Total iron concentration.

Reproduced with permission of the copyright owner. Further reproduction prohibited without permission.

APPENDIX I.B

Chemical analysis for alkali loss test in electron microprobe analysis of some experimental glass compositions

Reproduced with permission of the copyright owner. Further reproduction prohibited without permission.

Table I.B1. Variance in glass chemical analysis with respect to counting time measured at one micron beam diameter.

SAMPLE I.D. : 48115 Run $T^{o}C$=1149

	counting times in second			
	5	10	20	30
SiO_2	42.07	42.48	42.31	42.26
TiO_2	1.02	1.20	1.32	1.21
Al_2O_3	14.73	14.55	14.61	14.77
Cr_2O_3	0.00	0.05	0.05	0.02
FeO_t	15.94	15.85	15.69	15.49
MnO	0.27	0.32	0.25	0.29
MgO	4.97	4.94	4.95	4.89
CaO	13.70	13.49	13.54	13.36
Na_2O	1.03	1.06	1.07	1.06
K_2O	3.00	2.99	3.02	2.98
P_2O_5	0.78	1.02	0.92	0.94
TOTAL	97.51	97.96	97.70	97.26

FeO_t =Total iron concentration.

Reproduced with permission of the copyright owner. Further reproduction prohibited without permission.

Table I.B2. Variance in glass chemical analysis with respect to beam diameter measured at 30 second counting time.

SAMPLE I.D. : 48134 Run $T^{o}C$=1248

	beam diameter in microns 1	5	15	25	30
SiO_2	47.30	46.90	46.98	47.42	47.33
TiO_2	0.78	1.88	0.71	0.80	0.83
Al_2O_3	13.84	13.69	13.81	13.80	13.75
Cr_2O_3	0.05	0.00	0.04	0.00	0.05
FeO_t	10.09	9.95	10.00	9.77	9.82
MnO	0.20	0.24	0.20	0.22	0.12
MgO	7.75	7.84	7.79	7.76	7.67
CaO	13.26	13.25	13.26	13.18	13.29
Na_2O	1.76	1.88	1.89	1.84	1.88
K_2O	2.99	3.01	3.04	3.00	3.02
P_2O_5	0.34	0.34	0.35	0.32	0.37
TOTAL	98.35	97.99	98.07	98.10	98.12

SAMPLE I.D. : 67127 Run $T^{o}C$=1248

	beam diameter in microns 1	5	15	25	30
SiO_2	50.77	50.54	51.04	51.13	51.38
TiO_2	0.69	0.52	0.64	0.61	0.54
Al_2O_3	16.20	16.21	16.47	16.17	16.24
Cr_2O_3	0.03	0.04	0.03	0.03	0.00
FeO_t	6.51	6.57	6.50	6.52	6.22
MnO	0.14	0.11	0.18	0.12	0.18
MgO	6.34	6.60	6.22	6.47	6.39
CaO	10.13	10.01	9.52	9.93	9.87
Na_2O	2.11	2.08	2.30	2.19	2.22
K_2O	4.84	4.82	5.17	4.77	4.86
P_2O_5	0.50	0.46	0.34	0.44	0.36
TOTAL	98.26	97.98	98.40	98.39	98.28

FeO_t =Total iron concentration.

Reproduced with permission of the copyright owner. Further reproduction prohibited without permission.

Table I.B2. Variance in glass chemical analysis with respect to beam diameter measured at 30 second counting time, cont.

SAMPLE I.D. : 67130 Run $T^{o}C$=1248

	beam diameter in microns				
	1	5	15	25	30
SiO_2	49.44	49.31	49.45	49.40	49.37
TiO_2	0.70	0.68	0.73	0.87	0.75
Al_2O_3	13.97	14.17	14.14	14.09	14.11
Cr_2O_3	0.06	0.05	0.00	0.03	0.05
FeO_t	7.51	7.70	7.72	7.58	7.63
MnO	0.14	0.16	0.16	0.20	0.16
MgO	8.21	8.13	8.25	8.13	8.10
CaO	12.03	12.04	11.99	11.96	12.05
Na_2O	2.35	2.45	2.42	2.42	2.38
K_2O	3.19	3.27	3.21	3.20	3.22
P_2O_5	0.61	0.56	0.60	0.60	0.57
TOTAL	98.21	98.52	98.66	98.48	98.39

SAMPLE I.D. : 67137 Run $T^{o}C$=1243

	beam diameter in microns				
	1	5	15	25	30
SiO_2	48.78	49.01	49.00	48.71	48.92
TiO_2	0.70	0.77	0.85	0.69	0.77
Al_2O_3	16.52	16.54	16.45	16.44	16.32
Cr_2O_3	0.04	0.00	0.00	0.01	0.00
FeO_t	8.11	8.27	8.14	7.93	7.95
MnO	0.17	0.15	0.17	0.19	0.19
MgO	6.13	6.21	6.02	6.16	6.11
CaO	10.79	10.87	10.94	10.88	10.80
Na_2O	2.64	2.73	2.76	2.78	2.75
K_2O	3.49	3.46	3.46	3.50	3.49
P_2O_5	0.60	0.65	0.56	0.56	0.57
TOTAL	97.97	98.67	98.36	97.85	97.88

FeO_t =Total iron concentration.

Reproduced with permission of the copyright owner. Further reproduction prohibited without permission.

Table I.B2. Variance in glass chemical analysis with respect to beam diameter measured at 30 second counting time, cont.

SAMPLE I.D. : L-MID Run T°C=1243

	beam diameter in microns				
	1	5	15	25	30
SiO_2	55.36	54.54	53.99	54.22	53.94
TiO_2	2.00	1.96	2.05	2.08	2.10
Al_2O_3	14.49	14.37	14.21	14.13	14.15
Cr_2O_3	0.05	0.05	0.07	0.04	0.06
FeO_t	6.92	6.70	6.93	6.72	6.82
MnO	0.13	0.08	0.12	0.08	0.10
MgO	5.76	5.76	5.75	5.73	5.74
CaO	5.63	5.42	5.27	5.28	5.31
Na_2O	2.42	3.29	3.52	3.63	3.59
K_2O	5.07	5.21	5.18	5.24	5.28
P_2O_5	0.59	0.54	0.57	0.56	0.66
TOTAL	98.43	97.91	97.67	97.71	97.75

SAMPLE I.D. : L-UP Run T°C=1243

	beam diameter in microns				
	1	5	15	25	30
SiO_2	55.08	54.26	54.73	54.06	54.38
TiO_2	1.99	1.96	1.96	1.84	1.90
Al_2O_3	14.47	14.46	14.26	14.17	14.17
Cr_2O_3	0.04	0.02	0.04	0.01	0.01
FeO_t	7.00	6.92	6.81	6.74	6.83
MnO	0.14	0.13	0.08	0.11	0.10
MgO	5.74	5.77	5.73	5.78	5.62
CaO	5.41	5.32	5.31	5.25	5.27
Na_2O	2.63	3.38	3.61	3.73	3.65
K_2O	5.19	5.24	5.31	5.24	5.31
P_2O_5	0.67	0.70	0.63	0.64	0.62
TOTAL	98.38	98.16	98.46	97.56	97.85

FeO_t =Total iron concentration.

Reproduced with permission of the copyright owner. Further reproduction prohibited without permission.

Table I.B2. Variance in glass chemical analysis with respect to beam diameter measured at 30 second counting time, cont.

SAMPLE I.D. : H-5 Run $T^{o}C$=1243

	beam diameter in microns				
	1	5	15	25	30
SiO_2	51.40	50.88	50.77	50.72	50.72
TiO_2	1.85	1.92	1.80	1.82	1.91
Al_2O_3	14.09	13.92	13.78	13.75	13.86
Cr_2O_3	0.02	0.10	0.02	0.00	0.02
FeO_t	8.04	7.98	8.01	7.79	7.91
MnO	0.17	0.08	0.11	0.13	0.14
MgO	6.96	7.03	6.89	6.92	6.89
CaO	8.09	7.87	7.89	7.84	7.85
Na_2O	2.87	3.58	3.65	3.66	3.62
K_2O	4.03	4.09	4.08	4.05	4.06
P_2O_5	0.79	0.72	0.69	0.78	0.69
TOTAL	98.33	98.18	97.69	97.47	97.67

FeO_t =Total iron concentration.

Reproduced with permission of the copyright owner. Further reproduction prohibited without permission.

APPENDIX II.A

Calculation of standard state chemical potentials of melt and mineral components.

Reproduced with permission of the copyright owner. Further reproduction prohibited without permission.

Standard state chemical potential of mineral and melt components at one atmosphere is defined as:

$$(IIA.1) \quad {}^{o}G_{i,f,Pr,T} = {}^{o}H_{i,Pr,T} - T*{}^{o}S_{i,Pr,T}$$

where

Pr = Standard state pressure (=1 bar).

T = Temperature in Kelvin

${}^{o}H_{i,Pr,T}$ = Standard molal enthalpy of ith component at Pr and T.

${}^{o}S_{i,Pr,T}$ = Standard molal entropy of ith component at Pr and T.

Standard state heat capacity of component i is given by

$${}^{o}Cp_{i} = a + bT + (c/T^{2}) + (d/T^{0.5})$$

Standard molal enthalpy and entropy of ith mineral component at Pr and T are expressed as:

$$(IIA.2) \quad {}^{o}H_{i,Pr,T} = {}^{o}H_{i,Pr,Tr} + a(T-Tr) + 0.5b(T^{2}-Tr^{2}) - c(1/T-1/Tr) + 2d(T^{0.5}-Tr^{0.5})$$

$$(IIA.3) \quad {}^{o}S_{i,Pr,T} = {}^{o}S_{i,Pr,Tr} + a\ln(T/Tr) + b(T-Tr) - 0.5c(1/T^{2}-1/Tr^{2}) - 2d(1/T^{0.5}-1/Tr^{0.5})$$

Reproduced with permission of the copyright owner. Further reproduction prohibited without permission.

respectively, where

$H^{o}_{i,Pr,Tr}$ =Standard molal enthalpy of ith mineral componet at Pr and Tr.

$S^{o}_{i,Pr,Tr}$ =Standard molal entropy of ith mineral component at Pr and Tr.

a,b,c,d =Standard molal heat capacity coefficients.

Tr =Standard state temperature (=298.15 ^{o}K).

Standard molal enthalpy and entropy of ith melt component at Pr and T are expressed as:

$$(IIA.4)\quad H^{o}_{i,Pr,T}=H^{o}_{i,Pr,Tr}+a(Tm-Tr)+0.5b(Tm^{2}-Tr^{2})-c(1/Tm-1/Tr)+2d(Tm^{0.5}-Tr^{0.5})+H^{fusion}_{i,Tm,Tr}+Cp_{i}(T-Tm_{i})$$

$$(IIA.5)\quad S^{o}_{i,Pr,T}=S^{o}_{i,Pr,Tr}+a\ln(Tm/Tr)+b(Tm-Tr)-0.5c(1/Tm^{2}-1/Tr^{2})-2d(1/Tm^{0.5}-1/Tr^{0.5})+S^{fusion}_{i,Tm,Pr}+Cp_{i}\ln(T/Tm_{i})$$

respectively, where

$H^{o}_{i,Pr,Tr}$=Standard molal enthalpy of ith melt component at Pr and Tr.

$S^{o}_{i,Pr,Tr}$=Standard molal entropy of ith melt component at Pr and Tr.

$S^{fusion}_{i,Tm,Tr}$=Entropy of fusion of i th melt component.

Tm=Melting temperature.

Cp_{i}=Heat capacity of i th melt component.

Reproduced with permission of the copyright owner. Further reproduction prohibited without permission.

a,b,c,d =Standard molal heat capacity coefficients.

$^{fusion}H_{i,Tm,Tr}$ is the enthalpy of fusion of ith melt component defined as:

$$(IIA.6) \quad {}^{fusion}H_{i,Tm,Tr} = Tm * {}^{fusion}S_{i,Tm,Tr}$$

Values of these variables are listed in Table II.A1 and Table II.A2.

Reproduced with permission of the copyright owner. Further reproduction prohibited without permission.

Table II.A1. Standard state thermodynamic data for mineral components.

COMPONENT	H_i^o (Tr,Pr) (cal)	S_i^o (cal/mol-K)	$Cp_i^o = a + bT + (c/T^2) + (d/T^{0.5})$ a	b	c	d
Mg_2SiO_4 Forsterite	-518350	22.75	54.489	8.1594E-4	-213660	-416.97
Fe_2SiO_4 Fayalite	-352370	35.45	36.510	9.3600E-3	-670000	0.0
$CaMgSi_2O_6$ Diopside	-767390	34.20	52.870	7.8400E-3	-1570000	0.0
$Mg_2Si_2O_6$ C-Enstatite	-739482	32.44	98.260	-6.1166E-3	570080	-1098.32
$Fe_2Si_2O_6$ C-Ferrosilite	-569468	47.32	42.000	1.8000E-2	0.0	0.0
$MgSiO_3$ Enstatite	-369921	16.22	49.130	-3.0583E-3	285040	-549.16
$FeSiO_3$ Ferrosilite	-284734	23.66	21.000	9.0000E-3	0.0	0.0
$CaAl_2Si_2O_8$ Anorthite	-1013700	47.63	63.311	1.4794E-4	-1544000	0.0
$NaAlSi_3O_8$ Albite	-938700	54.11	67.329	8.9172E-3	-2035400	0.0
$KAlSi_3O_8$ Sanidine	-943919	55.66	65.908	1.0209E-2	-1932400	0.0
$NaAlSiO_4$ Nepheline	-500241	29.72	35.908	6.4580E-3	-732800	0.0
$KAlSiO_4$ Kalsilite	-509408	31.85	29.430	1.7360E-2	-532000	0.0
$KAlSi_2O_6$ Leucite	-728830	34.16	46.958	6.6123E-3	2930400	0.0
$NaAlSi_2O_6$ Dehydrated Analcime	-714678	41.90	42.090	2.4140E-2	-888000	0.0

* Data is after Ghiorso et al. (1983,1985) Analcime, nepheline and kalsilite data after Helgeson et al. (1978).

Reproduced with permission of the copyright owner. Further reproduction prohibited without permission.

Table II.A2. Standard state thermodynamic data for melt components.

COMPONENT	H_i^o (cal) (Tr,Pr)	S_i^o (cal/mol-K) (Tr,Pr)	$Cp_i^o = a + bT + (c/T^2) + (d/T^{0.5})$ (cal/mol-K) a	b	c	d
Si_4O_8	-867448	48.61	69.556	1.2432E-3	-3950300	0.0
Ti_4O_8	-909543	48.08	60.304	1.0810E-2	-942890	-5.3692
$Al_{16/3}O_8$	-1069406	32.45	100.293	4.5827E-4	-1209000	-629.7300
$Cr_{16/3}O_8$	-723200	51.73	75.856	6.0525E-4	-918990	-2.1698
$Fe_{16/3}O_8$	-563990	80.99	-698.320	1.7379E-1	-6525900	21644.00
$Fe_4Si_2O_8$	-704730	70.90	73.020	1.8720E-2	-134000	0.0
$Mn_4Si_2O_8$	-826038	78.02	78.510	7.4953E-3	-1822900	0.0
$Mg_4Si_2O_8$	-1036701	45.50	108.977	1.6319E-3	-427330	-833.94
$Ca_4Si_2O_8$	-1109070	36.44	98.000	0.0	0.0	0.0
$Na_{16/3}Si_{8/3}O_8$	-987623	72.56	83.040	2.5600E-2	-1725300	0.0
$K_{16/3}Si_{8/3}O_8$	-990064	93.15	79.280	4.4933E-2	-954670	0.0
$P_{16/5}O_8$	-575488	44.18	13.400	8.6402E-2	0.0	0.0

* Data is after Ghiorso et al. (1983,1985).

Reproduced with permission of the copyright owner. Further reproduction prohibited without permission.

Table II.A2. Standard state thermodynamic data for melt components, cont.

COMPONENT	(K) Tm	(cal/mol-K) S^{fusion}	Cp_i^o
Si_4O_8	1996.00	3.908	83.16
Ti_4O_8	2143.00	39.200	106.96
$Al_{16/3}O_8$	2327.00	32.080	65.71
$Cr_{16/3}O_8$	2603.00	31.760	100.00
$Fe_{16/3}O_8$	1895.00	34.800	122.27
$Fe_4Si_2O_8$	1490.00	29.570	114.60
$Mn_4Si_2O_8$	1620.00	26.460	116.20
$Mg_4Si_2O_8$	2163.00	37.610	128.06
$Ca_4Si_2O_8$	2403.00	20.810	118.96
$Na_{16/3}Si_{8/3}O_8$	1362.00	24.240	113.01
$K_{16/3}Si_{8/3}O_8$	1249.00	25.620	114.67
$P_{16/5}O_8$	853.00	10.680	93.60

* Data is after Ghiorso et al. (1983,1985).

Reproduced with permission of the copyright owner. Further reproduction prohibited without permission.

APPENDIX II.B

Adapted activity formulations of mineral components

Reproduced with permission of the copyright owner. Further reproduction prohibited without permission.

Activity-composition relations in the solid (mineral) solutions are expressed using mixing on site(s) model. For minerals olivine, plagioclase, nepheline, and leucite mixing on a single site is considered. According to this model, activity of i th component in the j th mineral defined as:

$$a_i^j = \left(X_i^s \gamma_i^s\right)^c \qquad \text{(II.B1)}$$

where, c is the stoichiometric number of s th site occupied by i th atom in one mole of the i th component. γ_i^s is the activity coefficient of i th atom in the s th site. X_i^s is the mole fraction of the i th atom in the s th site, expressed as:

$$X_i^s = \frac{n_i^s}{\sum_{i=1}^{ns} n_i^s} \qquad \text{(II.B2)}$$

where

n_i^s=Number of i atom in the mineral formula per s th site.

ns=Number of atoms in the s th site.

For ideal mixing of atoms in a site ($\gamma_i^s=1$) eq. (II.B1) reduces to,

Reproduced with permission of the copyright owner. Further reproduction prohibited without permission.

$$a_i^j = (X_i^{sc})^c \qquad \text{(II.B3)}$$

Using equation (II.B3), activities of the end-member components of olivine, plagioclase, nepheline, and leucite minerals are formulated as follows:

Olivine :

$$a_{Fo} = (X_{Mg}^{OL\ oct})^2 \qquad a_{Fa} = (X_{Fe}^{OL\ oct})^2$$

Plagioclase :

$$a_{An} = (X_{Ca}^{PL\ A}) \qquad a_{Ab} = (X_{Na}^{PL\ A}) \qquad a_{Sn} = (X_K^{PL\ A})$$

Nepheline :

$$a_{Ne} = (X_{Na}^{NE\ A}) \qquad a_{Ks} = (X_K^{NE\ A})$$

Leucite :

$$a_{Da} = (X_{Na}^{LC\ A}) \qquad a_{Le} = (X_K^{LC\ A})$$

For clinopyroxene and orthopyroxene, mixing on a multisite model is adapted. According to this model, activity of i th component in the j th mineral is defined as:

$$a_i^j = \gamma_i^j \prod_{i=1}^{sn} (X_i^{sc}) \qquad \text{(II.B4)}$$

Reproduced with permission of the copyright owner. Further reproduction prohibited without permission.

where

sn=Number of sites in the i th component of j th mineral.

γ_i^j is the ionic activity coefficient of the i th component in the j th mineral, defined as:

$$\text{(II.B5)} \qquad \gamma_i^j = \gamma_i^r \prod_{i=1}^{sn} \gamma_i^s$$

where

γ_i^s=Site activity coefficient of the i th atom in the s th site.

γ_i^r=Reciprocal activity coefficient of the i th component in the j th mineral.

Reciprocal avtivity coefficient is expressed as:

$$\text{(II.B6)} \qquad \gamma_i^r = EXP[(+/-)(G_{Re}/RT) \prod_{i=1}^{sn} (1-X_i)^s$$

Where G_{Re} is the standard free energy change of the reciprocal (site) reaction. The sign of the exponential term is positive for the reactant components negative for the product components in the reciprocal reaction. For detailed explanation of these parameters see Wood and Nicholls (1978).

For ideal interaction within individual sites ($\gamma_i^s=1$) and for ideal interaction between the sites in a given

Reproduced with permission of the copyright owner. Further reproduction prohibited without permission.

mineral (G_{Re}=0.0), then activity of the ith component in the j th mineral reduces to

$$a_i^j = \prod_{i=1}^{sn} X_i^s \qquad \text{(II.B7)}$$

Using equation (II.B7), activities of the end-member components of clinopyroxene and orthopyroxene minerals are formulated as follows:

Clinopyroxene:

Clinopyroxene composition is defined in quadrilateral using Di-Cen-Cfs-Hd end-member components. Since the chemical potentials of Di-Cen-Cfs-Hd components in clinopyroxene are not mutually independent and they are linearly dependent one each other through reciprocal reaction, it is assumed that whenever Di-Cen-Cfs components are in equilibrium in clinopyroxene, Hd component is also in equilibrium with these components (G_{Re}=0). And ideal activity relations for Di-Cen-Cfs are expressed as follows:

$$a_{Di}^{cpx} = X_{Ca}^{M2} * X_{Mg}^{M1} \qquad a_{C\text{-}en}^{cpx} = X_{Mg}^{M2} * X_{Mg}^{M1} \qquad a_{C\text{-}fs}^{cpx} = X_{Fe}^{M2} * X_{Fe}^{M1}$$

where

$$X_{Mg}^{M1} = 1 - X_{Fe}^{M1} \qquad X_{Fe}^{M2} = 1 - X_{Ca}^{M2} - X_{Mg}^{M2}$$

Reproduced with permission of the copyright owner. Further reproduction prohibited without permission.

Given site mole fractions in clinopyroxene formulae are related to molecular mole fractions of $X_{Ca2Si2O6}$ ($=X_{Ca}$) $X_{Fe2Si2O6}$ ($=X_{Fe}$), and $X_{Mg2Si2O6}$ ($=X_{Mg}$) as follows:

$$X_{Ca}=2*X_{Ca}^{M2} \quad ; \quad X_{Mg}+X_{Mg}=2*X_{Mg}^{M1\ M2} \quad ; \quad X_{Fe}+X_{Fe}=2*X_{Fe}^{M1\ M2}$$

Distribution of the cations in the sites is calculated from following equation:

$$\frac{X_{Mg}^{M2}\ X_{Fe}^{M1}}{X_{Mg}^{M1}\ X_{Fe}^{M2}}=EXP(-G_E^{cpx}/RT) \qquad \text{(II.B8)}$$

G_E^{cpx} is the standard free energy for intercrystalline ion-exchange in clinopyroxene. Value for this parameter is taken from Mc Callister et al.(1976) where it is given as:

$$G_E^{cpx}=3246.176-T*0.737906 \quad \text{(units are in cal/mol-K)}$$

T=temperature in Kelvin.

Orthopyroxene:

Assuming again $\gamma_i^s=1$ and $G_{Re}=0.0$, ideal activity relations of orthopyroxene components expressed as :

$$a_{En}^{opx}=(X_{Mg}^{M2}*X_{Mg}^{M1})^{0.5} \qquad a_{Fs}^{opx}=(X_{Fe}^{M2}*X_{Fe}^{M1})^{0.5}$$

Reproduced with permission of the copyright owner. Further reproduction prohibited without permission.

where

$$X_{Mg}^{M1}=1-X_{Fe}^{M1} \qquad X_{Fe}^{M2}=1-X_{Mg}^{M2}$$

Given site mole fractions in orthopyroxene formulae are related to molecular mole fractions of $X_{Mg2Si2O6}$ ($=X_{Mg}$) and $X_{Fe2Si2O6}$ ($=X_{Fe}$) as follows:

$$X_{Mg}^{M1}+X_{Mg}^{M2}=2*X_{Mg} \; ; \; X_{Fe}^{M1}+X_{Fe}^{M2}=2*X_{Fe}$$

Distribution of the cations in the sites is calculated from following equation:

$$\text{(II.B9)} \qquad \frac{X_{Mg}^{M2} X_{Fe}^{M1}}{X_{Mg}^{M1} X_{Fe}^{M2}}=EXP(-G_E^{opx}/RT)$$

where G_E^{opx} is the standard free energy for intercrystalline ion-exchange in orthopyroxene. Value for this parameter is taken from Ganguly (1982) where it is reported as:

$$G_E^{opx}=3103.723-T*0.285172 \qquad \text{(units are in cal/mol-K)}$$

T=temperature in Kelvin.

Reproduced with permission of the copyright owner. Further reproduction prohibited without permission.

APPENDIX II.C

Model Parameters

Reproduced with permission of the copyright owner. Further reproduction prohibited without permission.

Table II.C1. Modeled melt-mineral reactions.

R1) Melt = Forsterite

$0.5\ Mg_4Si_2O_8 = Mg_2SiO_4$

R2) Melt = Fayalite

$0.5\ Fe_4Si_2O_8 = Fe_2SiO_4$

R3) Melt = Clino-enstatite

$0.5\ Mg_4Si_2O_8 + 0.25\ Si_4O_8 = Mg_2Si_2O_6$

R4) Melt = Clino-ferrosillite

$0.5\ Fe_4Si_2O_8 + 0.25\ Si_4O_8 = Fe_2Si_2O_6$

R5) Melt = Diopside

$0.25\ Ca_4Si_2O_8 + 0.25\ Mg_4Si_2O_8 + 0.25\ Si_4O_8 = CaMgSi_2O_6$

R6) Melt = Ortho-enstatite

$0.25\ Mg_4Si_2O_8 + 0.125\ Si_4O_8 = MgSiO_3$

R7) Melt = Ortho-ferrosillite

$0.25\ Fe_4Si_2O_8 + 0.125\ Si_4O_8 = FeSiO_3$

R8) Melt = Anorthite

$0.25\ Ca_4Si_2O_8 + 0.375\ Al_{16/3}O_8 + 0.375\ Si_4O_8 = CaAl_2Si_2O_8$

R9) Melt = Albite

$0.1875\ Na_{16/3}Si_{8/3}O_8 + 0.1875\ Al_{16/3}O_8 + 0.625\ Si_4O_8 = NaAlSi_3O_8$

R10) Melt = Sanidine

$0.1875\ K_{16/3}Si_{8/3}O_8 + 0.1875\ Al_{16/3}O_8 + 0.625\ Si_4O_8 = KAlSi_3O_8$

R11) Melt = Nepheline

$0.1875\ Na_{16/3}Si_{8/3}O_8 + 0.1875\ Al_{16/3}O_8 + 0.125\ Si_4O_8 = NaAlSiO_4$

R12) Melt = Kalsilite

$0.1875\ K_{16/3}Si_{8/3}O_8 + 0.1875\ Al_{16/3}O_8 + 0.125\ Si_4O_8 = KAlSiO_4$

R13) Melt = Leucite

$0.1875\ K_{16/3}Si_{8/3}O_8 + 0.1875\ Al_{16/3}O_8 + 0.375\ Si_4O_8 = KAlSi_2O_6$

R14) Melt = Dehydrated analcime

$0.1875\ Na_{16/3}Si_{8/3}O_8 + 0.1875\ Al_{16/3}O_8 + 0.375\ Si_4O_8 = NaAlSi_2O_6$

Reproduced with permission of the copyright owner. Further reproduction prohibited without permission.

Table II.C2. Regressed melt-mineral REX coefficients.

	C_1	C_2	C_3
R1	-518350	165.40511	37.15095
R2	-352370	97.21134	28.75716
R3	-739482	228.67559	53.99478
R4	-569468	175.21113	42.77422
R5	-767390	234.47932	56.46490
R6	-369921	117.21210	26.87629
R7	-284734	83.69810	22.89502
R8	-1013700	318.04967	72.21256
R9	-938700	277.06206	70.55802
R10	-943919	264.15400	72.78905
R11	-500241	153.25671	36.05626
R12	-509408	145.24978	37.70139
R13	-728830	224.30565	52.48657
R14	-714678	211.82844	53.01777

Reproduced with permission of the copyright owner. Further reproduction prohibited without permission.

Table II.C2. Regressed REX coefficients, cont.

Following coefficients are the same in all reactions:

C_4=-0.21813	
CN_1= -2.86715	CD_1= 4
CN_2= -5.73429	CD_2= 4
CN_3= 16.53672	CD_3=1/0.375
CN_4= -5.73429	CD_4=1/0.375
CN_5= 18.23947	CD_5=2/0.375
CN_6= 16.54675	CD_6=6
CN_7= -1.43357	CD_7=6
CN_8= 20.31199	CD_8=6
CN_9= -1.72603	CD_9=6
CN_{10}= -9.44395	CD_{10}=2/0.375
CN_{11}=-11.16501	CD_{11}=2/0.375
CN_{12}= -5.73429	CD_{12}=1.6
CN_{13}= 5.73429	

Reproduced with permission of the copyright owner. Further reproduction prohibited without permission.

APPENDIX II.D

Numerical programming procedure applied to open oxygen system multiple saturation calculations of olivine, clinopyroxene, plagioclase, and leucite

Reproduced with permission of the copyright owner. Further reproduction prohibited without permission.

Thermodynamic equilibrium condition between the minerals olivine-, clinopyroxene-, plagioclase-, leucite- and a melt defines thirty-nine variables in a system that iron is open to oxygen exchange with its surroundings.

- 12 variables are the compositions of initial melt components.
- 1 variable is the amount of initial melt.
- 12 variables are the compositions of residual melt components that are in equilibrium with saturated minerals.
- 1 variable is the amount of residual melt.
- 4 variables are the amounts of minerals.
- 6 variables are the compositions of minerals.
- 2 variables are pressure and temperature.
- 1 variable is the oxygen fugacity in the system.

Since equilibrium crystallization calculations is performed at a given pressure, temperature, and f_{O2}, these variables are fixed. Thus, twelve component system with unknown ferric and ferrous iron concentration ratio requires (39-12-3=24) twenty-four linearly independent equations for the solution of the equilibrium state of defined magmatic system. Thirteen of these equations come from the conservation of mass in the system. Ten of remaining eleven equations come from the thermodynamic equilibrium reactions between the end-member components

Reproduced with permission of the copyright owner. Further reproduction prohibited without permission.

of the minerals and coexisting components of the melt phase. The last equation is the one that determines oxidation state of iron concentration in the melt phase. Because these calculations were performed at oxygen buffer QFM, Sack et al. (1980) equation was used as twentyfourth equation. The functions used to describe the equilibrium state of magmatic system are as follows:

```
f(1)=x(13)*x(1)+0.25*x(19)*{x(20)+[1-x(20)-x(21)]+x(21)}
     +x(16)*{0.375*x(17)+0.625*x(18)+0.625*[1-x(17)
     -x(18)]}+0.375*x(22)*{x(23)+[1-x(23)]}-NB(1)    =0.0

f(2)=x(13)*x(2)-NB(2)                                =0.0

f(3)=x(13)*x(3)+x(16)*{0.375*x(17)+0.1875*x(18)+0.1875
     *[1-x(17)-x(18)]}+0.1875*x(22)*{x(23)+[1-x(23)]}
     -NB(3)                                          =0.0

f(4)=x(13)*x(4)-NB(4)                                =0.0

f(5)=x(13)*x(5)-x(24)                                =0.0

f(6)=x(13)*x(6)+0.5*{x(14)*[1-x(15)]+x(19)*x(21)}
     -0.25*NBFEOT+(1/0.375)*x(24)                    =0.0

f(7)=x(13)*x(7)-NB(7)                                =0.0

f(8)=x(13)*x(8)+0.5*{x(14)*x(15)+x(19)*x(20)}
     +0.25*x(19)*[1-x(20)-x(21)]-NB(8)               =0.0

f(9)=x(13)*x(9)+0.25*{x(19)*[1-x(20)-x(21)]+x(16)
     *x(17)}-NB(9)                                   =0.0
f(10)=x(13)*x(10)+0.1875*{x(16)*x(18)+x(22)*[1-x(23)]}
      -NB(10)                                        =0.0
f(11)=x(13)*x(11)+0.1875*{x(16)*[1-x(17)-x(18)]+x(22)
      *x(23)}-NB(11)                                 =0.0

f(12)=x(13)*x(12)-NB(12)                             =0.0

f(13)=x(1)+x(2)+x(3)+x(4)+x(5)+x(6)+x(7)+x(8)+x(9)+
                              x(10)+x(11)+x(12)-1=0.0
```


Reproduced with permission of the copyright owner. Further reproduction prohibited without permission.

f(14)=R1 (forsterite-melt reaction) =0.0

f(15)=R2 (fayalite-melt reaction) =0.0

f(16)=R8 (anorthite-melt reaction) =0.0

f(17)=R9 (albite-melt reaction) =0.0

f(18)=R10 (sanidine-melt reaction) =0.0

f(19)=R3 (c-enstatite-melt reaction) =0.0

f(20)=R4 (c-ferrosilite-melt reaction) =0.0

f(21)=R5 (diopside-melt reaction) =0.0

f(22)=R13 (leucite-melt reaction) =0.0

f(23)=R14 (dehyd. analcime-melt reaction) =0.0

f(24)=Sack et. al. (1980) eq. =0.0

where known variables are:

NB(i)=Number of moles of bulk components (initial melt composition) (i=1 to 12).

NBFEOT=Total iron concentration in bulk.

and unknown variables are;

i=1 to 12, x(i) =Mole fractions of melt components (residual melt composition).

x(13)=Total number of moles of melt components.

x(14)=Total number of moles of olivine.

x(15)=Mole fraction of forsterite component in olivine.

[1-x(15)]=Mole fraction of fayalite component in olivine.

x(16)=Total number of moles of plagioclase.

x(17)=Mole fraction of anorthite component in plagioclase.

Reproduced with permission of the copyright owner. Further reproduction prohibited without permission.

x(18)=Mole fraction of albite component in plagioclase.

[1-x(17)-x(18)]=Mole fraction of sanidine component in plagioclase.

x(19)=Total number of moles of clinopyroxene.

x(20)=Mole fraction of c-enstatite component in clinopyroxene ($=X_{Mg}-X_{Ca}$).

x(21)=Mole fraction of c-ferrosilite component in clinopyroxene ($=X_{Fe}$).

[1-x(20)-x(21)]=Mole fraction of diopside component in clinopyroxene ($=2*X_{Ca}$).

x(22)=Total number of moles of leucite.

x(23)=Mole fraction of leucite component in leucite.

[1-x(23)]=Mole fraction of dehyd. analcime component in leucite.

x(24)=Ferric iron concentration in bulk under given temperature and f_{O2} conditions.

The non-linear system with twentyfour unknowns needed to be solved simultaneously. Newton-Raphson method for the systems of non-linear equations was used for the numerical solution of these equations. Numerical algorithm used in the calculations is given in Table II.D1. Jacobian matrix (partial differentials of functions with respect to unknowns) inversions were performed using LU decomposition subroutines given in Press et al. 1986.

Outputs of the equilibrium crystallization calculations are given in the following pages.

Reproduced with permission of the copyright owner. Further reproduction prohibited without permission.

Table II.D1. Numerical algorithm used for equilibrium crystallization calculations.

STEP 1 INPUT initial guess vector for n unknowns

[X] $(x_1,.....,x_n)$

for iter=1 to itmax

STEP 2 calculate [F(x)] vector at [X(x)]

STEP 3 calculate Jacobian matrix [J(x)] which is partial differentials of functions with respect to unknowns [X].

STEP 4 solve for [Y] vector $[Y]=-[F(x)]*[J(x)]^{-1}$

STEP 5 set [X]=[X]+[Y]

STEP 6 if SUM |[Y]| < TOL then OUTPUT [X] STOP

next iter

STEP 7 OUTPUT "maximum number of iterations exceeded" STOP

---

where

[X]=solution vector
[F]=function vector
[J]=Jacobian matrix
TOL=tolerance value for changes in [X] (1.0E-5).
itmax=maximum number of iterations.

Reproduced with permission of the copyright owner. Further reproduction prohibited without permission.

SACK BS-501 #13

COMPOSITION OF INITIAL LIQUID PHASE (Wt%)

SiO2	TiO2	Al2O3	Cr2O3	Fe2O3	FeO	MnO	MgO	CaO	Na2O	K2O	P2O5
49.48	1.60	13.51	0.00	2.84	5.36	0.15	9.80	9.07	2.78	3.69	0.99

Total grams= 99.27

****

Equilibrium T (in celcius)= 1116 ln fO2=-22.08179

****

COMPOSITION OF RESIDUAL LIQUID PHASE (Wt%)

SiO2	TiO2	Al2O3	Cr2O3	Fe2O3	FeO	MnO	MgO	CaO	Na2O	K2O	P2O5
50.79	3.31	16.86	0.00	1.00	4.41	0.31	4.94	7.60	4.98	3.74	2.05

Total grams= 48.31018

COMPOSITION OF SOLID PHASES (Wt%)

OLIVINE

38.27	0.00	0.00	0.00	0.00	23.66	0.00	38.08	0.00	0.00	0.00	0.00

Components	Grams	Moles	Mole Frac.
FORSTERITE	8.28973	0.05891	0.74150
FAYALITE	4.18524	0.02054	0.25850
TOTAL	12.47497	0.07945	1.00000

HIGH-CALCIUM PYROXENE

53.45	0.00	0.00	0.00	0.00	10.70	0.00	14.53	21.33	0.00	0.00	0.00

Components	Grams	Moles	Mole Frac.
DIOPSIDE	15.08936	0.06968	0.85504
C-ENSTATI	-0.36680	-0.00183	-0.02242
C-FERROSI	3.59905	0.01364	0.16738
TOTAL	18.32160	0.08149	1.00000

PLAGIOCLASE

49.47	0.00	32.37	0.00	0.00	0.00	0.00	0.00	15.16	2.77	0.22	0.00

Components	Grams	Moles	Mole Frac.
ANORTHITE	7.38730	0.02655	0.74164
ALBITE	2.57501	0.00878	0.24529
SANIDINE	0.15236	0.00047	0.01308
TOTAL	10.11467	0.03580	1.00000

LEUCITE

55.38	0.00	23.49	0.00	0.00	0.00	0.00	0.00	0.00	1.10	20.03	0.00

Components	Grams	Moles	Mole Frac.
LEUCITE	10.49858	0.03956	0.92267
ANALCIME	0.77299	0.00332	0.07733
TOTAL	11.27157	0.04288	1.00000

Reproduced with permission of the copyright owner. Further reproduction prohibited without permission.

SACK BS-501 #20

COMPOSITION OF INITIAL LIQUID PHASE (Wt%)

SiO2	TiO2	Al2O3	Cr2O3	Fe2O3	FeO	MnO	MgO	CaO	Na2O	K2O	P2O5
49.48	1.60	13.51	0.00	2.84	5.36	0.15	9.80	9.07	2.78	3.69	0.99

Total grams= 99.27

****

Equilibrium T (in celcius)= 1092.5 ln fO2=-22.91072

****

COMPOSITION OF RESIDUAL LIQUID PHASE (Wt%)

SiO2	TiO2	Al2O3	Cr2O3	Fe2O3	FeO	MnO	MgO	CaO	Na2O	K2O	P2O5
50.08	4.65	17.58	0.00	0.88	3.69	0.44	4.35	5.94	6.21	3.31	2.88

Total grams= 34.38384

COMPOSITION OF SOLID PHASES (Wt%)

OLIVINE

37.82	0.00	0.00	0.00	0.00	26.05	0.00	36.13	0.00	0.00	0.00	0.00

Components	Grams	Moles	Mole Frac.
FORSTERITE	8.60079	0.06113	0.71200
FAYALITE	5.03847	0.02473	0.28800
TOTAL	13.63926	0.08585	1.00000

HIGH-CALCIUM PYROXENE

53.40	0.00	0.00	0.00	0.00	10.84	0.00	14.37	21.38	0.00	0.00	0.00

Components	Grams	Moles	Mole Frac.
DIOPSIDE	19.40876	0.08962	0.85813
C-ENSTATI	-0.58628	-0.00292	-0.02796
C-FERROSI	4.68020	0.01774	0.16983
TOTAL	23.50268	0.10444	1.00000

PLAGIOCLASE

51.02	0.00	31.31	0.00	0.00	0.00	0.00	0.00	13.92	3.43	0.32	0.00

Components	Grams	Moles	Mole Frac.
ANORTHITE	9.93337	0.03570	0.67872
ALBITE	4.67182	0.01593	0.30288
SANIDINE	0.31493	0.00097	0.01840
TOTAL	14.92012	0.05261	1.00000

LEUCITE

55.40	0.00	23.50	0.00	0.00	0.00	0.00	0.00	0.00	1.20	19.89	0.00

Components	Grams	Moles	Mole Frac.
LEUCITE	14.12606	0.05323	0.91571
ANALCIME	1.14235	0.00490	0.08429
TOTAL	15.26841	0.05813	1.00000

Reproduced with permission of the copyright owner. Further reproduction prohibited without permission.

SACK 94-08 #13

COMPOSITION OF INITIAL LIQUID PHASE (Wt%)

SiO2	TiO2	Al2O3	Cr2O3	Fe2O3	FeO	MnO	MgO	CaO	Na2O	K2O	P2O5
47.84	1.24	17.90	0.00	1.88	6.21	0.17	3.87	8.68	2.78	7.43	0.92

Total grams= 98.92

****

Equilibrium T (in celcius)= 1116 ln fO2=-22.08179

****

COMPOSITION OF RESIDUAL LIQUID PHASE (Wt%)

SiO2	TiO2	Al2O3	Cr2O3	Fe2O3	FeO	MnO	MgO	CaO	Na2O	K2O	P2O5
44.37	2.26	19.43	0.00	1.69	8.24	0.31	3.65	9.13	4.39	4.86	1.68

Total grams= 54.87915

COMPOSITION OF SOLID PHASES (Wt%)

OLIVINE

37.56	0.00	0.00	0.00	0.00	27.43	0.00	35.01	0.00	0.00	0.00	0.00

Components	Grams	Moles	Mole Frac.
FORSTERITE	0.10056	0.00071	0.69465
FAYALITE	0.06402	0.00031	0.30535
TOTAL	0.16458	0.00103	1.00000

HIGH-CALCIUM PYROXENE

53.03	0.00	0.00	0.00	0.00	12.38	0.00	13.40	21.19	0.00	0.00	0.00

Components	Grams	Moles	Mole Frac.
DIOPSIDE	11.03798	0.05097	0.85627
C-ENSTATI	-0.61570	-0.00307	-0.05151
C-FERROSI	3.06658	0.01162	0.19524
TOTAL	13.48886	0.05953	1.00000

PLAGIOCLASE

48.74	0.00	32.86	0.00	0.00	0.00	0.00	0.00	15.74	2.44	0.21	0.00

Components	Grams	Moles	Mole Frac.
ANORTHITE	4.02092	0.01445	0.77105
ALBITE	1.19011	0.00406	0.21654
SANIDINE	0.07573	0.00023	0.01242
TOTAL	5.28677	0.01874	1.00000

LEUCITE

55.36	0.00	23.48	0.00	0.00	0.00	0.00	0.00	0.00	1.03	20.13	0.00

Components	Grams	Moles	Mole Frac.
LEUCITE	26.77726	0.10091	0.92771
ANALCIME	1.83324	0.00786	0.07229
TOTAL	28.61050	0.10878	1.00000

Reproduced with permission of the copyright owner. Further reproduction prohibited without permission.

SACK 9418 #6A

COMPOSITION OF INITIAL LIQUID PHASE (Wt%)

SiO2	TiO2	Al2O3	Cr2O3	Fe2O3	FeO	MnO	MgO	CaO	Na2O	K2O	P2O5
48.02	0.99	17.87	0.00	2.50	5.36	0.15	3.99	8.43	2.75	7.90	0.82

Total grams= 98.78001

****

Equilibrium T (in celcius)= 1133 ln fO2=-21.48312

****

COMPOSITION OF RESIDUAL LIQUID PHASE (Wt%)

SiO2	TiO2	Al2O3	Cr2O3	Fe2O3	FeO	MnO	MgO	CaO	Na2O	K2O	P2O5
46.49	1.51	17.41	0.00	1.64	7.44	0.23	4.47	10.53	3.74	5.27	1.25

Total grams= 65.51444

COMPOSITION OF SOLID PHASES (Wt%)

OLIVINE

38.14	0.00	0.00	0.00	0.00	24.34	0.00	37.52	0.00	0.00	0.00	0.00

Components	Grams	Moles	Mole Frac.
FORSTERITE	0.83173	0.00591	0.73312
FAYALITE	0.43850	0.00215	0.26688
TOTAL	1.27023	0.00806	1.00000

HIGH-CALCIUM PYROXENE

53.22	0.00	0.00	0.00	0.00	11.63	0.00	13.92	21.24	0.00	0.00	0.00

Components	Grams	Moles	Mole Frac.
DIOPSIDE	3.44078	0.01589	0.85503
C-ENSTATI	-0.14101	-0.00070	-0.03779
C-FERROSI	0.89609	0.00340	0.18276
TOTAL	4.19587	0.01858	1.00000

PLAGIOCLASE

48.01	0.00	33.37	0.00	0.00	0.00	0.00	0.00	16.33	2.13	0.17	0.00

Components	Grams	Moles	Mole Frac.
ANORTHITE	3.16072	0.01136	0.80124
ALBITE	0.78529	0.00268	0.18888
SANIDINE	0.04560	0.00014	0.00988
TOTAL	3.99161	0.01418	1.00000

LEUCITE

55.34	0.00	23.48	0.00	0.00	0.00	0.00	0.00	0.00	0.97	20.21	0.00

Components	Grams	Moles	Mole Frac.
LEUCITE	25.02723	0.09432	0.93190
ANALCIME	1.60682	0.00689	0.06810
TOTAL	26.63404	0.10121	1.00000

Reproduced with permission of the copyright owner. Further reproduction prohibited without permission.

SACK K-14 #13

COMPOSITION OF INITIAL LIQUID PHASE (Wt%)

SiO2	TiO2	Al2O3	Cr2O3	Fe2O3	FeO	MnO	MgO	CaO	Na2O	K2O	P2O5
45.51	2.10	16.93	0.00	2.30	6.43	0.19	7.06	10.72	4.09	2.18	0.48

Total grams= 97.99001

****

Equilibrium T (in celcius)= 1116 ln fO2=-22.08179

****

COMPOSITION OF RESIDUAL LIQUID PHASE (Wt%)

SiO2	TiO2	Al2O3	Cr2O3	Fe2O3	FeO	MnO	MgO	CaO	Na2O	K2O	P2O5
45.62	3.70	18.38	0.00	1.47	6.15	0.34	4.17	9.25	6.30	3.77	0.85

Total grams= 56.6992

COMPOSITION OF SOLID PHASES (Wt%)

OLIVINE

37.89	0.00	0.00	0.00	0.00	25.67	0.00	36.44	0.00	0.00	0.00	0.00

Components	Grams	Moles	Mole Frac.
FORSTERITE	5.47815	0.03893	0.71666
FAYALITE	3.13660	0.01539	0.28334
TOTAL	8.61475	0.05433	1.00000

HIGH-CALCIUM PYROXENE

53.22	0.00	0.00	0.00	0.00	11.55	0.00	13.89	21.34	0.00	0.00	0.00

Components	Grams	Moles	Mole Frac.
DIOPSIDE	9.23748	0.04266	0.85905
C-ENSTATI	-0.40339	-0.00201	-0.04046
C-FERROSI	2.37685	0.00901	0.18141
TOTAL	11.21094	0.04965	1.00000

PLAGIOCLASE

49.08	0.00	32.64	0.00	0.00	0.00	0.00	0.00	15.48	2.60	0.20	0.00

Components	Grams	Moles	Mole Frac.
ANORTHITE	15.30944	0.05503	0.75774
ALBITE	4.90782	0.01674	0.23048
SANIDINE	0.27841	0.00086	0.01178
TOTAL	20.49567	0.07262	1.00000

Reproduced with permission of the copyright owner. Further reproduction prohibited without permission.

SACK K-15 #20

COMPOSITION OF INITIAL LIQUID PHASE (Wt%)

SiO2	TiO2	Al2O3	Cr2O3	Fe2O3	FeO	MnO	MgO	CaO	Na2O	K2O	P2O5
48.50	1.49	18.86	0.00	2.78	5.74	0.22	3.28	8.26	5.85	3.01	0.45

Total grams= 98.44

****

Equilibrium T (in celcius)= 1092.5 ln fO2=-22.91072

****

COMPOSITION OF RESIDUAL LIQUID PHASE (Wt%)

SiO2	TiO2	Al2O3	Cr2O3	Fe2O3	FeO	MnO	MgO	CaO	Na2O	K2O	P2O5
49.06	2.26	17.30	0.00	1.85	7.28	0.33	3.00	6.17	7.62	4.44	0.68

Total grams= 65.98988

COMPOSITION OF SOLID PHASES (Wt%)

OLIVINE

36.99	0.00	0.00	0.00	0.00	30.48	0.00	32.53	0.00	0.00	0.00	0.00

Components	Grams	Moles	Mole Frac.
FORSTERITE	1.31048	0.00931	0.65539
FAYALITE	0.99794	0.00490	0.34461
TOTAL	2.30842	0.01421	1.00000

HIGH-CALCIUM PYROXENE

52.92	0.00	0.00	0.00	0.00	12.84	0.00	13.13	21.11	0.00	0.00	0.00

Components	Grams	Moles	Mole Frac.
DIOPSIDE	3.40375	0.01572	0.85469
C-ENSTATI	-0.21284	-0.00106	-0.05764
C-FERROSI	0.98476	0.00373	0.20295
TOTAL	4.17567	0.01839	1.00000

PLAGIOCLASE

51.04	0.00	31.29	0.00	0.00	0.00	0.00	0.00	13.91	3.44	0.32	0.00

Components	Grams	Moles	Mole Frac.
ANORTHITE	16.41304	0.05900	0.67784
ALBITE	7.74315	0.02641	0.30342
SANIDINE	0.53086	0.00163	0.01874
TOTAL	24.68705	0.08703	1.00000

Reproduced with permission of the copyright owner. Further reproduction prohibited without permission.

SACK SSC-1 #19

COMPOSITION OF INITIAL LIQUID PHASE (Wt%)

SiO2	TiO2	Al2O3	Cr2O3	Fe2O3	FeO	MnO	MgO	CaO	Na2O	K2O	P2O5
45.81	2.44	15.01	0.00	2.13	8.83	0.10	8.33	11.75	3.01	1.04	0.65

Total grams= 99.10001

****

Equilibrium T (in celcius)= 1121 ln fO2=-21.89758

****

COMPOSITION OF RESIDUAL LIQUID PHASE (Wt%)

SiO2	TiO2	Al2O3	Cr2O3	Fe2O3	FeO	MnO	MgO	CaO	Na2O	K2O	P2O5
44.49	4.89	18.64	0.00	1.68	8.17	0.20	3.91	9.51	5.18	2.03	1.30

Total grams= 49.91137

COMPOSITION OF SOLID PHASES (Wt%)

OLIVINE

37.73	0.00	0.00	0.00	0.00	26.55	0.00	35.73	0.00	0.00	0.00	0.00

Components	Grams	Moles	Mole Frac.
FORSTERITE	6.37542	0.04531	0.70575
FAYALITE	3.84963	0.01889	0.29425
TOTAL	10.22505	0.06420	1.00000

HIGH-CALCIUM PYROXENE

53.08	0.00	0.00	0.00	0.00	12.19	0.00	13.54	21.19	0.00	0.00	0.00

Components	Grams	Moles	Mole Frac.
DIOPSIDE	16.46027	0.07601	0.85545
C-ENSTATI	-0.84648	-0.00422	-0.04745
C-FERROSI	4.50128	0.01706	0.19200
TOTAL	20.11507	0.08885	1.00000

PLAGIOCLASE

48.68	0.00	32.92	0.00	0.00	0.00	0.00	0.00	15.80	2.44	0.17	0.00

Components	Grams	Moles	Mole Frac.
ANORTHITE	13.58950	0.04885	0.77411
ALBITE	3.99813	0.01364	0.21610
SANIDINE	0.20103	0.00062	0.00979
TOTAL	17.78865	0.06310	1.00000

Reproduced with permission of the copyright owner. Further reproduction prohibited without permission.

SACK SSC-2 #13

COMPOSITION OF INITIAL LIQUID PHASE (Wt%)

SiO2	TiO2	Al2O3	Cr2O3	Fe2O3	FeO	MnO	MgO	CaO	Na2O	K2O	P2O5
50.20	2.43	16.65	0.00	1.69	8.76	0.24	3.62	7.53	5.27	2.16	0.82

Total grams= 99.37

****

Equilibrium T (in celcius)= 1116 ln fO2=-22.08179

****

COMPOSITION OF RESIDUAL LIQUID PHASE (Wt%)

SiO2	TiO2	Al2O3	Cr2O3	Fe2O3	FeO	MnO	MgO	CaO	Na2O	K2O	P2O5
50.65	2.68	16.67	0.00	1.71	8.11	0.26	3.82	7.16	5.66	2.37	0.90

Total grams= 90.64152

COMPOSITION OF SOLID PHASES (Wt%)

OLIVINE

37.61	0.00	0.00	0.00	0.00	27.17	0.00	35.22	0.00	0.00	0.00	0.00

Components	Grams	Moles	Mole Frac.
FORSTERITE	-0.09426	-0.00067	0.69790
FAYALITE	-0.05909	-0.00029	0.30210
TOTAL	-0.15336	-0.00096	1.00000

HIGH-CALCIUM PYROXENE

53.06	0.00	0.00	0.00	0.00	12.39	0.00	13.55	21.00	0.00	0.00	0.00

Components	Grams	Moles	Mole Frac.
DIOPSIDE	1.25331	0.00579	0.84817
C-ENSTATI	-0.05963	-0.00030	-0.04352
C-FERROSI	0.35173	0.00133	0.19536
TOTAL	1.54540	0.00682	1.00000

PLAGIOCLASE

49.63	0.00	32.27	0.00	0.00	0.00	0.00	0.00	15.04	2.86	0.21	0.00

Components	Grams	Moles	Mole Frac.
ANORTHITE	3.55711	0.01279	0.73522
ALBITE	1.28857	0.00439	0.25271
SANIDINE	0.06835	0.00021	0.01208
TOTAL	4.91403	0.01739	1.00000

Reproduced with permission of the copyright owner. Further reproduction prohibited without permission.

SACK SSC-2 #20

COMPOSITION OF INITIAL LIQUID PHASE (Wt%)

SiO2	TiO2	Al2O3	Cr2O3	Fe2O3	FeO	MnO	MgO	CaO	Na2O	K2O	P2O5
50.20	2.43	16.65	0.00	1.69	8.76	0.24	3.62	7.53	5.27	2.16	0.82

Total grams= 99.37

****

Equilibrium T (in celcius)= 1092.5 ln fO2=-22.91072

****

COMPOSITION OF RESIDUAL LIQUID PHASE (Wt%)

SiO2	TiO2	Al2O3	Cr2O3	Fe2O3	FeO	MnO	MgO	CaO	Na2O	K2O	P2O5
50.63	3.25	16.81	0.00	1.86	8.38	0.32	2.85	5.54	6.43	2.83	1.10

Total grams= 74.78565

COMPOSITION OF SOLID PHASES (Wt%)

OLIVINE

36.83	0.00	0.00	0.00	0.00	31.32	0.00	31.85	0.00	0.00	0.00	0.00

Components	Grams	Moles	Mole Frac.
FORSTERITE	0.89445	0.00636	0.64439
FAYALITE	0.71487	0.00351	0.35561
TOTAL	1.60931	0.00986	1.00000

HIGH-CALCIUM PYROXENE

52.83	0.00	0.00	0.00	0.00	13.30	0.00	12.92	20.95	0.00	0.00	0.00

Components	Grams	Moles	Mole Frac.
DIOPSIDE	6.11932	0.02826	0.84970
C-ENSTATI	-0.40233	-0.00200	-0.06025
C-FERROSI	1.84756	0.00700	0.21055
TOTAL	7.56455	0.03326	1.00000

PLAGIOCLASE

51.19	0.00	31.19	0.00	0.00	0.00	0.00	0.00	13.79	3.51	0.31	0.00

Components	Grams	Moles	Mole Frac.
ANORTHITE	8.94957	0.03217	0.67195
ALBITE	4.35000	0.01484	0.30989
SANIDINE	0.28297	0.00087	0.01816
TOTAL	13.58254	0.04787	1.00000

Reproduced with permission of the copyright owner. Further reproduction prohibited without permission.

SACK CSQ-3 #19

COMPOSITION OF INITIAL LIQUID PHASE (Wt%)

SiO2	TiO2	Al2O3	Cr2O3	Fe2O3	FeO	MnO	MgO	CaO	Na2O	K2O	P2O5
46.58	2.41	15.08	0.00	2.09	8.60	0.19	9.42	8.86	3.42	1.51	0.52

Total grams= 98.67999

****

Equilibrium T (in celcius)= 1121 ln fO2=-21.89758

****

COMPOSITION OF RESIDUAL LIQUID PHASE (Wt%)

SiO2	TiO2	Al2O3	Cr2O3	Fe2O3	FeO	MnO	MgO	CaO	Na2O	K2O	P2O5
48.64	4.25	17.07	0.00	1.51	6.89	0.34	4.27	8.25	5.27	2.61	0.92

Total grams= 56.71487

COMPOSITION OF SOLID PHASES (Wt%)

OLIVINE

37.92	0.00	0.00	0.00	0.00	25.49	0.00	36.59	0.00	0.00	0.00	0.00

Components	Grams	Moles	Mole Frac.
FORSTERITE	10.35687	0.07361	0.71895
FAYALITE	5.86344	0.02877	0.28105
TOTAL	16.22031	0.10238	1.00000

HIGH-CALCIUM PYROXENE

53.20	0.00	0.00	0.00	0.00	11.75	0.00	13.89	21.16	0.00	0.00	0.00

Components	Grams	Moles	Mole Frac.
DIOPSIDE	6.25591	0.02889	0.85225
C-ENSTATI	-0.25209	-0.00126	-0.03704
C-FERROSI	1.65268	0.00626	0.18479
TOTAL	7.65650	0.03390	1.00000

PLAGIOCLASE

49.10	0.00	32.63	0.00	0.00	0.00	0.00	0.00	15.46	2.62	0.19	0.00

Components	Grams	Moles	Mole Frac.
ANORTHITE	12.69529	0.04563	0.75679
ALBITE	4.10548	0.01400	0.23221
SANIDINE	0.21581	0.00066	0.01100
TOTAL	17.01658	0.06030	1.00000

Reproduced with permission of the copyright owner. Further reproduction prohibited without permission.

SACK CSQ-3 #20

COMPOSITION OF INITIAL LIQUID PHASE (Wt%)

SiO2	TiO2	Al2O3	Cr2O3	Fe2O3	FeO	MnO	MgO	CaO	Na2O	K2O	P2O5
46.58	2.41	15.08	0.00	2.09	8.60	0.19	9.42	8.86	3.42	1.51	0.52

Total grams= 98.67999

****

Equilibrium T (in celcius)= 1092.5 ln fO2=-22.91072

****

COMPOSITION OF RESIDUAL LIQUID PHASE (Wt%)

SiO2	TiO2	Al2O3	Cr2O3	Fe2O3	FeO	MnO	MgO	CaO	Na2O	K2O	P2O5
47.76	5.80	18.05	0.00	1.40	5.92	0.46	3.41	6.20	6.29	3.46	1.25

Total grams= 41.52635

COMPOSITION OF SOLID PHASES (Wt%)

OLIVINE

37.26	0.00	0.00	0.00	0.00	29.05	0.00	33.69	0.00	0.00	0.00	0.00

Components	Grams	Moles	Mole Frac.
FORSTERITE	10.75362	0.07643	0.67396
FAYALITE	7.53399	0.03697	0.32604
TOTAL	18.28761	0.11340	1.00000

HIGH-CALCIUM PYROXENE

53.08	0.00	0.00	0.00	0.00	12.18	0.00	13.53	21.21	0.00	0.00	0.00

Components	Grams	Moles	Mole Frac.
DIOPSIDE	11.16072	0.05154	0.85627
C-ENSTATI	-0.58297	-0.00290	-0.04824
C-FERROSI	3.04863	0.01155	0.19197
TOTAL	13.62638	0.06019	1.00000

PLAGIOCLASE

50.83	0.00	31.44	0.00	0.00	0.00	0.00	0.00	14.07	3.35	0.31	0.00

Components	Grams	Moles	Mole Frac.
ANORTHITE	16.84433	0.06055	0.68636
ALBITE	7.64533	0.02607	0.29558
SANIDINE	0.51837	0.00159	0.01806
TOTAL	25.00802	0.08821	1.00000

Reproduced with permission of the copyright owner. Further reproduction prohibited without permission.

SACK TB-253 #6A

COMPOSITION OF INITIAL LIQUID PHASE (Wt%)

SiO2	TiO2	Al2O3	Cr2O3	Fe2O3	FeO	MnO	MgO	CaO	Na2O	K2O	P2O5
47.41	2.13	15.78	0.00	2.18	7.87	0.18	8.04	8.75	3.73	1.72	0.55

Total grams= 98.34001

****

Equilibrium T (in celcius)= 1133 ln fO2=-21.48312

****

COMPOSITION OF RESIDUAL LIQUID PHASE (Wt%)

SiO2	TiO2	Al2O3	Cr2O3	Fe2O3	FeO	MnO	MgO	CaO	Na2O	K2O	P2O5
50.05	3.09	15.95	0.00	1.55	7.05	0.26	4.70	9.19	4.91	2.46	0.80

Total grams= 68.97916

COMPOSITION OF SOLID PHASES (Wt%)

OLIVINE

38.22	0.00	0.00	0.00	0.00	23.92	0.00	37.86	0.00	0.00	0.00	0.00

Components	Grams	Moles	Mole Frac.
FORSTERITE	8.23901	0.05855	0.73823
FAYALITE	4.23094	0.02076	0.26177
TOTAL	12.46996	0.07932	1.00000

HIGH-CALCIUM PYROXENE

53.27	0.00	0.00	0.00	0.00	11.50	0.00	14.08	21.15	0.00	0.00	0.00

Components	Grams	Moles	Mole Frac.
DIOPSIDE	0.42843	0.00198	0.85072
C-ENSTATI	-0.01462	-0.00007	-0.03130
C-FERROSI	0.11081	0.00042	0.18058
TOTAL	0.52463	0.00233	1.00000

PLAGIOCLASE

48.56	0.00	33.00	0.00	0.00	0.00	0.00	0.00	15.90	2.39	0.16	0.00

Components	Grams	Moles	Mole Frac.
ANORTHITE	11.42560	0.04107	0.77902
ALBITE	3.27463	0.01117	0.21185
SANIDINE	0.15673	0.00048	0.00914
TOTAL	14.85695	0.05272	1.00000

Reproduced with permission of the copyright owner. Further reproduction prohibited without permission.

SACK HC-63 #4A

COMPOSITION OF INITIAL LIQUID PHASE (Wt%)

SiO2	TiO2	Al2O3	Cr2O3	Fe2O3	FeO	MnO	MgO	CaO	Na2O	K2O	P2O5
48.63	1.07	17.39	0.00	1.76	7.97	0.18	8.64	11.10	2.80	0.22	0.12

Total grams= 99.88001

****

Equilibrium T (in celcius)= 1137 ln fO2=-21.34497

****

COMPOSITION OF RESIDUAL LIQUID PHASE (Wt%)

SiO2	TiO2	Al2O3	Cr2O3	Fe2O3	FeO	MnO	MgO	CaO	Na2O	K2O	P2O5
51.79	2.73	15.33	0.00	1.77	8.87	0.46	4.51	8.75	5.03	0.46	0.31

Total grams= 39.12449

COMPOSITION OF SOLID PHASES (Wt%)

OLIVINE

38.09	0.00	0.00	0.00	0.00	24.59	0.00	37.31	0.00	0.00	0.00	0.00

Components	Grams	Moles	Mole Frac.
FORSTERITE	9.48259	0.06739	0.73002
FAYALITE	5.07888	0.02492	0.26998
TOTAL	14.56148	0.09232	1.00000

HIGH-CALCIUM PYROXENE

53.15	0.00	0.00	0.00	0.00	12.05	0.00	13.83	20.97	0.00	0.00	0.00

Components	Grams	Moles	Mole Frac.
DIOPSIDE	8.44844	0.03901	0.84530
C-ENSTATI	-0.32273	-0.00161	-0.03483
C-FERROSI	2.30802	0.00875	0.18953
TOTAL	10.43374	0.04615	1.00000

PLAGIOCLASE

48.55	0.00	33.02	0.00	0.00	0.00	0.00	0.00	15.91	2.41	0.11	0.00

Components	Grams	Moles	Mole Frac.
ANORTHITE	27.23813	0.09790	0.77957
ALBITE	7.87759	0.02687	0.21392
SANIDINE	0.26590	0.00082	0.00651
TOTAL	35.38162	0.12559	1.00000

Reproduced with permission of the copyright owner. Further reproduction prohibited without permission.